Accessible Hand Prostheses

3D Printing meet Smartphones

Cuellar Lopez, J.S.

DOI
10.4233/uuid:7caf6926-a673-4e01-9f2b-673f58828b9b

Publication date
2021

Document Version
Final published version

Citation (APA)
Cuellar Lopez, J. S. (2021). *Accessible Hand Prostheses: 3D Printing meet Smartphones*. [Dissertation (TU Delft), Delft University of Technology]. https://doi.org/10.4233/uuid:7caf6926-a673-4e01-9f2b-673f58828b9b

Important note
To cite this publication, please use the final published version (if applicable).
Please check the document version above.

Accessible Hand Prostheses:

3D Printers meet Smartphones

Juan Sebastian Cuellar Lopez

Title: Accessible hand prostheses: 3D printers meet smartphones
Author: Juan Sebastian Cuellar Lopez (juanqr7@hotmail.com)
Cover illustration by:
ISBN:
This research was funded by the Delft Global Initiative

An electronic version of this dissertation is available at

Accessible Hand Prostheses:

3D Printers meet Smartphones

PROEFSCHRIFT

ter verkrijging van de graad van doctor aan de Technische Universiteit Delft,
op gezag van de Rector Magnificus prof. dr. ir. T.H.J.J. van der Hagen
voorzitter van het College voor Promoties, in het openbaar te verdedigen op donderdag 25 februari 2021 om 12:00 uur

door

Juan Sebastian CUELLAR LOPEZ

Werktuigkundig Ingenieur, Technische Universiteit Delft, Nederland
geboren te Bogotá, Colombia

Dit proefschrift is goedgekeurd door de promotoren.

Samenstelling promotiecomissie bestaat uit:
Rector Magnificus voorzitter
Prof. dr. ir. P. Breedveld, Technische Universiteit Delft, promotor
Prof. dr. ir. A.A. Zadpoor, Technische Universiteit Delft, promotor
Dr. ir. G. Smit, Technische Universiteit Delft, copromotor

Onafhankelijke leden:
Prof. dr. L.P.J. Kenney, University of Salford, Manchester, UK
Prof. dr. -Ing. H. Vallery, Technische Universiteit Delft
Prof. dr. J.S. Rietman, U. Twente/Roessingh Res. & Development
Prof. dr. ir. J.L, Herder, Technische Universiteit Delft
Prof. dr. J. Dankelman, Technische Universiteit Delft

Contents

SUMMARY

The World Health Organization (WHO) estimates that there are ≈40 million amputees in developing countries and that only ≈5% of them have access to prosthetic devices. In low income countries, there are only a few big cities capable of providing reasonable healthcare services and transportation from rural areas is usually complicated, expensive, and may take several days. In most of the cases, there is a general lack of trained personnel and materials making, prosthetic workshops limited, difficult to reach, or even non-existent. 3D printing is a manufacturing method that enables fabrication of structures with unusual geometries without the need for any particular manual skill, elaborate tooling, or labour-intensive procedures. Many 3D printing techniques have become easily accessible and have opened a window for creating low-cost functional parts in a simpler way than conventional procedures. The main purpose of the research described in this thesis is to increase the accessibility of prosthetic hands among people living in low-income settings. To achieve this, the goal of the research is twofold: one, to design a transradial hand prosthesis that can be 3D printed with very few and simple post assembly steps and suffice basic user requirements; and two, to develop a 3D modelling process based on 2D photographs for the design of transradial (below the elbow) sockets that can be 3D printed.

This thesis began exploring possibilities of non-assembly fabrication using 3D printing techniques. Chapter 2 contains a literature review describing a number of mechanisms fabricated in a non-assembly manner by 3D printing. Chapter 3 reviews the results of fatigue testing in 3D printed polymers in order to determine the 3D printing material and 3D printing settings that ensure best fatigue performance. Chapter 4 continues with a number of design considerations that were formulated for the fabrication of non-assembly mechanisms with 3D printing. We followed these guidelines to design a functional multi-articulated hand prosthesis that was then manufactured by material extrusion 3D printing. This design procedure concluded in a hand prosthesis concept that reduces manufacturing requirements to a single 3D printer and its building material. Chapter 5 contains a functional evaluation of

the 3D printed prosthetic hand including mechanical and user testing. To further explore the capabilities of non-assembly 3D printing, in Chapter 6 we initiated a new design process aimed at producing articulated fingers (two degrees of freedom per finger) under this manufacturing framework. For this process, we adopted a bio-inspired design approach by studying the anatomical structures of the human hand that can be translated into components of prosthetic hands and have the potential of offering improved functionality. This bio-inspired designed prosthetic hand achieved superior pinch force as compared to our previous non-assembly BP prosthetic hand. Chapter 7 describes the method employed to obtain and process the 3D models of a stump. The method is based on photos from a smartphone and a Statistical Shape Model (SSM). The algorithm translates the photos into a 3D digital shape and then introduces the digital outcome into the process of automatic anthropometry. The outcome was later used for determining the parameters of a parametric design of a transradial socket that can be 3D printed and fitted onto the user's residual limb. The error resulting from the automatic measurement was still too large for an acceptable socket design. The thesis ends in Chapter 8 with a pilot study of our new bio-inspired 3D printed hand design in Colombia. We employed a manual measuring method using visual cues of the stump and a measuring tape to obtain the dimensions required for the design of the socket. Through the manual measuring method and parametric socket and shaft designs, the components of the prosthetic device were produced easily and locally on a material extrusion 3D printer. The field testing in Colombia concluded that our design and manufacturing processes based on 3D printing are fast and easy to implement and opens a gateway for the production of prosthetic devices in developing countries.

Chapter 1: Introduction

1.1 Background

This PhD project was carried out in the context of a challenging but significant research question: how to improve access to prosthetic devices for amputees in developing countries? In other words, the project aspires to contribute to global development by facilitating the rehabilitation of poor and disabled people in countries where an absence of trained prosthetists exists and healthcare infrastructures are either completely absent, or difficult to access and/or poorly equipped. How? by designing prosthetic limbs that meet the users' requirements, but are also easy to produce without the need for the specialist manual skills possessed by prosthetists.

Let's start by framing the context that inspired the development of this project. In 2015 the World Health Organization (WHO) estimated that there are about 40 million amputees, both for upper and lower extremities, in developing countries [1]. More recently, McDonald et al. estimated that in 2017 57.7 million people were living with limb amputation only by traumatic causes [2]. By taking out the central-west European region and the North American region the prevalence of limb amputation adds up to 42 million. There are several reasons that explain this high figure. The greatest and maybe most dramatic one relates to violent events in war zones and post-war zones [3]. For instance, the 1994 civil war/genocide in Rwanda left hundreds of thousands of amputees. Similarly, a disproportionate number of people have had their limbs amputated during the 1991-2002 civil war in Sierra Leone. Humanitarian crises related to natural disasters also often result in a large number of people having this devastating condition. For instance, the WHO estimates that up to 4000 people had an amputation after the 2010 earthquake in Haiti [4]. Amputations are often performed by surgeons as a last resort measure to save the life of a patient, when all other treatment options are no longer viable to salvage extremely damaged or infected tissues [5-7]. Thanks to the advanced level of medical knowledge and technological development, amputations are relatively rare in Western countries. However, in low-income countries, the situation is unfortunately quite different: amputations are performed frequently and data seems to suggest that this scenario will not change in the next decades [8].

Apart from war-related amputations, traffic accidents or accidents in the workplace, especially in remote rural and mining regions, often result in limbs removal operations, as victims are not timely and adequately treated. In fact, even when the limb could be easily salvaged with proper medical care, patients get to the hospital when the wound has already reached an irreversible stage, or the infection is too advanced [6]. Healthcare facilities are often simply too far away, too crowded or too expensive for people living in rural, remote areas [9].

It is important to underline that amputation is linked to much more than the loss of a limb. It implies a lifelong disability that seriously jeopardizes the amputee's physical, psychological and social well-being. Amputations are traumatic, irreversible events that can be emotionally devastating for the victims and consequently also for their family [10]. For instance, evidence shows that in Nigeria, most amputees have no other option than living as homeless or beggars in the street [11]. Another study conducted in India demonstrates a clear link between amputation and the development of psychiatric disorders, including depression, post-traumatic stress disorder and even suicide [10]. The social stigmatization of amputees is very difficult to deal with, as people missing a limb are often perceived and treated as being somehow "incomplete individuals" or even as a burden for society, especially in the context of a political, economic and/or environmental crisis.

So, how to treat an individual with a missing body part? (Figure 1). A common and frequently used solution is to replace the specific body part with something artificial that at least partly fulfils the lost biomechanical functionality [12]. This is what defines the concept of a prosthesis. Upper limb prostheses are therefore devices that try to replicate the function of the human arm and hand. The human hand is so complex that still today, the anatomical and physiological functions are far to be fully replaceable with a prosthesis. The current upper limb prostheses are therefore substitutes that can execute only a limited number of functions, either in a passive or an active way. A passive prosthesis can be static, usually serving only for cosmetic purposes, or adjustable, where the other sound hand or the environment can adapt the grasping mechanism in different positions [13]. An active prosthesis uses force

delivered internally to the grasping mechanisms either by external actuation, mostly in the form of electronic actuators, or a body-powered cable. External actuators use energy provided by any means other than the human body. Batteries are the most used in this case. Body-powered (BP) prostheses use a shoulder harness and are cable-driven by shoulder and/or arm movement [14] (See Figure 2 [15]). According to a number of authors BP prostheses offer advantages such as proprioceptive feedback, lower weight and easier maintenance [14, 16-18] as compared to prostheses driven by external actuators. BP prostheses are also generally simpler to produce and therefore more affordable, which makes them more suitable for low-income settings and usually a more acceptable solution for upper limb amputation [16].

Figure 1.1: Person with transradial amputation in Colombia.

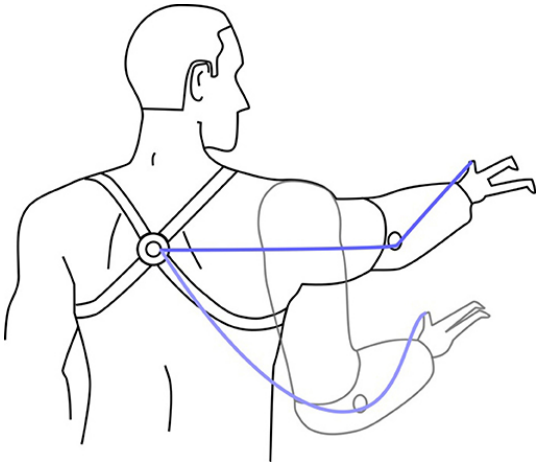

Figure 1.2: Diagram of how a Body-powered (BP) prosthesis works. Reprinted under the terms of the https://creativecommons.org/licenses/by/4.0/ [15].

Prosthetic devices play a fundamental role in improving the life of amputees, as they facilitate mobility and the capacity to perform everyday tasks independently. Prostheses can help a person to overcome social stigmatization, to regain self-confidence and to perform an active, decent "new" life [12]. In other words, prostheses are important to foster emotional and physical empowerment. Yet, prostheses are not easily accessible to all those who need them. Data by the WHO suggests that only about 5 - 15% of amputees in developing countries have access to these devices [1]. In fact, in low-income countries, few facilities exist that have the necessary personnel and advanced technology to design and construct robust, affordable and functioning prostheses [6]. A quick comparison in Figure 3 between a prosthetic workshop in Nepal and in the Netherlands depicts some of the differences. Furthermore, these facilities are most often only located in a few major cities, and cannot be easily reached by people living in remote rural areas. This is particularly the case in war and post-war zones. Even when amputees manage to get a prosthesis, they cannot afford to go back for follow-up checks, maintenance or repair [9, 19].

Figure 1.3: Workbench in a prosthetic workshop in Nepal (top) vs prosthetic workshop in the Netherlands (bottom). In the Netherlands state-of-the art tools and prosthetic devices are available whereas in Nepal the workbench is outdated and underequipped.

Most prostheses delivered to amputees in developing countries are provided by governmental and non-governmental organizations or private entities, trying to offer low-cost functional devices. However, these organizations face a wide range of technical, economic and infrastructural challenges [19]. In fact, the majority of the prostheses available in developing countries are second-hand prostheses from Western countries transported and provided to the user

through Non-governmental Organizations (NGOs) [19]. However, different studies show that up to 50% of these second-hand prostheses need repair work, or fail to perform adequately [20]. Beneficiaries complain about mechanical issues and high repair costs [9]. Moreover, fit issues between second-hand prostheses and users' residual limbs also create severe problems, including high level of discomfort, pain, and even wounds. In short, second-hand prostheses are not a sustainable option. If sockets are not personalized; they are eventually or immediately abandoned.

1.2 Scope of the project

Prostheses need to be easily accessible, affordable and custom-made. And it is here that the idea of this project unfolds: The starting point is the assumption that nowadays a great portion of the world's population owns a smartphone that can easily connect to an internet network. This is the case also in the developing world, where phones and internet access are increasingly widespread. The other core part of our project is 3D printing technology, which offers the unique possibility of fabricating complex 3D-shapes adjustable to the customers' needs. Mick Ebeling's recent "Not Impossible" project in Sudan is an inspiring example in this sense as it proved that it is possible to design and create simple but functional prostheses using basic 3D printing technology [21]. Other NGOs like e-NABLE [22] or "Doctors Without Borders" [23] have used 3D printing in this way as well, just like a large group of enthusiastic developers and research groups that have created a number of prosthetic hands with this manufacturing technology [24]. Little information is however available regarding whether basic user requirements are met for short- or long-term use by prosthetic hands produced this way [24]. Moreover, additional post-printing assembly actions are yet necessary to provide functional prostheses to users. Those assembly steps usually need to be performed by skilled personnel and may necessitate extra tools, thereby again reducing the overall accessibility.

1.3 Goal of the research

The main purpose of the research described in this thesis is to increase the accessibility of prosthetic hands among people living in low-income settings and poverty conditions. To achieve this, the goal of the research is twofold: one, to design a transradial hand prosthesis that can be 3D printed with very few and simple post assembly steps and suffice basic user requirements; and two, to develop a 3D modelling process based on 2D photographs for the design of transradial (below the elbow) sockets that can be 3D printed.

The overall idea is to develop a free smartphone app that scans the amputee's arm remnant with a smartphone camera and, with supplementary info of the contralateral limb, completely automates the complex prosthetic design process to make it able for 3D printing. This means that patients do not have to visit a clinic to have their stump measured: they just need a smartphone with an integrated camera that creates the design drawings of a personalized socket. Via the internet and the local mobile phone network, the design drawings are then sent to a 3D printer located in a private person's home, in a specialized workshop, hospital or company. Here, a customized prosthesis can be printed entirely in such a way that it contains just a few robust functional parts that are easily assembled by any handy person. The finished prosthesis can then be transported directly to the amputee using available local supply chains. Through this process, patients, even in remote, isolated areas can receive their custom-made artificial limb promptly, without much effort or financial resources.

1.4 Target region and collaborations

This project was possible with the financial support of the Delft Global Initiative, a TU Delft fellowship committed to use "science for the benefit of people, all people, worldwide" [25]. In the beginning of this research project we decided to select a relevant country in the developing world that contains a large population of people in need of prosthetic hands. Colombia is one of the countries that has endured civil conflict and violence in the last decades. This, combined with the socioeconomic conditions of some areas of the country, makes it an interesting target location for the development of this project. The production and fitting of low-cost prostheses in real scenarios is very much dependent on the coordination with individuals and organizations that are in

direct contact with people in need of a prosthesis and that are able to provide logistical information and support related to specific local contexts. The project thus needs the collaboration of several partners. We partnered with the Secretary of Health of the city of Ibague, Colombia, and the University of Ibague. Ibague is a city in the mid-western region of Colombia, approximately 200 km west from Bogota, the capital of the country. With a population of nearly 600.000 inhabitants the city has few general providers of prosthetic/orthotic devices and no specialized prosthetic workshops for treatment of upper limb amputations. The Secretary of Health helped to analyse local supply chains and to contact potential beneficiaries of our project. The University of Ibague provided logistic support and help to spot strategic locations of the workshop for the actual fabrication of the prostheses. The work described in this thesis is the start of an ambitious long-term project that entails several technical and financial challenges, yet also shows the great potential to advance scientific knowledge on manufacturing with 3D printing while greatly improving the accessibility to prosthetic technology to unprivileged people in developing countries.

1.5 Outline

This thesis is divided in two parts. Part 1 (Chapters 2-6) deals with the design and manufacture of prosthetic hands optimized for settings in developing countries with the aim to reduce manufacturing requirements to only one inexpensive 3D printer and common tools. The prosthetic devices are designed in such a way that after a 3D printing job, post assembly and other post processing steps are avoided or reduced to a minimum. Chapter 2 contains a state-of-the-art review of attempts to produce assembled mechanisms in a single step by 3D printing technologies. As opposed to a laboratory setting, in real life, prosthetic hands undergo many loading cycles. Chapter 3 contains a state-of-the-art review on the fatigue behaviour of 3D printed polymers where we establish whether the lifespan of 3D printed mechanisms could be predicted from the published data for the materials used in our designs. We present an overview of current data available and give directions for future research.

Chapter 4 deals with the development of a novel prosthetic hand that can be produced fully assembled in a single 3D printing job and establishes a set of design guidelines that can be used to facilitate the production of non-assembly mechanisms. Chapter 5 assesses the mechanical and functional characteristics of the non-assembly prosthetic hand from Chapter 4 and compares it with current solutions. As the non-assembly manufacturing paradigm was explored, some limitations on the design possibilities were encountered. Chapter 6 describes the development and functional assessment of a new minimal assembly 3D printed prosthetic hand design with improved features. To improve the functional characteristics we opted for a bio-inspired design approach combined with the advantages of 3D printing to create a prosthetic hand that features fully articulated fingers with just a few post-assembly requirements. The design principles used to create this bio-inspired hand and a functional assessment are described. The chapter finishes with a description of the manufacturing of the prosthetic hand and the functional prototype.

Part 2 of the thesis (Chapters 7 and 8) deals with the personalization of transradial prosthetic sockets using 2D photographs. Chapter 7 describes a new fitting method for prosthetic sockets based on automatic 3D anthropometry using statistical shape models and a new parametric design that can be 3D printed. The process uses pictures taken by a smartphone, creates a 3D model, measures important parts of the 3D model and resizes the socket design accordingly. Chapter 8 deals with the application of both the 3D printing and the 3D modelling technologies to produce fully working prosthetic devices in developing countries. We first combine both the fabrication by the 3D printing technology and the socket personalization by a smartphone to create a new framework of accessible and automatic design and manufacturing of upper limb prosthetic devices. In collaboration with our local partners in Colombia we set a small prosthetic workshop in the city of Ibague and used this new fabrication methodology to deliver prosthetic devices to Colombian people in need. We registered the feedback provided by the users and carried out a functional evaluation. Lastly, Chapter 9 contains a general discussion of the entire

fabrication process and the experience of the users with our novel 3D printed prosthetic hand.

1.6 References

[1] W.H. Organization, Standards for P&O Service Provision | ISPO, 2015. http://www.ispoint.org/standards-P-O-Services.

[2] C.L. McDonald, S. Westcott-McCoy, M.R. Weaver, J. Haagsma, D. Kartin, Global prevalence of traumatic non-fatal limb amputation, Prosthet Orthot Int (2020) 309364620972258.

[3] T.B. Staats, The rehabilitation of the amputee in the developing world: a review of the literature, Prosthet Orthot Int 20(1) (1996) 45-50.

[4] M.G. Randolph, L. Elbaum, P.S. Wen, D. Brunt, J. Larsen, A. Kulwicki, M. De la Rosa, Functional and psychosocial status of Haitians who became users of lower extremity prostheses as a result of the 2010 earthquake, J Prosthet Orthot 26(4) (2014) 177-182.

[5] L. Magnusson, G. Ahlstrom, Experiences of providing prosthetic and orthotic services in Sierra Leone--the local staff's perspective, Disabil Rehabil 34(24) (2012) 2111-8.

[6] R.A. Gosselin, D.A. Spiegel, R. Coughlin, L.G. Zirkle, Injuries: the neglected burden in developing countries, Bull World Health Organ 87(4) (2009) 246-246a.

[7] W. Yinusa, M.E. Ugbeye, Problems of amputation surgery in a developing country, Int Orthop 27(2) (2003) 121-4.

[8] A. Sabzi Sarvestani, A. Taheri Azam, Amputation: a ten-year survey, Trauma Mon 18(3) (2013) 126-129.

[9] C.S. Harkins, A. McGarry, A. Buis, Provision of prosthetic and orthotic services in low-income countries: a review of the literature, Prosthet Orthot Int 37(5) (2013) 353-61.

[10] A. Sahu, R. Sagar, S. Sarkar, S. Sagar, Psychological effects of amputation: A review of studies from India, Ind Psychiatry J 25(1) (2016) 4-10.

[11] C. Nwosu, M.O. Babalola, M.H. Ibrahim, S.I. Suleiman, Major limb amputations in a tertiary hospital in North Western Nigeria, Afr Health Sci 17(2) (2017) 508-512.

[12] J.M. Malone, L.L. Fleming, J. Roberson, T.E. Whitesides, Jr., J.M. Leal, J.U. Poole, R.S. Grodin, Immediate, early, and late postsurgical management of upper-limb amputation, J Rehabil Res Dev 21(1) (1984) 33-41.

[13] B. Maat, G. Smit, D. Plettenburg, P. Breedveld, Passive prosthetic hands and tools: A literature review, Prosthet Orthot Int 42(1) (2018) 66-74.
[14] A.L. Muilenburg, M.A. LeBlanc, Body-Powered Upper-Limb Components, in: D.J. Atkins, R.H. Meier (Eds.), Comprehensive Management of the Upper-Limb Amputee, Springer New York, New York, NY, 1989, pp. 28-38.
[15] L.F. Engels, C. Cipriani, Nature's Masterpiece: How Scientists Struggle to Replace the Human Hand, 2019. https://kids.frontiersin.org/article/10.3389/frym.2019.00083. (Accessed 20/10/2020 2020).
[16] S.L. Carey, D.J. Lura, M.J. Highsmith, Cp, Faaop, Differences in myoelectric and body-powered upper-limb prostheses: Systematic literature review, J Rehabil Res Dev 52(3) (2015) 247-62.
[17] S.G. Millstein, H. Heger, G.A. Hunter, Prosthetic use in adult upper limb amputees: a comparison of the body powered and electrically powered prostheses, Prosthet Orthot Int 10(1) (1986) 27-34.
[18] L.M. Kruger, S. Fishman, Myoelectric and body-powered prostheses, J Pediatr Orthop 13(1) (1993) 68-75.
[19] M. Marino, S. Pattni, M. Greenberg, A. Miller, E. Hocker, S. Ritter, K. Mehta, Access to Prosthetic Devices in Developing Countries: Pathways and Challenges, Proceedings of the Fifth Ieee Global Humanitarian Technology Conference Ghtc 2015 (2015) 45-51.
[20] L. Magnusson, N. Ramstrand, E.I. Fransson, G. Ahlstrom, Mobility and satisfaction with lower-limb prostheses and orthoses among users in Sierra Leone: a cross-sectional study, J Rehabil Med 46(5) (2014) 438-46.
[21] M. Ebeling, Project Daniel - Not Impossible's 3D Printing Arms for Children of War-Torn Sudan, 2013. https://www.youtube.com/watch?v=SDYFMgrjeLg.
[22] e-NABLE, The Raptor Hand, Enabling The Future, 2014.
[23] S. Herfat, P. Moreau, Evaluating 3D technologies for upper limb prosthesis design (Amman, Jordan), 2018. https://doi.org/10.7490/f1000research.1115497.1. (Accessed 28/04/2020).
[24] J. ten-Kate, G. Smit, P. Breedveld, 3D-printed upper limb prostheses: a review, Disabil Rehabil Assist Technol 12(3) (2017) 300-314.
[25] T. Delft, Delft Global Initiative, 2020. https://www.tudelft.nl/global/. (Accessed 08/10/2020).

Chapter 2: Additive manufacturing of non-assembly mechanisms

Juan Sebastian Cuellar, Gerwin Smit, Dick Plettenburg and Amir A. Zadpoor

Published as:

Additive manufacturing of non-assembly mechanisms, Addit Manuf 21 (2018) 150-158.

Abstract

Fabrication of complex and multi-articulated mechanisms is often seen as a time consuming and demanding process. The development of functional multi-articulated mechanisms that could be fabricated in a single step without the need for post-manufacturing assembly is therefore very attractive. Additive manufacturing (AM) has been pointed out as a feasible solution due to its numerous advantages and high versatility in comparison to other manufacturing techniques. Nevertheless, AM techniques also present different shortcomings that limit the complexity of the mechanism for single step fabrication. Here, we review the applications of AM techniques in fabrication of non-assembly multi-articulated mechanisms and highlight the involved challenges, thereby providing a perspective regarding the advantages and limitations of current AM techniques for production of complex mechanical devices. The paper starts off with basic joint elements in rigid-body and compliant configurations and proceeds with presenting an overview of multiple arrangements of joints and assemblies with embedded mechanical components. For every case of non-assembly fabrication, the limitations of the applicable AM processes are presented and further discussed. This work concludes with a discussion of the major shortcomings found in current non-assembly mechanisms fabricated by AM and recommending alternative techniques and future developments on AM.

2.1 Introduction

Fabrication of complex and multi-articulated mechanisms is often seen as a time consuming and demanding process. Conventional manufacturing techniques are often limited to simple mechanisms, thus requiring complex assembly procedures to construct multi-articulated mechanisms. For that reason, the development of functional multi-articulated mechanisms that could be fabricated in a single step without the need for post-manufacturing assembly is very attractive. Mechanisms fabricated whose fabrication process does not involve an assembly step are often referred to as non-assembly mechanisms, a term introduced first early in the 21st century [1].

Over the last two decades, many research groups have approached this problem by adopting additive manufacturing (AM) techniques, which are also referred to as 3D printing techniques, as the most feasible solution. This manufacturing method creates 3D constructs through sequential addition of material in a layer-by-layer [2] approach. The advantages of this method are numerous, but most importantly, it enables the fabrication of structures with complex geometries regardless of any specialized manufacturing skill or labor demanding procedures. The versatility of AM techniques is the core motivation for a thorough change in the current way of designing and constructing complex mechanisms.

In fact, it has been pointed out that multi-articulated mechanisms whose main specific function is that of mechanical motion could be built directly with satisfactory precision using current AM technologies without requiring any post-assembly [3]. Furthermore, several groups have already achieved successful fabrication of non-assembly mechanisms with different AM techniques. Joints were fabricated from polymer [1, 4, 5] and metallic [6-8] materials, soft robots were produced with flexible materials and fluids [9, 10] and fully assembled actuators were conceived with more elaborate AM-based techniques [11]. Overall, the mechanisms were successfully created with good kinematic characteristics and satisfactory performance.

Despite the existence of successful cases of non-assembly fabrication with 3D-printing, some limitations could be also identified. A comprehensive analysis on the design and manufacturing of such examples expose the constraints of each AM technique, consequently narrowing the spectrum of mechanism complexity.

An alternative approach for non-assembly fabrication lies in a promising technology based on AM often termed as hybrid or multiprocess 3D-printing. Parts can be produced not only in a non-assembly approach but also with increased functionality by using AM in combination with complementary processes (such as machining, manual embedding of parts, direct printing of electronic components and more) [12]. Especially when referring to non-assembly fabrication of mechanical parts, some of those complementary

manufacturing procedures could hold an equivalent or even higher level of complexity as compared to traditional manufacturing techniques because automation has not been fully achieved and skilled human involvement is still necessary [13], [14]. Adding to this the underlying limitations of AM, understanding thoroughly each 3D-printing technique becomes a critical matter in an attempt to exploit their potential and reduce their shortcomings in order to recognize up to what point mechanism complexity is feasible for a single-step fabrication.

The purpose of this manuscript is to review the applications of AM techniques in the construction of non-assembly mechanical parts and to discuss the challenges involved, thus providing perspective regarding the advantages and limitations of current AM techniques in the production of complex mechanisms. This paper focuses on the conception of multi-body mechanical assemblies at the macro-scale. Single step fabrication of structural electronics and microelectromechanical systems (MEMS) are, for example, not covered here, as they are reviewed elsewhere [12], [15] and [16].

2.2 Background on Additive Manufacturing (AM) processes and Joints

2.2.1 AM processes

AM allows for fabrication of models from three-dimensional computer-aided designs (CAD) by sequentially adding layers of material [2]. At present, AM techniques are classified in seven groups according to the ASTM standards [17]. These groups differ from each other in the way the layers are created and the way the layers are bonded to each other. *Vat photopolymerization* processes use liquid photo-curable resins that react to ultraviolet radiation (UV) and become solid after a chemical reaction. The most common technique is known as stereolithography (SL) [18]. *Powder Bed Fusion (PBF)* process uses energy to generate fusion of particulate material, a methodology to control the fusion of particulate material over a predefined track in every layer, and lastly, components destined to smooth and add new particulate layers [19]. PBF often

requires no support structures, because unused polymeric powder serves as a support basis for overhang structures. In contrast, support structures may be still needed during metallic PBF fabrication to prevent excessive warping due to high residual stresses [20]. *Material extrusion* process uses pressure (and high temperature) to force the material through a nozzle in a semi-solid state. The most widely known material extrusion technology is the fused deposition modelling (FDM^{TM}) [21]. *Material jetting (MJ)* process uses specialized nozzles to deposit drops of liquid material over a building platform. The new layer is then solidified commonly by UV light and moved downwards. In many cases, more than one jetting head is used, enabling deposition of support material and different part materials simultaneously. Support structures could be removed using a chemical agent such as sodium hydroxide solution or with a water jet [22]. *Binder Jetting (BJ)* process ejects binder droplets over a powder bed to form spherical agglomerates and bond them to the previous layer [23]. *Sheet lamination* processes use a laser to cut the shape of each cross-sectional layer out of a paper material sheet. Each new layer is then bonded to the previous layer via chemical compounds, clamping mechanisms, heat, or ultrasonic welding [24]. *Directed energy deposition (DED)* process uses an energy source to melt material, which is being deposited onto the building platform. After the material is fixed and solidified, a new layer is deposited on top [25].

2.2.2 Mechanical joints

AM principles permit the construction of complex geometries in a single-step, thereby removing the need for skilled technical personnel and labor-intensive procedures. Streamlining of the manufacturing process may therefore be possible through proper adjustment of the fabrication process of basic elements, i.e. links and joints. Joints, as a means of constraining the number of degrees of freedom (DoF), often play a central role in the function of mechanisms and deserve special attention, because their successful production often necessitate precisely-controlled geometric dimensions. Two separate groups, traditional rigid-body joints and compliant joints, have been considered here to review the joints fabricated with AM. Joints like the rolling toothed

geometry shown in Figure 2.1 are examples of precise fabrication that could be achieved with AM. Further background on joint concepts and a classification based on working principles and DoF could be found in reference [26].

Figure 2.1: Rolling toothed joint fabricated by AM.

2.3 Rigid-body joints

Traditional link connections in a mechanism are accomplished by placing rigid bodies between two or more of its elements. These joints generally comprise multiple bodies and are required to restrain specific DoF without deforming. Successful joint performance is therefore highly dependent on the surface quality of parts and the clearance between bodies. Strict geometrical dimensions and a proper surface finish reduce backlash and friction, both major concerns in the design and manufacturing of mechanisms. Hence, high accuracy is critical for fabrication of rigid-body joints with AM. Moreover, the use of support structures is an issue, because (1) removal procedures that generally deteriorate the surface quality of parts are usually necessary and (2) purge areas are sometimes required when trapped material is difficult to reach. For high-end joint manufacturing, AM should provide high accuracy of features and reduced layer thickness during fabrication, no or easy-to-remove support material, and easy cleaning of residual material when needed. Studies

introducing non-assembly fabrication of these rigid and multi-bodied joints are grouped by the AM process employed and are presented next.

2.3.1 Vat photopolymerization

Single-step fabrication of joints using the vat photopolymerization process has been reported with the SL technique using a SLA 190 machine with a Cibatool® SL 5170 resin. The fabrication process was adjusted through a trial-and-error approach by changing different manufacturing parameters such as clearance, size, and support structures. The clearances were optimized by sequentially fabricating joints with initial clearances of 1 mm which were reduced by 0.1 mm in every subsequent step until the joint stopped to work properly. Afterwards, the clearance was raised by 0.05 mm in new steps until a smooth motion was again present in the joint. Optimal clearances were found to be 0.5 mm for circular surfaces and 0.3 mm for planar surfaces. These clearances guaranteed smooth joint mobility made possible through sufficient surface quality while avoiding blockage that may be caused by support structures inserted between the surfaces. Revolute, prismatic, spherical, and universal joints were fabricated as shown in Figure 2.2a-d [1].

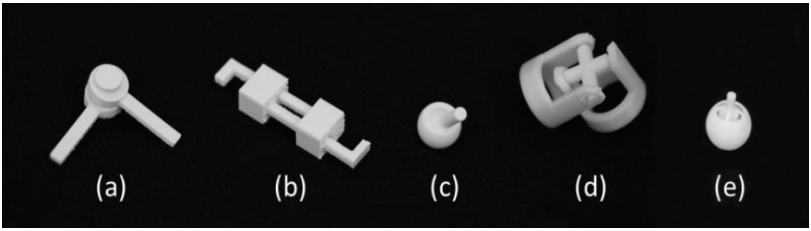

Figure 2.2: Joint concept designs for AM non-assembly fabrication. (a) Revolute joint[1], (b) Prismatic joint[1] (c) Spherical joint[1], (d) Universal joint[1] and (e) Cage-in-socket joint[4].

2.3.2 Powder Bed Fusion (PBF)

Polymer PBF

Non-assembly fabrication of joints using PBF was achieved first by Mavroidis et al.[1] using the SLS technique. A Sinterstation 2000 machine (DTM Corporation,

Austin, TX) was used for that purpose. Based on their previous experience with SL technique and taking into consideration that the Sinterstation 2000 machine had better accuracy, similar clearances were established (0.5 mm for spherical surfaces and 0.3 mm for planar surfaces). Revolute and spherical joints were successfully fabricated as shown in Figure 2.2a and 2.2c.

Modified spherical joints were also fabricated following a better residual extraction principle [4]. After experimenting with different concept designs, a cage-in-socket design (Figure 2.2e) was adopted. This design was created specifically to present contact between the moving parts. This was achieved by introducing gaps between the surface of the socket and the cage to prevent the parts from joining during fabrication. To find suitable parameters for this design, different features were tested including gap distance and size. The different set of joints were built using the SLS technique (EOS FORMIGA P 100 machine). The minimum gap achieved before the parts were fused together was 0.3 mm. Additionally, the authors reported that residuary material was easier to reach and remove due to the cage-shaped design.

Metallic PBF

Metallic non-assembly mechanisms are highly desirable, because their high mechanical properties expand the range of possible engineering applications. Assemblies fabricated with AM from metallic materials could withstand higher loads as compared to polymeric assemblies.

Since a large joint clearance could lead to vibration and instability, new design concepts have been introduced to reduce the minimum clearance achievable in pin joints. Three new alternatives are presented in Figure 2.3b-d. Stress analyses were carried out to explore the mechanical behavior of alternative joints. It was found that the drum-shape configuration shown in Figure 2.3d exhibited the best mechanical performance [7]. Furthermore, based on the perception of reduced joint functionality due to residuary stuck material between clearances, the drum-shaped joint was claimed to allow easy support cleaning [7]. Grounded on these findings, fully working drum-shaped pin joints were fabricated by SLM technique in universal joint configurations. This pin

design makes use of the wider space in the outer ends as purge areas, thus allowing a reduction of the clearance in the center of the joint. Pins were built using a Dimetal 280 machine with 316L stainless steel, achieving minimum operating joint clearances of 0.2 mm [3], 0.3 mm [7] and 0.1 mm [8]. In addition, different conclusions were drawn after completion of different experiments regarding the processability of the SLM technique for non-assembly mechanism fabrication [27, 28]. Processability issues like scanning speed, extraction of residual and support materials, build direction, and critical fabrication angle were considered. Scanning speeds are directly related to the amount of energy employed to melt the metallic powder. In case of improper use of energy, the transmission of heat could melt the powder inside the clearances, thus sticking residuary material to the surfaces. The minimum joint clearance achievable is therefore dependent on the particle size of the powder and the quantity of the employed laser energy [3, 28]. As previously mentioned, even though the SLM technique is a powder-based technology, support structures may still be needed when facing overhang fabrication. These structures are generally undesired, because the extraction procedure normally deteriorates the surface [3]. Moreover, support structures are difficult to reach when they are inserted inside the clearances, consequently compromising the surface quality and the functionality of the mechanisms. Nevertheless, avoiding the insertion of support structures inside the clearances is often possible through proper choice of process parameters, i.e. fabrication direction, scanning speed, particle size, etc., which enable suitable critical fabrication angles [27, 28]. Universal joints (Figure 2.4a), a crank rocker mechanism (Figure 2.4b) [8], a rocker- slider mechanism (Figure 2.4c) [27] and an abacus [29] were successfully built using modified fabrication directions and proper process parameters. A correct selection of processing strategies successfully could be used to avoid the insertion of support structures inside the clearances.

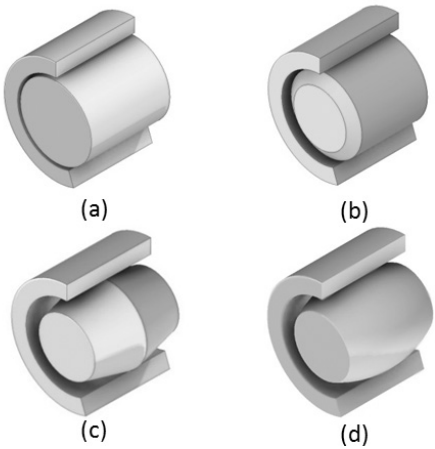

Figure 2.3. Pin joint concept designs considered for non-assembly fabrication (a) traditional pin (b) with chamfered ends (c) Double cone (d) Drum-shaped[7].

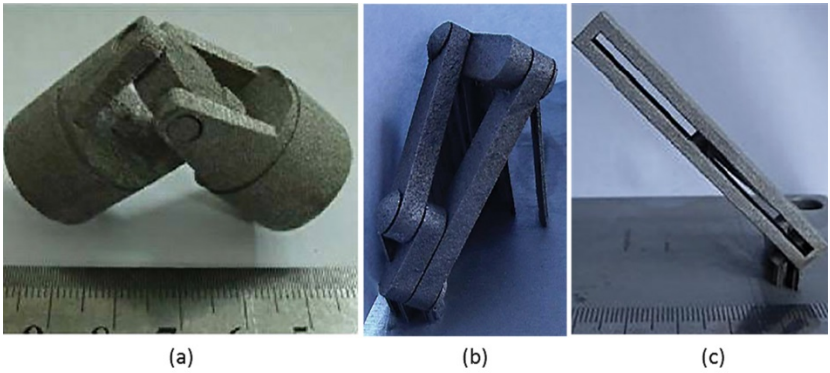

Figure 2.4: Non-assembly joint samples fabricated in stainless steel material using metallic PBF processes. (a) Universal joint, (b) crank rocker mechanism[8] and (c) rocker-slider mechanism[27].

Alternative joint designs have been also built from aluminum and titanium alloys using a DMLS machine (EOSINT M270 Xtended version) [6]. Concave and convex shapes were adopted for the pin joints using well-defined curvatures as

self-supporting structures. Optimal process parameters for the highest density and best surface quality of parts fabricated with aluminum alloys had been stablished in previous investigations [30, 31]. These parameters were used to fabricate a simple gear train mechanism with concave-shaped pins and concave-shaped hole joints from an aluminum alloy (Figure 2.5). Alternatively, default machine parameters were used to fabricate a simple joint with a convex-shaped pin and a concave-shaped hole joint from a titanium alloy (Figure 2.5). Aluminum parts exhibited smooth mobility at a minimum joint clearance of 0.1 mm, while titanium parts achieved the same at a minimum joint clearance of 0.08 mm.

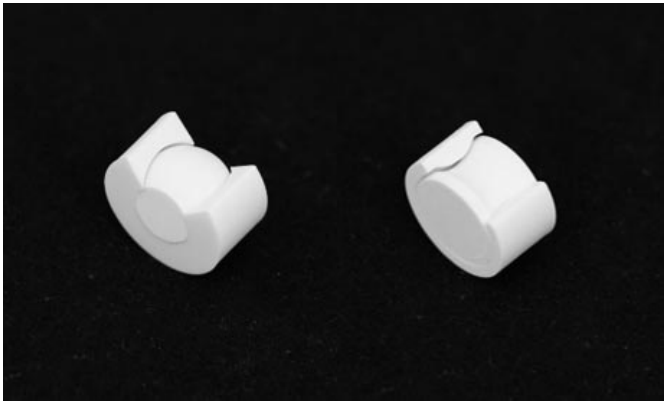

Figure 2.5: Non-assembly joint concepts for AM in aluminum and titanium alloy[6].

2.3.3 Material Jetting (MJ)

As previously mentioned, drum-shaped designs for pin joints could reduce the achievable clearance in non-assembly joints [7]. To validate this new concept, several universal joints were fabricated with conventional pins and drum-shaped pins with an MJ process. An Objet (2010) Eden 350V machine was used with two different materials (Fullcure 720 and VeroWhite) for that purpose. The constructs achieved 0.2 mm of minimum clearance for the conventional joint

and 0.1 mm of minimum clearance for the drum-shaped joint [32]. In a study by Calì et al. [4], modified spherical joints were also fabricated using MJ. Likewise, a cage-in-socket design was adopted and different sets of joints were built using an Objet Polyjet machine following the same methodology used for the polymer PBF technique. The authors reported identical results as the experiments involving the SLS technique, i.e. a minimum gap of 0.3 mm and the easier cleaning of residuary material and support structures.

2.3.4 Material extrusion

A recent work by [33] assessed the performance of new joint designs based on drum-shaped and cylindrical-shaped revolute joints. A new worm-shaped design was fabricated with a Stratasys Vantage™ machine using ABS material and dissolvable supports. The worm-shaped joint showed significant dynamical improvements compared to other non-assembly joint designs as it achieved a minimum joint clearance of 0.05 mm. Even though no other rigorous research was found regarding non-assembly fabrication of rigid-body joints via Material Extrusion based technologies, online hobbyist community of entry-level FDM™ users have shown successful production of revolute joints reaching a minimum clearance of 0.3 mm [34]. Although Material Extrusion based processes are commonly perceived to be the less precise of main commercially available AM techniques, recent developments have reached reasonable part accuracy levels and also dual deposition of part and soluble support material. As shown by [33], industrial-grade FDM™ 3D printers could equate other AM technologies in terms of minimum achievable clearance when building non-assembly joints.

The high versatility and easy accessibility makes the Material Extrusion technology a valuable choice for prototyping non-assembly constructs especially in settings where high-end technology is out of reach. To explore the full potential of new Material Extrusion technologies into the non-assembly rigid-body joint framework, additional research is required.

2.4 Compliant joints

Compliant joints allow the relative motion of elements through deformation of elastic members. Manufactured as a continuous and flexible body, these joints offer an interesting alternative for fabrication of non-assembly mechanisms with AM techniques, because joint clearance between rigid links is non-existent. Successful performance is therefore not affected by the lack of high precision manufacturing. Instead, the building materials and geometric configurations are the most important features determining the mechanical performance of such joints. Since AM allows practically full geometric freedom, the key drawback lies in the mechanical properties of the building materials. Although acceptable elastic behavior of building materials is basically present with all AM techniques, precise mechanical properties, like elastic modulus or yield strength, are difficult to predict and should be also provided to enable AM of complaint joints for high-end applications.

To accomplish different types of motion, several compliant shapes have been fabricated with AM techniques. Flexural hinge-type joints were created with SLS [35] and Material Extrusion [36, 37] technologies. A translational joint [38] and a trispiral joint [39] were made with FDM™, while twist compliant mechanisms have been produced using SLA [40], and lattice flexures have been fabricated from titanium using the electron beam melting technique [41]. Further complexity has been achieved using a MJ-based Polyjet (Stratasys) process by fabricating multi-material compliant joints. A helical-shaped compliant joint [42] and a compliant force-inverter [43] were conceived using multiple phases of rigid and soft materials, thus providing stiff structural parts to hold the construct as a robust entity and localized flexible points. AM techniques were also used to provide solutions for stability and parasitic motion, both major concerns in the design of compliant joints. The addition of multiple joints and links in parallel layers was successfully assessed and supplementary guidelines for compliant joints designs were proposed for correct performance of compliant mechanisms [44].

2.5 Advanced non-assembly mechanisms

Arrangements of multiple joint and link elements compose the basic structure of several robots and actuators. Such arrangements have also been fabricated with AM technologies in a single step and are presented in this section as advanced mechanisms.

Successful fabrication of an advanced mechanism consisting of traditional rigid-body links and joints in a single step with AM technologies is reported by Wei et al. [11]. The MJ Polyjet technique was employed in order to build a pneumatic robot. An Objet Eden 350V machine was used with the VeroClear 950 as main building material. Although parts were conceived completely assembled in a single step, the clearance achieved between movable parts affected deeply the transmission efficiency of the mechanism. The final construct eventually showed instability, vibration, and inaccuracy after performance tests.

Further development on compliant mechanisms allowed the formation of alternative advanced mechanisms. Inspired by biological systems, soft robotics have recently gained important attention and have been extensively studied over the last decade [45]. Fabricated out of compliant materials, these robots are safer for human interaction, can move in a large number of degrees-of-freedom and have the potential to adapt their shape to the environment [46]. Despite the advantages of soft robotics, manufacturing and design of these devices is still challenging. Even though several manufacturing techniques have been used [47], design concepts have a tendency towards more complex geometric features [48], thereby demanding challenging fabrication procedures. Moreover, embedded components are usually included into the designs due to the actuation principles employed, thus contributing additional complexity to the fabrication. Since many AM techniques are compatible with soft material and due to the aforementioned capability of producing complex geometries, AM has been proposed as a suitable process to create fully working soft robotics. Although several soft robotic examples produced via AM techniques could be found in the literature [49, 50], they still require manual post-processing steps. Overall, research regarding single step fabrication of soft

robotics and actuators is very limited and scarce. Two examples are presented next.

An actuator inspired by the tentacle muscle of octopus was fabricated using an SL-based technique. The Digital Mask Projection Stereolithography (DMP–SL) technique was employed, because it allowed photopolymerization of a whole layer in a single step. The complex pleated structure shown in Figure 2.6a was fabricated using the commercial Spot-e resin (Spot-A Materials, Inc.). Each air inlet is connected directly to one chamber allowing pressure differentials between two opposing cavities. The actuator bends when pleated structures on one side expand and the opposing side contracts. Multiple 3d trajectories were achieved at a reasonable speed (< 70ms) [10].

An alternative approach embraced the option of printing both fluids and solids in parallel. By tricking a commercial MJ machine (Stratasys Objet260) control system, certain fluids could be deposited along with photocurable resins. A list of design rules was created after iteratively manufacturing different geometries in different directions. Different hydraulic robots were conceived encasing the fluid with soft photocurable material. A six-legged robot was built enclosing fluid into bellows structures as shown in Figure 2.6b. The bellows structures exert force by applying pressure differentials into the fluid via an electric motor. Likewise, a fully housed gear pump and a soft gripper were successfully fabricated in a single step following the abovementioned design rules [9].

Even tough fully working soft robotics were conceived, current building materials are very limited and provide poor mechanical properties. For both SL and MJ techniques, the authors reported insufficient fatigue lifetime, specifically tears appearing after continuous actuation [10]. Alternative options for single-step fabrication of soft robotics includes direct deposition of soft actuators, i.e. smart materials that activate and bend with different stimuli (e.g. heat, magnetism, light, moisture, pH, electricity). Additional literature on non-assembly AM soft actuators can could be found in [51].

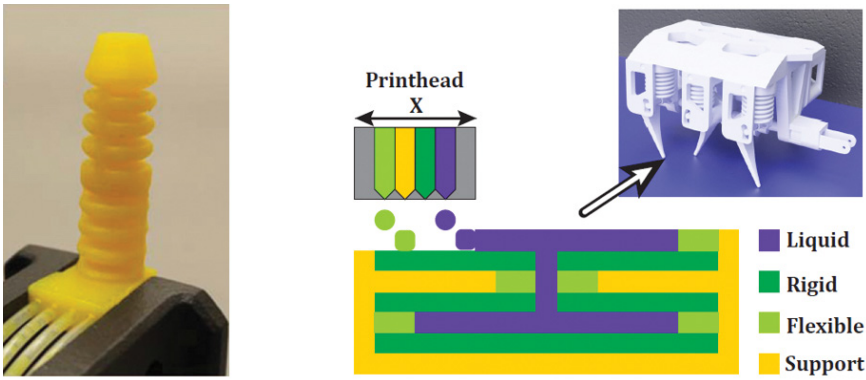

(a) (b)

Figure 2.6: Soft robots produced by AM single-step fabrication (a) soft actuator with pleated structure [10], (b) Scheme showing deposition of liquid and solid materials in parallel to create the bellows structure in a six-legged robot [9].

2.6 Non-assembly advanced mechanisms with embedded components

Embedding of different components (either manually or in combination with other manufacturing procedures) during AM fabrication of parts has become a technique extensively used in recent years. Here the applications of the embedding techniques facilitating fabrication of non-assembly mechanical parts are shown. A few examples of embedded electronics are addressed since a more thorough review can be found in [12].

One of the many advantages of AM is the possibility to access the internal geometry of manufactured parts and incorporate functional components during their fabrication. Embedded components during a layer-based fabrication could be traced back to the early 90s, where they were used as fundamental parts of electromechanical devices. This embedding process was more extensively used after the introduction of the technique referred to as shape deposition manufacturing (SDM) [52]. These techniques not only deposit material onto a layer but also use computer numerically controlled

(CNC) machining to precisely define the surface of the part by removing material. The CNC machining step could be used to define cavities in which different components may be inserted. The deposition of layers could be resumed on top of the inserts to fully encase the components. SDM has been used for embedding pneumatic actuators, servo motors, and flexible inserts to create insect-like robots [53, 54], fibers and electrical wires to create flexible mechanisms [55], and sensors for measuring and monitoring purposes [56-60]. Although the outcome has been successful, the SDM process is still laborious, slow, and limited to a small spectrum of materials [61].

Stereolithography (SL) has been also used to embed different components during the fabrication of mechanisms. Initially used to embed sensors [62], the SL technique has proved to be a suitable procedure to embed other types of components. Procedure recommendations were established after successfully embedding screwdrivers, electric motors, gears, nuts, and screws in a robot [63]. Fabrication issues like laser shadowing, support structures, and re-coating of the vat of building material have been reported and addressed. Different strategies such as the inclusion of shape converters were introduced and subsequently taken into consideration for successful fabrication of a radio-controlled vehicle [5], a robotic hand [64], a fan and encased joints [65]. Despite the fact that successful mechanisms were produced, real-world applications are very limited due to the arduous work implicit when trying to circumvent the aforementioned problems and the lack of compatible materials with the SL technique. Different electronic components have been also extensively embedded for the past decade using manual operations and/or extra manufacturing processes (e.g. [66], [67]). A comprehensive study on the SL technique and the different techniques for embedding electronics can be found in [68].

The Material Jetting (MJ) process, and more specifically the Stratasys Polyjet process, has been used to embed electronics [69] and more recently SMA actuators [14, 70]. SMA fibers were embedded (Figure 2.7) to conceive active compliant finger and knee. A multi-material Polyjet machine was used for fabricating rigid parts with VeroWhite material and flexible parts with

TangoBlack material. Guideline procedures for successful embedding and anchoring of SMA fibers have been established [14]. Further work established additional guidelines for embedding and fixing SMA fibers and springs into more complex configurations. Using a clever cavity design a compliant construct with embedded spring SMA actuators was produced. Likewise, the VeroWhite material was used for the rigid parts and the TangoBlack was used for the flexible parts [70].

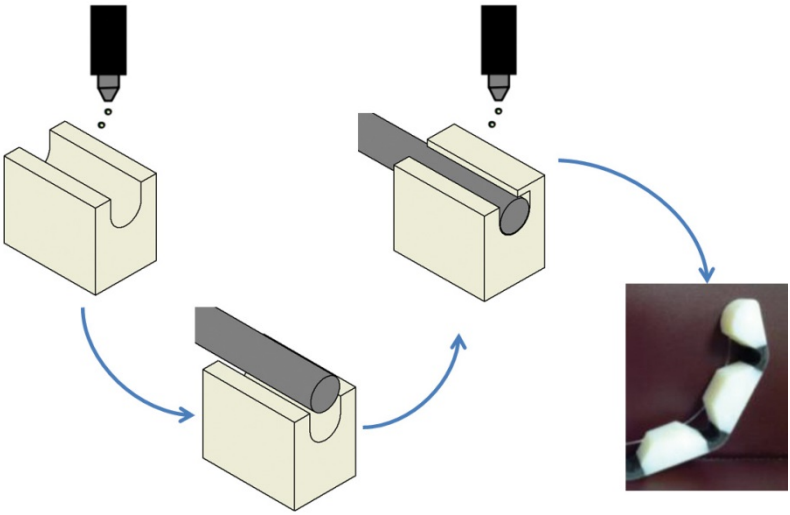

Figure 2.7: Embedding scheme of SMA fibers [14]. (1) The base is made with AM, (2) The AM process is stopped and the fibers are inserted, (3) The AM process is resumed on top to fully embed the fiber, (4) the mechanisms is completed.

Material extrusion based technologies have been mostly used to embed different electronic components such as sensors [71], functional circuits [72] [73], transmission lines [74] and more. In addition, successful non-assembly fabrication of a multi-articulated electromechanical device was achieved by Aguilera et al [13]. A rotational motor was conceived by manually embedding

magnets, electromagnets, bearings and an electronic speed controller into the thermoplastic substrate delivered by the AM technology. The material extrusion process was stopped in five stages, in where different components were manually inserted, and subsequently resumed on top in order to fully encase all parts [13].

2.7 Discussion

2.7.1 Rigid-body joints

The review of literature shows several examples of mechanisms fabricated using AM without any need for manual post-assembly. Throughout this search, the MJ-based Polyjet technique was found to be the most widely used AM process for the fabrication of non-assembly mechanisms. Both compliant and traditional mechanisms were successfully conceived achieving reasonable levels of (geometrical) complexity. The remarkable feature of some 3D printer (e.g. Objet, Stratasys) for parallel deposition of part and support material has proven to be significantly advantageous over other AM fabrication principles. Nevertheless, complex internal structures are more challenging to fabricate, because purge connections must be taken into consideration for support removal of encased constructs. Clever deposition of fluid and support material (in parallel with part material) circumvent this problem when fabricating actuators for hydraulic applications. Parts could be fabricated surrounded by a small layer of liquid, thus preventing the fusion of material part with the inner walls of the casing and fragile support structures. As in MacCurdy et al. [9] pump design, liquid and support material may be removed as normal mechanism actuation is executed.

Although PBF process is also recognized to facilitate overhang fabrication, extraction of the residual material is still challenging and could strongly influence the performance of the fabricated joints. Trapped powder inside joint clearances could lead to high friction and poor mechanical performance. As with the Objet Polyjet technology, purge openings and connections must be taken into consideration for encased mechanisms and

tight clearances. Moreover, and in addition to the typical “staircase effect” of every AM technique, final surface roughness of parts is still difficult to control and mostly unsuitable for high-precision applications. Related research has studied the effect of different fabrication parameters on the final surface roughness of polymeric [75] and metallic [30] parts. Despite previous research, high-end surface quality remains uniquely achievable through additional post processing steps.

The addition of support structures in metallic PBF techniques is a limiting factor, because arduous post processing removal steps are unavoidable and their extraction contributes to a poor surface quality. Fortunately, evidence of successful evasion of support structures has been shown and is possible by providing proper critical fabrication angles. This could be achieved by adjusting the fabrication parameters to their optimum values and choosing the appropriate build direction.

Despite early introduction of the vat photopolymerization processes to the development of non-assembly mechanisms, this type of processes was rarely used in further investigations of traditional joint fabrication. As previously shown, clearances achieved in jointed structures by this technique are inferior and the addition of support structures may be problematic. However, different alternatives to the SL technique, like the DMP-SL, and further developments on photocurable materials are promising options for fast conception of robust soft robotics and compliant mechanisms.

2.7.2 Compliant joints

Application of compliant mechanisms is highly advantageous in the context of manufacturing, because joint clearance between rigid links is non-existent. Still, when it comes to fabrication by AM techniques, material selection presents a major limitation because many are unsuited for large deformation applications and the effect of multiple printing parameters in the compliant behavior of parts has not been studied thoroughly. Even though satisfactory kinematic performances were achieved, little attention was paid to the kinetics of the joints. For instance, the stiffness of joints was rarely explored. To reach an

optimal mechanical performance, additional tools that could provide the mechanical behavior of joints should be considered. As an example, a setup for stiffness calculation of material extrusion based flexure hinges could be taken into consideration [37, 76]. Given availability of a limited number of flexible materials that could be processed with AM technique, the use of multi-material deposition and new topology optimization algorithms could significantly increase the mechanical behavior of compliant bodies [43].

Furthermore, the design freedom of complex geometries permits the manipulation of the inertial and stiffness properties of 3D printed parts, thereby allowing enhanced compliancy of joints. Careful design choices must be taken in order to achieve consistent stiffness over active and inactive axis with the aim of allowing flexural motion while preventing parasitic motion of compliant parts. Detailed stiffness analysis on numerous compliant designs can be found in [77]. Even though several compliant shapes have been proposed both in polymeric and metallic parts so far, there exist more joint type possibilities that could be fabricated with AM and could be potentially more suited for certain mechanical applications.

2.7.3 Embedding of external components

Embedding of several components during AM fabrication has proven to enhance mechanical properties and increase the features of the fabricated parts. Parts could be produced with new features by adding sensors, actuators, joints, links, and smart materials during the fabrication process. The embedding processes have the potential to conceive advanced mechanisms without any post-processing requirements. Nevertheless, the design processes need to take into consideration the correct positioning and encasing of embedded parts. Furthermore, careful monitoring of fabrication processes may be needed for just-in-time pausing of the manufacturing process, manual insertion of the embedded parts, and resuming the production process. Overall, the embedding process requires skilled manual operations and time-consuming procedures to achieve successful performances. The concomitant complexity during fabrication therefore introduces difficulties and needs further assessment.

2.7.4 Final remarks and future directions

We envision a new paradigm of manufacturing of mechanisms. Fully working mechanisms could be fabricated in a single step without any requirement for post-manufacturing assembly. By replacing the traditional manufacturing process with AM, robust assemblies could be produced on-demand and *in situ*, thereby eliminating several logistic problems. Customized devices could be produced for any kind of engineering applications. For example, patient-specific surgical instruments could be fabricated as a disposable medical devices while prosthetics and orthotics may be produced in different settings without the need for a well-equipped workshop or laboratory.

Current technologies, however, lack sufficient versatility for fabrication of fully-assembled and multi-articulated complex mechanisms. Accurate joint clearances with satisfactory surface roughness are still difficult to achieve, encased complex features require purge channels or elaborated strategies for support removal, available materials are still limited and lack sufficient mechanical performance and embedding techniques require complex and demanding processing steps. Yet, clever use of multi-material AM techniques could combine rigid and soft materials to create both structural parts and compliant joints. Multi-material AM requires compatibility of building substances and their corresponding printing processes, thus limiting the range of suitable materials that can be combined in a single printing job. However, clear examples of dual deposition of polymers with rigid and soft characteristics into mechanical parts have been demonstrated using MJ based technologies. Due to the physics of material deposition into the building platform by processes like MJ or Material Extrusion, multi-material AM is accomplished by adding multiple nozzles, as found in commercially available equipment, loaded with materials capable of compatible bonding [78]. Other than materials used for the PolyJet (Stratasys) technology, no material combinations suitable for multi-material AM have achieved desired mechanical behavior for both structural and compliant parts. Bonding of rigid and soft materials with sufficient position accuracy is a main concern that should be addressed in order to expand the range of compliant and rigid non-assembly constructs achieved

by multi-material AM. Other processes, such as SL or SLS, require more elaborated techniques and present a limited variety of compatible materials. Therefore, they have never been used to fabricate either compliant or rigid-body assemblies with multi-material AM. Essentially dissimilar materials like polymers and metals could be processed in a single printing job by using hybrid 3D-printing in where different AM and conventional manufacturing techniques can be combined [12]. Depending on the ultimate use, correct design of compliant joints could smartly replace traditional joints, eliminating the tight tolerance requirements. Certainly, further development on the field of design for additive manufacturing could set the stage for increasing the complexity achievable in non-assembly fabrication [79, 80].

New emerging research fields that may be potentially embraced by this non-assembly fabrication framework contemplate direct deposition of smart materials into structural parts [51], self-assembly of components using bonding forces [81], shape-shifting of 2D structures into 3D structures, as in origami where sheets of paper fold into 3D figures [82], and control of mechanical properties in localized areas of monolithic structures via meta-material design [83].

2.8 Conclusion

There is no doubt that the progress in AM has allowed for considerable design freedom and is a promising opportunity for the development of non-assembly fabrication. Still, AM is several steps away from replacing current assembly lines of traditional manufacturing. Assemblies produced in a single step by AM exhibit different shortcomings depending on the process employed. In general, important shortcomings found in current non-assembly mechanisms produced by AM are backlash, poor surface quality, weak mechanical properties (fatigue life, strength, toughness, etc.), and stuck support or/and residual material. Amongst all the limitations of manufacturing with AM, the need for overhang structures, limited range of building materials, inadequate fabrication accuracy stand out as the major drawbacks and are critical for further development of high-complexity fabrication of assemblies in a single step.

AM, nevertheless, has some unique characteristics that could potentially shift the current manufacturing practices to non-assembly paradigms. Given that AM processes parts could be used to fabricate shapes that would be impossible to manufacture with other manufacturing techniques, new design approaches could be used, leading to availability of parts that achieve equal or even higher performance than traditionally-assembled mechanisms. Alternative designs of monolithic compliant mechanisms that could replace traditional rigid-body joints is just one such example. Further development of the materials that could be processed with AM may also improve the mechanical properties of parts and establish new damage-free pathways to remove support structures. New emerging techniques for AM, like meta-material design, could also be introduced to facilitate non-assembly fabrication of high complexity parts and should be further implemented to recognize their full potential.

2.9 References

[1] C. Mavroidis, K.J. DeLaurentis, J. Won, M. Alam, Fabrication of Non-Assembly Mechanisms and Robotic Systems Using Rapid Prototyping, Journal of Mechanical Design 123(4) (2000) 516-524.

[2] I. Gibson, D.W. Rosen, B. Stucker, Introduction and Basic Principles, Additive Manufacturing Technologies, Springer US2010, pp. 20-35.

[3] Y. Yang, X. Su, D. Wang, Y. Chen, Rapid fabrication of metallic mechanism joints by selective laser melting, Proc. Inst. Mech. Eng. Pt. B: J. Eng. Manuf. 225(12) (2011) 2249-2256.

[4] J. Calì, D.A. Calian, C. Amati, R. Kleinberger, A. Steed, J. Kautz, T. Weyrich, 3D-printing of Non-assembly, Articulated Models, ACM Trans. Graph. 31(6) (2012) 130:1-130:8.

[5] K.J. De Laurentis, F.F. Kong, C. Mavroidis, Procedure for Rapid Fabrication of Non-Assembly Mechanisms With Embedded Components, (2002) 1239-1245.

[6] F. Calignano, D. Manfredi, E.P. Ambrosio, S. Biamino, M. Pavese, P. Fino, 24th CIRP Design ConferenceDirect Fabrication of Joints based on Direct Metal Laser Sintering in Aluminum and Titanium Alloys, Procedia CIRP 21 (2014) 129-132.

[7] Y. Chen, J. Lu, Minimise joint clearance in rapid fabrication of non-assembly mechanisms, International Journal of Computer Integrated Manufacturing 24(8) (2011) 726-734.
[8] X. Su, Y. Yang, D. Wang, Y. Chen, Digital assembly and direct fabrication of mechanism based on selective laser melting, Rapid Prototyping Journal 19(3) (2013) 166-172.
[9] R. MacCurdy, R. Katzschmann, Y. Kim, D. Rus, Printable hydraulics: A method for fabricating robots by 3D co-printing solids and liquids, 2016 IEEE International Conference on Robotics and Automation (ICRA), IEEE, 2016, pp. 3878-3885.
[10] B.N. Peele, T.J. Wallin, H. Zhao, R.F. Shepherd, 3D printing antagonistic systems of artificial muscle using projection stereolithography, Bioinspiration & Biomimetics 10(5) (2015) 055003.
[11] Y. Wei, Y. Chen, Y. Yang, Y. Li, Novel Design and 3-D Printing of Nonassembly Controllable Pneumatic Robots, IEEE/ASME Transactions on Mechatronics 21(2) (2016) 649-659.
[12] E. MacDonald, R. Wicker, Multiprocess 3D printing for increasing component functionality, Science 353(6307) (2016).
[13] E. Aguilera, J. Ramos, D. Espalin, F. Cedillos, D. Muse, R. Wicker, E. MacDonald, 3D Printing of Electro Mechanical Systems, Solid Freeform Fabrication Symposium Proceedings, 2013, pp. 950–961.
[14] J. Stiltner, A.M. Elliott, C.B. Williams, A method for creating actuated joints via fiber embedding in a polyjet 3D printing process, 22nd Annual International Solid Freeform Fabrication Symposium - An Additive Manufacturing Conference, SFF 2011, 2011, pp. 583-592.
[15] J. O'Donnell, M. Kim, H.-S. Yoon, A Review on Electromechanical Devices Fabricated by Additive Manufacturing, Journal of Manufacturing Science and Engineering 139(1) (2016) 010801.
[16] M. Vaezi, H. Seitz, S. Yang, A review on 3D micro-additive manufacturing technologies, The International Journal of Advanced Manufacturing Technology 67(5-8) (2012) 1721-1754.
[17] A. International, Standard terminology for additive manufacturing technologies: designation F2792 - 12a, ASTM International, West Conshohocken, PA, 2012.
[18] C.W. Hull, Apparatus for production of three-dimensional objects by stereolithography, Uvp, Inc., 1986.

[19] C.R. Deckard, Method and apparatus for producing parts by selective sintering, Board Of Regents, The University Of Texas System, 1989.
[20] T.H.C. Childs, C. Hauser, M. Badrossamay, Selective laser sintering (melting) of stainless and tool steel powders: Experiments and modelling, Proc. Inst. Mech. Eng. Pt. B: J. Eng. Manuf. 219(4) (2005) 339-357.
[21] S.S. Crump, Apparatus and method for creating three-dimensional objects, 1993.
[22] Z. Zagagi, H. Gothait, G. Miller, Method for building a three dimensional object, Objet Geometries Ltd., 2010.
[23] E.M. Sachs, J.S. Haggerty, M.J. Cima, P.A. Williams, Three-dimensional printing techniques, Massachusetts Institute Of Technology, 1994.
[24] T. Himmer, T. Nakagawa, M. Anzai, Lamination of metal sheets, Computers in Industry 39(1) (1999) 27-33.
[25] G.K. Lewis, R. Nemec, J. Milewski, D.J. Thoma, D. Cremers, M. Barbe, Directed Light Fabrication, Los Alamos National Lab., NM (United States), 1994.
[26] F. Jelínek, E.A. Arkenbout, P.W.J. Henselmans, R. Pessers, P. Breedveld, Classification of Joints Used in Steerable Instruments for Minimally Invasive Surgery—A Review of the State of the Art, J. Med. Device. 9(1) (2015) 010801-010801.
[27] X. Su, Y. Yang, D. Xiao, Y. Chen, Processability investigatation of non-assembly mechanisms for powder bed fusion process, The International Journal of Advanced Manufacturing Technology 64(5-8) (2012) 1193-1200.
[28] Y. Yang, Z. Luo, X. Su, D. Wang, Study on process and effective factors of stainless steel thin-wall parts manufactured by selective laser melting, Zhongguo Jiguang/Chinese Journal of Lasers 38(1) (2011).
[29] C. Song, Y. Yang, Z. Xiao, D. Wang, Y. Liu, R. Liu, Design and direct manufacture of non-assembly abacus by Selective Laser Melting, International Symposium on Optoelectronic Technology and Application 2014: Laser Materials Processing; and Micro/Nano Technologies, Beijing, China, 2014, p. 929510.
[30] F. Calignano, D. Manfredi, E.P. Ambrosio, L. Iuliano, P. Fino, Influence of process parameters on surface roughness of aluminum parts produced by DMLS, The International Journal of Advanced Manufacturing Technology 67(9-12) (2012) 2743-2751.
[31] D. Manfredi, F. Calignano, M. Krishnan, R. Canali, E.P. Ambrosio, E. Atzeni, From Powders to Dense Metal Parts: Characterization of a Commercial AlSiMg

Alloy Processed through Direct Metal Laser Sintering, Materials 6(3) (2013) 856-869.
[32] Y. Chen, C. Zhezheng, Joint analysis in rapid fabrication of non-assembly mechanisms, Rapid Prototyping Journal 17(6) (2011) 408-417.
[33] X. Wei, Y. Tian, A. Joneja, A study on revolute joints in 3D-printed non-assembly mechanisms, Rapid Prototyping Journal 22(6) (2016) 901-933.
[34] C. Westbrook, How to design 3D printed pin hinges: No assembly required, 2016. http://support.ponoko.com/hc/en-us/articles/220290728-How-to-design-3D-printed-pin-hinges-No-assembly-required. (Accessed 06.07.2016.
[35] M.W.M. Groenewegen, M.E. Aguirre, J.L. Herder, Design Of a partially compliant, three-phalanx underactuated prosthetic finger, Proceedings of the ASME Design Engineering Technical Conference, 2015.
[36] R. Mutlu, G. Alici, M.I.H. Panhuis, G. Spinks, Effect of flexure hinge type on a 3D printed fully compliant prosthetic finger, IEEE/ASME International Conference on Advanced Intelligent Mechatronics, AIM, 2015, pp. 790-795.
[37] S. Hill, S. Canfield, An Assessment of Fused Deposition Modeling for the Manufacturing of Flexural Pivots in an Anthropomorphic Robotic Hand Design, Proceedings of the Asme International Design Engineering Technical Conferences and Computers and Information in Engineering Conference, 2016, Vol 5b (2016).
[38] S.B. Ge, X.C. Duan, P. Li, T. Zheng, A compliant translational joint based force/displacement integrated sensor, Fifth Asia International Symposium on Mechatronics (AISM 2015), 2015, pp. 1-6.
[39] J.A. Mirth, An examination of trispiral hinges suitable for use in ABS-based rapid prototyping of compliant mechanisms, Proceedings of the ASME Design Engineering Technical Conference, 2014.
[40] Y. Tummala, M.I. Frecker, A.A. Wissa, J.E.H. Jr, Design optimization of a twist compliant mechanism with nonlinear stiffness, Smart Materials and Structures 23(10) (2014) 104010.
[41] E.G. Merriam, L.L. Howell, Lattice flexures: Geometries for stiffness reduction of blade flexures, Precision Engineering 45 (2016) 160-167.
[42] A. Bruyas, F. Geiskopf, P. Renaud, Towards statically balanced compliant joints using multimaterial 3D printing, Proceedings of the ASME Design Engineering Technical Conference, 2014.
[43] A.T. Gaynor, N.A. Meisel, C.B. Williams, J.K. Guest, Multiple-Material Topology Optimization of Compliant Mechanisms Created Via PolyJet Three-

Dimensional Printing, Journal of Manufacturing Science and Engineering-Transactions of the Asme 136(6) (2014) 061015.
[44] J.A. Mirth, Preliminary Investigations Into the Design and Manufacturing of Fully Compliant Layered Mechanisms (FCLMs), ASME 2013 International Design Engineering Technical Conferences and Computers and Information in Engineering Conference, Portland, Oregon, USA, 2013, p. V06AT07A017.
[45] D. Rus, M.T. Tolley, Design, fabrication and control of soft robots, Nature 521(7553) (2015) 467-475.
[46] D. Trivedi, C.D. Rahn, W.M. Kier, I.D. Walker, Soft Robotics: Biological Inspiration, State of the Art, and Future Research, Applied Bionics and Biomechanics 5(3) (2008) 99-117.
[47] K.-J. Cho, J.-S. Koh, S. Kim, W.-S. Chu, Y. Hong, S.-H. Ahn, Review of manufacturing processes for soft biomimetic robots, International Journal of Precision Engineering and Manufacturing 10(3) (2009) 171.
[48] H. Lipson, Challenges and Opportunities for Design, Simulation, and Fabrication of Soft Robots, Soft Robotics 1(1) (2013) 21-27.
[49] A. Rost, S. Schädle, The SLS-Generated Soft Robotic Hand - An Integrated Approach Using Additive Manufacturing and Reinforcement Learning, 2013 12th International Conference on Machine Learning and Applications (ICMLA), 2013, pp. 215-220.
[50] T. Umedachi, B.A. Trimmer, Design of a 3D-printed soft robot with posture and steering control, 2014 IEEE International Conference on Robotics and Automation (ICRA), 2014, pp. 2874-2879.
[51] A. Zolfagharian, A.Z. Kouzani, S.Y. Khoo, A.A.A. Moghadam, I. Gibson, A. Kaynak, Evolution of 3D printed soft actuators, Sensors and Actuators A: Physical 250 (2016) 258-272.
[52] R. Merz, F.B. Prinz, K. Ramaswami, M. Terk, L.E. Weiss, Shape Deposition Manufacturing, Proceedings of the Solid Freeform Fabrication Symposium, The University of Texas at Austin (1994).
[53] S.A. Bailey, J.G. Cham, M.R. Cutkosky, R.J. Full, Biomimetic Robotic Mechanisms via Shape Deposition Manufacturing, Robotics Research—International Symposium 9 (2000) 403-410.
[54] J.G. Cham, S.A. Bailey, J.E. Clark, R.J. Full, M.R. Cutkosky, Fast and robust: Hexapedal robots via shape deposition manufacturing, Int J Robot Res 21(10-11) (2002) 869-882.
[55] M. Hatanaka, M.R. Cutkosky, Process Planning for Embedding Flexible Materials in Multi-Material Prototypes, (2003) 325-333.

[56] A.M. Dollar, R.D. Howe, A robust compliant grasper via shape deposition manufacturing, IEEE/ASME Transactions on Mechatronics 11(2) (2006) 154-161.
[57] X. Li, J. Johnsen, J. Groza, F. Prinz, Processing and microstructures of fiber Bragg grating sensors embedded in stainless steel, Metallurgical and Materials Transactions A: Physical Metallurgy and Materials Science 33(9) (2002) 3019-3024.
[58] X. Li, F. Prinz, Embedded fiber Bragg grating sensors in polymer structures fabricated by layered manufacturing, Journal of Manufacturing Processes 5(1) (2003) 78-86.
[59] X.C. Li, A. Golnas, F. Prinz, Shape deposition manufacturing of smart metallic structures with embedded sensors, Proceedings of SPIE - The International Society for Optical Engineering 3986 (2000) 160-171.
[60] L.U. Odhner, L.P. Jentoft, M.R. Claffee, N. Corson, Y. Tenzer, R.R. Ma, M. Buehler, R. Kohout, R.D. Howe, A.M. Dollar, A compliant, underactuated hand for robust manipulation, Int J Robot Res 33(5) (2014) 736-752.
[61] R.R. Ma, J.T. Belter, A.M. Dollar, Hybrid Deposition Manufacturing: Design Strategies for Multimaterial Mechanisms Via Three-Dimensional Printing and Material Deposition, Journal of Mechanisms and Robotics 7(2) (2015) 021002-021002.
[62] H. Denham, G. George, L. Rintoul, P. Calvert, Fabrication of polymers and composites containing embedded sensors, Proceedings of SPIE - The International Society for Optical Engineering, 1996, pp. 742-747.
[63] A. Kataria, D.W. Rosen, Building around inserts: Methods for fabricating complex devices in stereolithography, Rapid Prototyping Journal 7(5) (2001) 253-261.
[64] K.J. De Laurentis, C. Mavroidis, Rapid fabrication of a non-assembly robotic hand with embedded components, Assembly Automation 24(4) (2004) 394-405.
[65] Y.S. Liao, H.C. Li, M.T. Chen, The study of rapid prototyping process with embedded functional inserts, Journal of Materials Processing Technology 192–193 (2007) 68-74.
[66] A.J. Lopes, E. MacDonald, R.B. Wicker, Integrating stereolithography and direct print technologies for 3D structural electronics fabrication, Rapid Prototyping Journal 18(2) (2012) 129-143.
[67] E. Macdonald, R. Salas, D. Espalin, M. Perez, E. Aguilera, D. Muse, R.B. Wicker, 3D Printing for the Rapid Prototyping of Structural Electronics, Ieee Access 2 (2014) 234-242.

[68] R.B. Wicker, E.W. MacDonald, Multi-material, multi-technology stereolithography, Virtual and Physical Prototyping 7(3) (2012) 181-194.
[69] K. Willis, E. Brockmeyer, S. Hudson, I. Poupyrev, Printed Optics: 3D Printing of Embedded Optical Elements for Interactive Devices, ACM, 2012, pp. 589-598.
[70] N.A. Meisel, A.M. Elliott, C.B. Williams, A procedure for creating actuated joints via embedding shape memory alloys in PolyJet 3D printing, Journal of Intelligent Material Systems and Structures (2014) 1045389X14544144.
[71] C. Shemelya, F. Cedillos, E. Aguilera, D. Espalin, D. Muse, R. Wicker, E. MacDonald, Encapsulated Copper Wire and Copper Mesh Capacitive Sensing for 3-D Printing Applications, Ieee Sens J 15(2) (2015) 1280-1286.
[72] A. Wild, Integration of Functional Circuits into FDM Parts, Advanced Materials Research 1038 (2014) 29-33.
[73] D. Espalin, D.W. Muse, E. MacDonald, R.B. Wicker, 3D Printing multifunctionality: structures with electronics, The International Journal of Advanced Manufacturing Technology 72(5-8) (2014) 963-978.
[74] P.I. Deffenbaugh, T.M. Weller, K.H. Church, Fabrication and Microwave Characterization of 3-D Printed Transmission Lines, Ieee Microw Wirel Co 25(12) (2015) 823-825.
[75] A. Sachdeva, S. Singh, V.S. Sharma, Investigating surface roughness of parts produced by SLS process, The International Journal of Advanced Manufacturing Technology 64(9-12) (2012) 1505-1516.
[76] R. Mutlu, G. Alici, M. in het Panhuis, G.M. Spinks, 3D Printed Flexure Hinges for Soft Monolithic Prosthetic Fingers, Soft Robotics 3(3) (2016) 120-133.
[77] D.F. Machekposhti, N. Tolou, J.L. Herder, A Review on Compliant Joints and Rigid-Body Constant Velocity Universal Joints Toward the Design of Compliant Homokinetic Couplings, Journal of Mechanical Design 137(3) (2015) 032301.
[78] M. Vaezi, S. Chianrabutra, B. Mellor, S. Yang, Multiple material additive manufacturing – Part 1: a review, Virtual and Physical Prototyping 8(1) (2013) 19-50.
[79] W. Gao, Y. Zhang, D. Ramanujan, K. Ramani, Y. Chen, C.B. Williams, C.C.L. Wang, Y.C. Shin, S. Zhang, P.D. Zavattieri, The status, challenges, and future of additive manufacturing in engineering, Computer-Aided Design 69 (2015) 65-89.
[80] S. Yang, Y.F. Zhao, Additive manufacturing-enabled design theory and methodology: a critical review, International Journal of Advanced Manufacturing Technology 80(1-4) (2015) 327-342.

[81] N.B. Crane, J. Tuckerman, G.N. Nielson, Self-assembly in additive manufacturing: opportunities and obstacles, Rapid Prototyping Journal 17(3) (2011) 211-217.
[82] S. Janbaz, R. Hedayati, A.A. Zadpoor, Programming the shape-shifting of flat soft matter: from self-rolling/self-twisting materials to self-folding origami, Mater. Horiz. 3(6) (2016) 536-547.
[83] A. Ion, J. Frohnhofen, L. Wall, R. Kovacs, M. Alistar, J. Lindsay, P. Lopes, H.-T. Chen, P. Baudisch, Metamaterial Mechanisms, 29th Annual Symposium on User Interface Software and Technology. ACM, 2016, pp. 529-539.

Chapter 3: A review of the fatigue behavior of 3D printed polymers

Lauren Safai, Juan Sebastián Cuellar, Gerwin Smit, Amir A. Zadpoor

Published as:

A review of the fatigue behavior of 3D printed polymers. Addit Manuf 28 (2019) 87-97.

Abstract

As additive manufacturing of polymeric materials is becoming more prevalent throughout industry and research communities, it is important to ensure that 3D printed parts are able to withstand mechanical and environmental stresses that occur when in use, including the sub-critical cyclic loads that could result in fatigue crack propagation and material failure. There has so far been only limited research on the fatigue behavior of 3D printed polymers to determine which printing or material parameters result in the most favorable fatigue behavior. To better understand the effects of the printing technique, printing materials, and printing parameters on the fatigue behavior of 3D printed materials, we present here an overview of the data currently available in the literature including fatigue testing protocols and a quantitative analysis of the available fatigue data per type of the AM technology. The results of our literature review clearly show that, due to the synergism between printing parameters and the properties of the printed material, it is challenging to determine the best combination of variables for fatigue resistance. There is therefore a need for more experimental and computational fatigue studies to understand how the above-mentioned material and printing parameters affect the fatigue behavior.

3.1 Introduction

The use of additive manufacturing (AM), or 3D printing, has been increasing due to the growing interest from both industry and research communities [1]. As additive manufacturing technology improves, high quality prints can be produced quickly and inexpensively. With a wider range of polymer materials available, the development and fabrication of products are continuously changing with technological advancement and consumer use [1]. Innovators and inventors are now able to build prototypes or complex geometries efficiently at minimal costs with the reduction of production time from weeks to hours [2]. As a result of these improvements in AM, various industries such as biomedical [3-10], aerospace [11], apparel [12, 13], dentistry [14], automotive

[15], electronics [2, 16], and oceanography [17] are researching this technique to produce parts.

As additive manufacturing becomes more widely used, parts must withstand both mechanical and environmental stresses that occur during use. Understanding the required strengths for specific loading conditions is vital for any load-bearing applications [18, 19]. Since a material may fail due to fatigue conditions, it is also important to understand a material's resistance to cyclic loading and unloading [20]. Repetitive sub-critical loading of material may result in fatigue damage, *i.e.* a progressive accumulation and permanent structural change, which could lead to cracking or rupturing of the part after a certain number of cycles. Polymers are susceptible to fatigue at applied stresses below yield, which can cause microcracking and eventual failure [21]. Understanding the fatigue behavior of AM parts is therefore essential for predicting and preventing fatigue failure.

This paper will review current literature investigating the fatigue life of 3D printed polymers (Appendix A). The aim is to see if there are trends between experiments that provide insight into which printing parameters and material properties lead to the best fatigue life for 3D printed polymers.

3.2 Fatigue

As previously mentioned, fatigue is the development of structural damage as a result of repetitive loads (i.e. cyclic loading) that are less than ultimate tensile strength and possibly yield strength. Fatigue failure in polymers occurs in two ways [22, 23]: (1) thermal failure due to softening and melting from hysteretic heating, or (2) mechanical failure from crack initiation and propagation. As a result of high damping, viscoelasticity, and low thermal conductivity, high frequencies or strain rates cause hysteretic heating in thermal fatigue [24, 25]. The hysteretic energy is mainly dissipated as heat, which causes the specimen temperature to increase and the stiffness to decrease. Stiffness loss causes an increase in specimen deflection and deformation. From a macroscopic viewpoint, the process of fatigue failure in polymers resembles that of metals [26, 27]: it starts with initial microcracks on the surface or stress concentrator

that grow into macroscopic cracks and cause the final failure. Depending on the type of polymer, the crack may originate in different ways. In semi-crystalline polymers, for example, the crack is likely to initiate in spherulites. Once the crack growth enters the micro-structurally independent stage, the crack continues until the final rupture of the material [28, 29]. According to reference [30], thermal failure does not necessarily have a crack at failure, while mechanical failure is a result of physical separation.

3.3 Fatigue Testing

3.3.1 Objectives of fatigue testing

There are several objectives when fatigue testing: material type testing, structural type testing, and actual service type testing [31]. Material testing investigates the material response to repeated stresses, various environments, geometrical factors, or surface finishes. In structural testing, different materials or structural designs are tested to analyze stress concentrations, fatigue life, or fabrication processes. Finally, actual service type testing is used for reliability or quality verification.

3.3.2 Types of fatigue testing

Fatigue testing machines are classified based on the applied stress method. For axial loading, a uniform stress or strain is directly applied to the cross-section of the specimen in tension or compression. The specimen is held at both ends and loaded cyclically between minimum and maximum values. During repeated or reciprocating bending, one end of the specimen is fixed while a stress or strain is applied to the other end such that the specimen bends in the same plane. In rotating bending, the specimen is revolved at a constant frequency while a load is applied at two clamping points on the either side of the specimen. In every rotational cycle, the stresses change from compressive to tensile and from tensile to compressive, making sure that the specimen experiences the full cycle of flexural stresses. For fracture mechanical testing, a notch is made in the specimen to examine fracture initiation and propagation during cyclic loading.

In torsion fatigue, each end of the specimen is either clamped or twisted to specified values through a stress or strain. Other types of fatigue tests include combined bending and torsion fatigue and biaxial and triaxial fatigue, which are used in more complicated fatigue analyses [31, 32].

3.3.3 Stress amplitude in fatigue testing

The simplest stress sequence uses a constant stress amplitude where all load cycles, or cycles, are identical (Figure 3.1). For each cycle, σ is the alternating stress, σ_m is the mean stress, σ_{max} is the maximum stress, and σ_{min} is the minimum stress. Load cycles can be expressed as $\sigma_m \pm \sigma$, with compressive loads taken as negative. It follows that:

$$\sigma_{max} = \sigma_m + \sigma \quad (3.1)$$

$$\sigma_{min} = \sigma_m - \sigma \quad (3.2)$$

$$\sigma_m = \frac{\sigma_{min} + \sigma_{max}}{2} \quad (3.3)$$

For constant amplitude loading, the stress range, S, and stress ratio, R, are expressed as:

$$S = 2\sigma = \sigma_{max} - \sigma_{min} \quad (3.4)$$

$$R = \frac{\sigma_{min}}{\sigma_{max}} \quad (3.5)$$

Depending on stress level, constant amplitude loading can be classified into several different testing categories [31]. Routine tests are chosen so the specimen fails at a moderate number of cycles (i.e. 10^4-10^7). In short-life tests, applied stress is chosen to surpass yield stress so statistically some specimens fail at the application of the load, while in long-life tests, load is set to be just above or below the fatigue limit so some specimens do not fail after an assigned number of cycles. The aim of the long-life test is to examine the distribution of fatigue strength at a pre-assigned cycle number, which is beneficial for determining the fatigue limit.

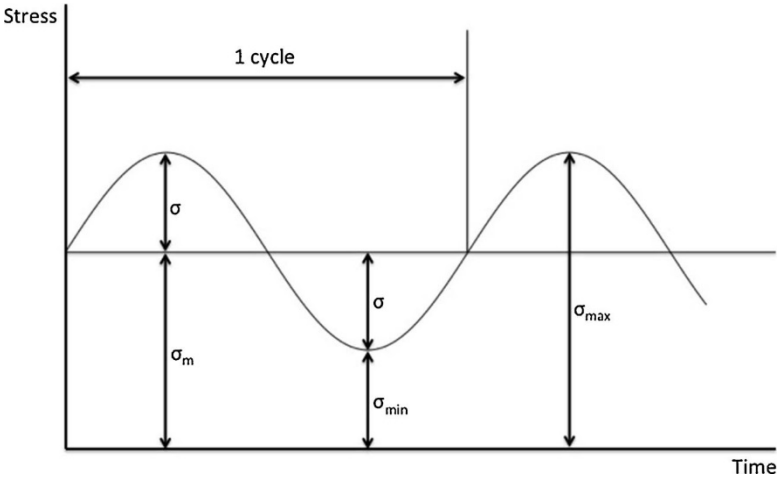

Figure 3.1: Nomenclature that describes testing parameters in constant amplitude loading.

In contrast to constant amplitude loading, variable amplitude loading (Figure 3.2) has complicated loading sequences that are more representative of what structures and components experience [28, 31]. Variable loading is used for cumulative damage analysis or the simulation of service life. Cumulative damage testing is performed at several stress levels with a simplified loading sequence, while service simulations have a more complicated loading pattern [31].

3.3.4 Stressing sources

In fatigue testing, force-controlled or displacement-controlled methods can be implemented, which is where a specific force or displacement is increased and decreased at a specified and controlled rate, respectively. Loads are produced by one of the following techniques: mechanical deflections, dead weights or constant springs, centrifugal forces, electromagnetic forces, hydraulic forces, or pneumatic forces. Load choice depends on factors such as frequency, control systems, required forces, costs, and simplifications of working loads [31].

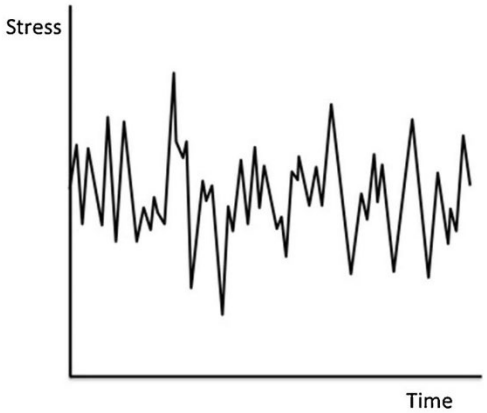

Figure 3.2: An example of a general variable amplitude loading.

3.3.5 Presentation of fatigue data

During fatigue testing, cyclic loads are applied with varied or constant stresses, which can be either positive or negative. A series of fatigue tests are conducted at several stress levels to create a stress-cycle plot or S-N curve, which is the conventional method of presenting fatigue behavior of polymers. Since current theories do not explain the mechanical behavior of polymers, empirical methods have been applied to analyze polymer fatigue [33]. S-N curves plot the stress endured against the number of cycles until failure. By lowering the stress value during testing, a fatigue limit can be established with the S-N curve, which is a value that does not result in failure and is sometimes referred to as fatigue limit, endurance limit, or fatigue strength [28]. The fatigue limit is affected by material surface conditions, such as roughness, damage, treatment, and residual stresses [28].

3.4 Fatigue testing machines and specimens

3.4.1 Components

Each fatigue-testing machine consists of the same basic structural components: (1) a load train that consists of a load-producing mechanism to generate the

desired load or displacement and a load-transmitting mechanism to produce the desired stress distribution; (2) controllers to set the upper and lower load limits and maintain the load throughout the test; (3) a counting and shut-off apparatus to stop the machine after failure or the pre-assigned number of cycles; and (4) a framework to support all of the necessary parts and reduce vibrations in the system [31, 32].

3.4.2 Specimens

Fatigue test specimens typically have three sections, including two grip ends and the test section [32]. The grips of the specimen are designed to transfer load from the test machine to the test section, and, depending on the test, may not be identical. Transitions between the grips and test section are designed with large radii so no stress concentrations build-up. The desired type of test and the objectives affect the design of the fatigue test specimen. Several fatigue test specimens are shown in Figure 3.3.

3.5 Fatigue testing of 3d printed polymers

3.5.1 Factors affecting fatigue characterization

Fatigue testing in 3D printed specimens is challenging due to the anisotropic properties and residual stresses that result from layer deposition [19]. Different variables associated with each type of printing technique affect the mechanical characterization of the specimens. The variables for extrusion-based printing include: raster orientation, build orientation, layer height and bead width, and air gap between filaments [19, 34-37]. The mechanical properties of powder bed fusion-based specimens are affected by the laser power, scan length, layer height, build orientation, recycled powder content, powder bed temperature, and crystallization temperature [19, 38]. Parts printed with material jetting techniques are affected by the presence of additives, unknown manufacturer resin formulations, printed on an over-cured surface, and the physics and chemistry of polymer fusion [19]. Due to the synergism between these variables, fatigue is challenging to predict. All of these variables influence the

microstructure of the part that, in turn, may significantly affect the mechanical behavior and failure mechanism. There was no literature regarding the fatigue testing of polymers fabricated using other categories of 3D printing techniques.

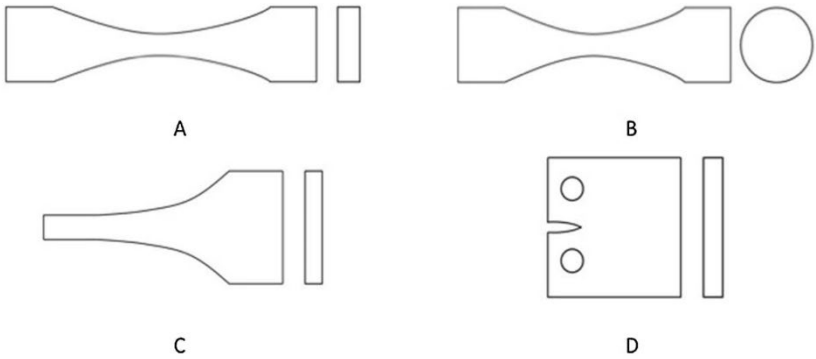

Figure 3.3: Four examples of fatigue testing specimens that include A) an axial loading specimen, B) a rotating bending specimen, C) a reverse bending specimen, and D) a fracture mechanical test specimen.

3.5.2 Standardization of fatigue testing

The American Society for Testing and Materials (ASTM) and the International Standards Organization (ISO) are two institutes that address the standardization of mechanical testing of AM specimens [19]. Currently, there is limited standardization in terms of the fatigue testing of 3D printed polymers.

With no ISO equivalent, the ASTM D7774 standard addresses uniaxial fatigue in tension or compression [39]. While it is recommended to test below a frequency of 5 Hz to reduce heat generation, specimens can be cycled between 1-25 Hz. The fatigue limit is defined when the specimen fails or reaches 10^7 cycles. Stress or strain is applied so the material does not experience plastic behavior. In addition to the previous standard, ASTM D3479 investigates tension fatigue for polymer matrix composites for specific loading and environmental conditions [40].

Two standards, ASTM D7791 and ISO 13003, address flexural fatigue in plastics [41, 42]. Both standards have sinusoidal loading, but are technically

different. ASTM D7791 tests specimens using three- or four-point bending, while ISO 13003 is applicable to all testing methods. For ASTM D7791, cyclic loading alternates between positive and negative values so that *R* is -1 and the stress or strain remains within the elastic limit. The fatigue limit is characterized in the same fashion as the previous standard. In ISO 13003, fiber-reinforced plastic composites undergo cyclic loading at a constant amplitude and frequency at four different stress or strain levels. For displacement control, the termination of the test is characterized as reaching the cycle limit or the specimen stiffness is reduced by 20%.

There are two standards, ASTM D6115 and ISO 15850, that address crack propagation (fatigue delamination) in the interlaminar region of a fiber composite [43, 44]. Since both standards are defined specifically for composites, it is unclear if 3D printed materials would fulfill the supporting assumptions. Finally, in order to perform statistical analyses of fatigue data, the standard ASTM E739 can be used [45].

3.6 Analysis of fatigue experiments

This section reviews the literature associated with the fatigue testing of 3D printed polymers, namely those printed using extrusion-based printing, selective laser sintering, and material jetting (*e.g.*, polyjet printing). The topics of interest include the effects of printing parameters, material properties, production methods, and geometric considerations on the fatigue life. Tables 3.1-3.3, following each section, summarize the experiments of each study and the conclusions drawn about fatigue life.

3.6.1 Extrusion-based printing

Axial loading fatigue

Various printing parameters, such as raster orientation, printing orientation, layer thickness, and feed rate, have been found to influence fatigue life of 3D printed parts. In several studies conducted by Ziemian et al., the effects of raster orientation were examined when printing with acrylonitrile butadiene styrene (ABS) [46-48]. In the first study [46], rectangular prism specimens

(190x12.7x2.6 mm^3) were printed with four raster orientations of 0° (Figure 3.4A), 45° (Figure 3.4C), 90° (Figure 3.4B), and 45°/45° (Figure 3.4D). The results indicated that the 45°/45° raster orientation has the best fatigue life. In the subsequent studies [47, 48], ASTM D638 dog bone specimens were printed with raster orientations of 0° (Figure 3.4A), 45° (Figure 3.4C), 90° (Figure 3.4B), 45°/45° (Figure 3.4D), 30°/60°, 15°/75°, and 0°/90° (for conventions used in defining raster orientations, see Figure 3.4) [49]. In accordance with the first study, the 45°/45° raster orientation exhibited the best performance (Figure 3.6).

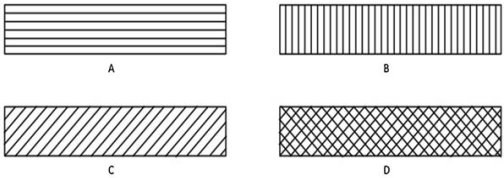

Figure 3.4: Four different raster orientations of A) 0°, B) 90°, C) 45°, and D) 45°/45°.

Both [50] and [51] investigated the effects of raster orientation, but in polylactic acid (PLA) specimens according to references [41] and [49], respectively. Three raster orientations of 0° (Figure 3.4A), 45° (Figure 3.4C), and 90° (for conventions used in defining raster orientations, see Figure 3.4) (Figure 3.4B) were cyclically loaded at 2 Hz in [50] and 1 Hz in reference [51]. Both studies had similar results, where the 45° orientation had the best fatigue life. In a different study [52], the effects of printing orientation on fatigue life in ABS and ABS*plus* specimens [53] were investigated. Nine specimens were printed in varying directions, where each print orientation dictated the raster orientation used by the printer (Figure 3.5). It was found that printing the specimen in the Flat-x (Figure 3.5) direction had the best fatigue life. In Figure 3.6, the S-N curves for the best results from [47, 50-52] are presented. From the curves, it can be concluded that ABS*plus* had better fatigue resistance than ABS since, at each stress level, the ABS*plus* material had a larger number of cycles. Comparing ABS and PLA, it was inconclusive which material had the better

fatigue life, since the PLA and ABS curves between studies provided conflicting results. Finally, in a cumulative study, reference [54] explored which printing parameter (layer thickness, extruder width, print orientation, feed rate) has the most influence on the fatigue life. Rectangular prisms (150x20x3 mm) of ABS were tested with 0.2 or 0.3 mm layer thickness, 0.35 or 0.45 mm extruder width, Flat-x or Flat-y (Figure 3.5) print orientation, and 2000 or 4000 mm/min feed rate. It was found that printing in the Flat-x direction and using a smaller layer height resulted in the best fatigue life. For feed rate and extruder width, while it appeared that smaller values resulted in better fatigue life, neither parameter had a significant impact on fatigue life. Printing parameters were found to have a substantial impact on the fatigue life in polymers.

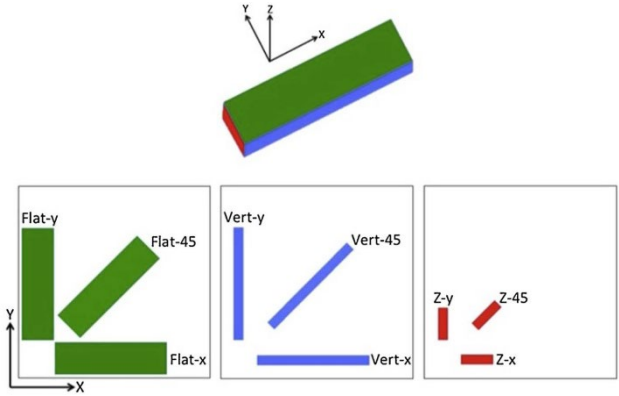

Figure 3.5: An arbitrary geometry that shows the notation of the nine different printing orientations on an XYZ stage.

Material properties and production methods, such as fabrication with injection molding or 3D printing and surface treatments, were investigated to see how fatigue life was affected. Both [55] and [56] studied and compared the fatigue lives of injection molded and 3D printed specimens [49] of ABS and polycarbonate urethane (75A, 85A, and 95A), respectively. In conflicting results, [55] found that the 3D printed specimens had worse fatigue life, while [56] found that 3D printed parts had a better fatigue life (Figure 3.7 and 3.8). From

Figures 3.7 and 3.8, it can be seen that the ABS injected molded specimens had the best fatigue life, but the injection molded polycarbonate specimens had a slightly worse fatigue life when compared with their 3D printed counterparts. In the case of polycarbonate urethane, the authors argued that the high temperature and cooling process of the 3D printing process may have affected the internal structures of the samples, thereby increasing its capacity to experience strain crystallization. This would lead to less strain hardening effects and could explain the small improvements in the fatigue behavior of 3D printed specimens. Overall, it was unclear whether or not injection molding had better fatigue resistance than 3D printing, since each study drew a different conclusion. Aside from comparing injection molding and 3D printing, reference [57] examined the differences in chemically post-treated and non-treated specimens from the commercially available polymer Ultem 9085. Ultem 9085 is manufactured by Stratasys, and is a high-performance thermoplastic composed of a polyetherimide and polycarbonate copolymer blend (Stratasys Ltd., Minnesota, USA). The results indicated that surface treatment did not have an effect on fatigue life.

Finally, the effects of topological design on the fatigue behavior of 3D printed porous scaffolds have been investigated in a few studies. In one of these studies [58], the effects of pore geometry and notch shape on the fatigue life in polycarbonate urethane (95A) and polyurethane 68A (EPU40) dog bone specimens was investigated, while another study [59] examined the effects of scaffold geometry in PLA. The test results from [58] indicated that pore geometry influenced fatigue life, with circular pore geometry and a circular notch shape having the best performance. In accordance with [58, 59], [61] also found that pore geometry affected fatigue life with a greater influence at high cycles. As well, for a crosshatch pattern, line spacing had a negligible effect on fatigue life.

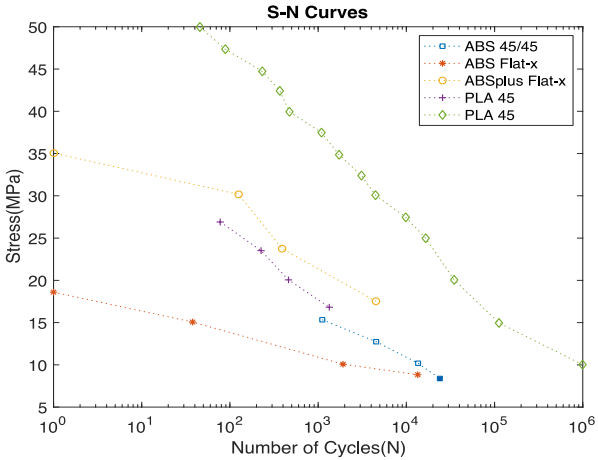

Figure 3.6: The S-N curves of the best raster and printing orientation experiments that used dog bone specimens during uniaxial loading. The blue square is the best raster orientation at 45°/45° for ABS specimens [49]. The red star and yellow circle lines are the best printing orientation, flat-x, for ABS and ABSplus, respectively [54]. The purple cross and green diamond lines are the best raster orientation at 45° for PLA specimens, from [53] and [52], respectively. Solid color points represent run-out data (For interpretation of the references to colour in this figure legend, the reader is referred to the web version of this article).

Rotating bending fatigue

The influence of four different printing parameters, *i.e.* layer height (0.1, 0.2, 0.3 mm), fill density (25, 50, 75 %), nozzle diameter (0.3, 0.4, 0.5 mm), and printing velocity (25, 30, 35 mm/min), were examined in [60] for two different infill patterns, *i.e.* rectilinear and honeycomb, in cylindrical, PLA test specimens. Fill density was found to have the most impact on fatigue life, while the effects of the layer height and nozzle diameter were dependent on the infill pattern, and velocity did not have a significant impact on fatigue. According to the authors, certain values of the layer height and nozzle diameter lead to an insufficient cohesion between layers, resulting in a reduced fatigue life. The influence of density was not linear between the three values, with the jump

from 50 to 75% density having a larger impact. The best combination of parameters was 75% density, 0.5 mm nozzle diameter, 0.3 mm layer height, and a honeycomb infill.

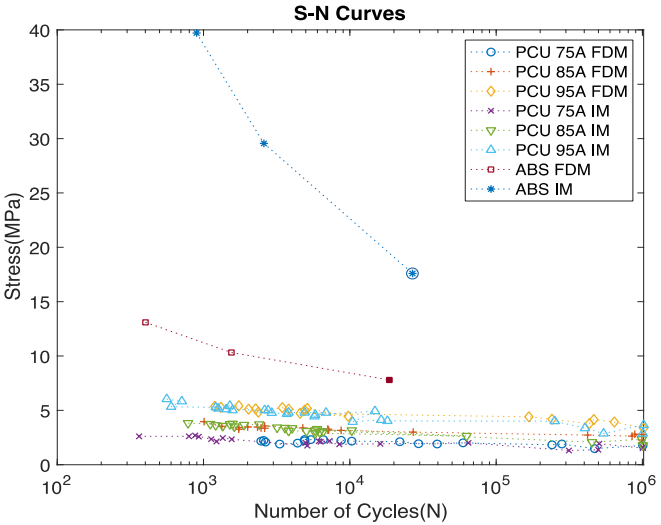

Figure 3.7: The S-N curves of the results from [57] and [58] using dog bone specimens made of ABS or polycarbonate urethane, respectively. The blue star and red square curves are the ABS specimens fabricated with 3D printing and injection molding (IM), respectively. The remaining curves are the results of the polycarbonate urethane specimens made with 3D printing and injection molding, which are shown enlarged in the following figure. Solid color points and circled points represent run-out data (For interpretation of the references to colour in this figure legend, the reader is referred to the web version of this article).

Reference [61] examined the mechanical properties of how cylindrical ABS specimens failed during fatigue testing. Each test specimen broke at the smallest cross section with both static and fatigue fractures. As stress was increased, the amount of static fatigue also increased. ABS had better a fatigue life as compared with PLA in rotating bending fatigue (Figure 3.9), since at

higher stress levels, the ABS specimens were able to last for a larger number of cycles.

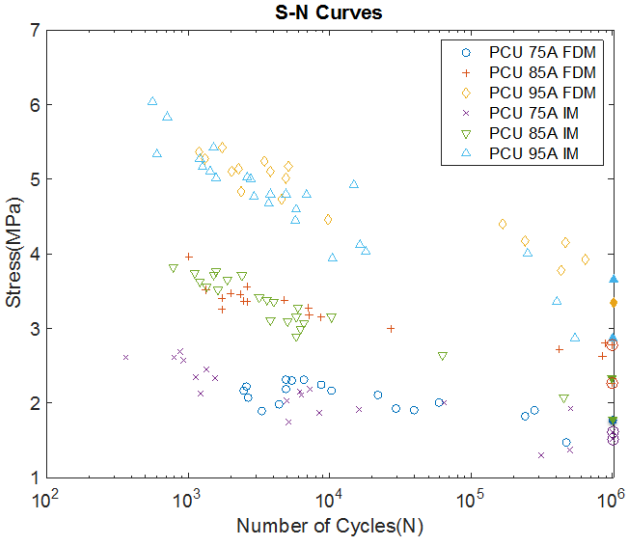

Figure 3.8: The S-N curves of the polycarbonate urethane 3D printed and injection molded (IM) specimens for [58]. The specimens were printed in three different types of polycarbonate urethane, 75 A, 85 A, and 95 A. The blue circle, red cross, and yellow diamond are the curves of the 3D printed specimens made with 75 A, 85 A, and 95 A, respectively. The purple cross, downward green triangle, and upward blue triangle are the injection molded specimens made of 75 A, 85 A, and 95 A, respectively. Solid color points and circled points represent run-out data (For interpretation of the references to colour in this figure legend, the reader is referred to the web version of this article).

Fracture mechanical fatigue

In reference [62], the effects of raster orientation on fatigue life in PLA compact tension specimens were examined. The specimens were printed in three different orientations with 0° (Figure 3.4A), 90° (Figure 3.4B), and 0°/90° (for conventions used in defining raster orientations, see Figure 3.4). The study concluded that raster orientation did not affect fatigue life, and that the fatigue

behavior was dominated by crack propagation at high loads, and crack initiation at low loads.

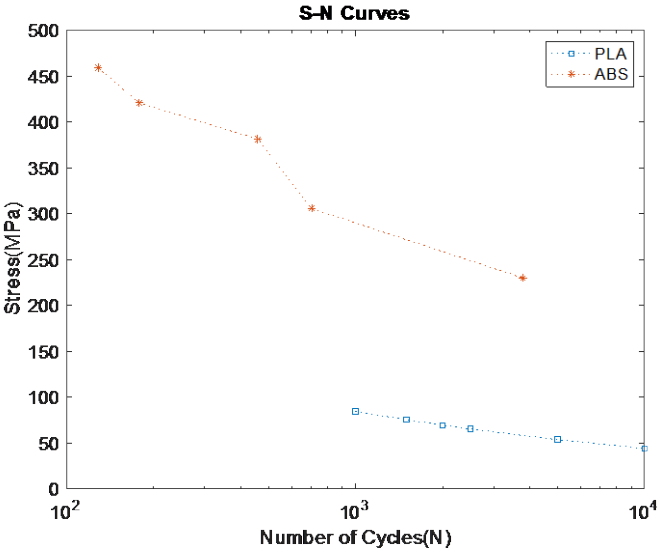

Figure 3.9: The S-N curves for the best combination of printing parameters from [62] for PLA hourglass and ABS hourglass specimens from [63]. The red star curve represents the ABS specimen, while the blue square represents the PLA specimen.

3.6.2 Selective laser sintering

Axial loading fatigue

Similar to extrusion-based printing, printing parameters, such as printing orientation, affect parts built using selective laser sintering. In one study [63], the effects of printing orientation on notched and un-notched Nylon-12 (PA12) hourglass specimens [64] were investigated. The results indicated that orientation does not affect the fatigue life, but that notched specimens had a longer fatigue life. This is a result of the reduced thermal load that the notched specimens experience, since a smaller volume is subjected to cyclic loading.

Table 3.1: A summary of fatigue testing parameters and results from the studies that used extrusion-based printing.

Testing Method	Material	Specimen Geometry	Results	Study
Tension-tension fatigue	ABS	Rectilinear Box	The 45°/45° fiber orientation had the best fatigue life	Ziemian et al. (2012)
Tension-tension fatigue	ABS	Dog Bone	The 45°/45° fiber orientation had the best fatigue life	Ziemian et al. (2015)
Tension-tension fatigue	ABS	Dog Bone	The 45°/45° fiber orientation had the best fatigue life	Ziemian et al. (2016)
Tension-tension fatigue	PLA	Dog Bone	Flat printing orientation at 45° had the best fatigue life	Afrose et al. (2015)
Tension-compression fatigue	PLA	Dog Bone	Flat printing orientation at 45° had the best fatigue endurance limit	Letcher and Waytashek (2014)
Tension-relaxation fatigue	ABS	Dog Bone	Flat printing orientation in X had the best fatigue life	Lee and Huang (2013)
Tension-tension fatigue	ABS	Rectilinear Box	Print orientation, layer thickness, and feed rate influenced fatigue life the most	Corbett et al. (2014)
Tension-tension fatigue	ABS	Dog Bone	3D-printed parts had worse fatigue life than injection molding	Padzi et al. (2017)
Tension-relaxation fatigue	Polycarbonate Urethane	Dog Bone	3D-printed parts had better fatigue life than injection molding	Miller et al. (2017a)
Tension-tension fatigue	Ultem 9085	Dog Bone	Surface treatment did not affect fatigue life	Fischer and Volker (2016)
Tension-relaxation fatigue	Polyurethane	Rectilinear Box	Circular pores had the best fatigue life	Miller et al. (2017b)
Compression Fatigue	PLA	Rectilinear Box	Circular pores had the best fatigue life	Gong et al. (2017)
Rotating Bending Fatigue	PLA	Hourglass	Fill density and layer height influenced fatigue life the most	Gomez-Gras et al. (2018)
Rotating Bending Fatigue	ABS	Hourglass	Cycling at higher stresses led to worse fatigue life	Zhang et al. (2017)
Fracture Mechanical Fatigue	PLA	Compact Tension	The 0°/90° fiber orientation had the best fatigue life	Arbeiter et al. (2018)

In addition to printing parameters, material properties, such as density, surface roughness, and printing with injection molding or 3D printing, also influence fatigue life. Studies conducted by [65] and [66] investigated the effects of density on the fatigue life. According to reference [65], there is no relationship between the fatigue life and density or surface roughness in the dog bone Nylon-12 (PA12), since different samples provided contrasting behaviors. In order to verify whether fabrication defects caused this, more testing was needed. However, [66] concluded that lower density PA12 hourglass specimens had a lower fatigue life (Figure 3.10). As seen from the curve, there was a positive relationship between the density and fatigue life. Aside from density, reference [67] studied the differences in the fatigue life between notched and un-notched injection molded and 3D printed PA12 parts [64], where the 3D printed parts were built in the Vert-x and Z-x directions (Figure 3.5).

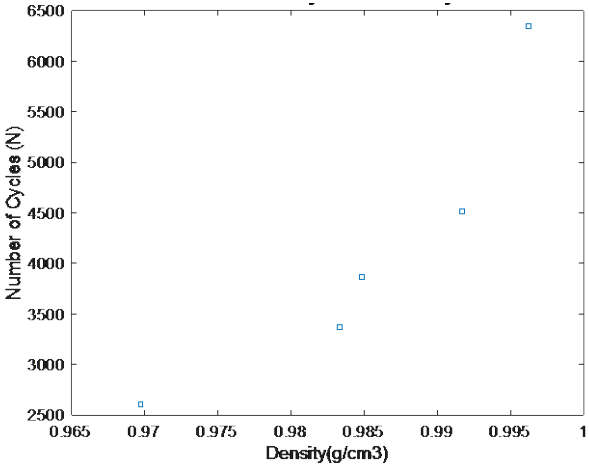

Figure 3.10. The results of [68], indicating that as part density increases so does the number of cycles that the specimen is able to withstand.

The results found that notched injection molded and 3D printed parts had similar fatigue lives (Figure 3.11). Moreover, there were no substantial differences in the fatigue life of the specimens printed in the Vert-x and Z-x directions when using SLS.

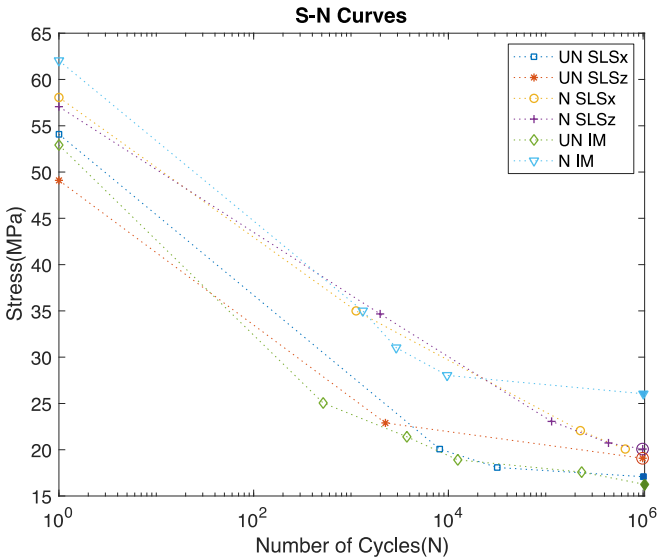

Figure 3.11: The S-N curves of the results from [69] using notched and un-notched hourglass specimens of PA12 fabricated using SLS or injection molding (IM). The blue square and red star curves are the SLS un-notched specimens fabricated in the Vert-x or Z-x directions, respectively. The yellow circle and purple cross are the SLS notched specimens fabricated in the Vert-x or Z-x directions, respectively. The green diamond and blue triangle are the un-notched and notched injection molded specimens. Solid color points and circled points represent run-out data (For interpretation of the references to colour in this figure legend, the reader is referred to the web version of this article).

In [68], the effects of geometry on the fatigue life was investigated by varying the section thickness (2, 4, and 6mm) in dog bone PA12 specimens under tension-tension and tension-compression uniaxial loading. In both cases, the fatigue life increased with the section thickness, but these results were not statistically significant for tension-tension loading. This may be due to temperature increasing more in smaller section thicknesses than in larger thicknesses.

Rotating bending fatigue

The effects of printing orientation was investigated in references [69] and [70] for PA12 hourglass specimens [71]. In reference [69], the specimens were printed in the direction of the X and Z-axes (Figure 3.5) and tested at two frequencies of 30 and 50 Hz. The results indicated that printing in the Z direction, though not significant, and testing at 50 Hz both reduced fatigue life (Figure 3.12). In reference [70], specimens for rotating bending [71] and reverse bending [72] were printed parallel to the Y and Z-axes (Figure 3.5). The results of both types of tests and orientations showed no significant differences, indicating isotropic behavior from the specimens (Figure 3.12). The curves seen in Figure 3.12 include both printing orientations that were tested.

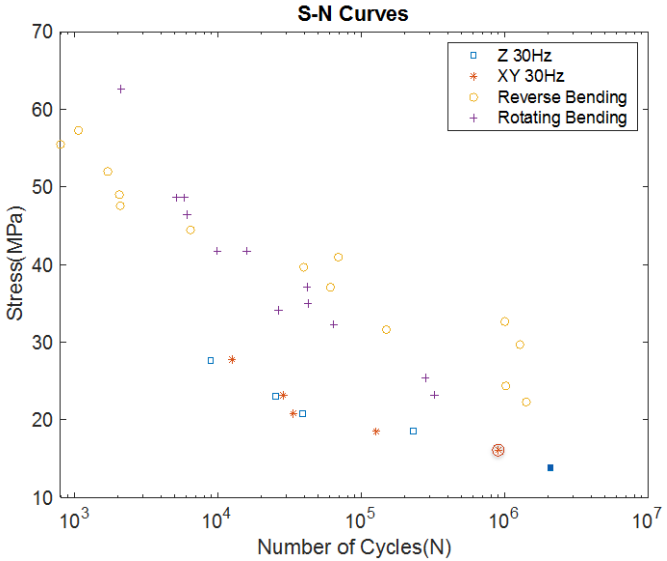

Figure 3.12: The S-N curves of the best results from [71] and [72] that each printed specimen made out of PA12. The blue square and red star are the curves for hourglass specimens that were printed along the z-axis and x-axis, respectively, and were tested at a frequency of 30 Hz. The yellow circle and purple cross curves represent specimens tested with reverse bending fatigue and rotating bending fatigue. Solid color points and circled points represent

run-out data (For interpretation of the references to colour in this figure legend, the reader is referred to the web version of this article).

Bending fatigue

In [73], two printing parameters, namely laser energy density and particle size, were varied to see their influence on the fatigue life of rectilinear boxes (35x5x1.4 mm^3) of polycaprolactone (PCL). The study found that a combination of smaller particles and large laser energy densities leads to a higher degree of sintering and improved fatigue life (Figure 3.13). The curve with the combination of small particles and a large energy density started off at a higher stress variation value, meaning that the specimen initially started off more rigid than the other specimens (Figure 3.13). This implies that a higher degree of sintering melted the particles together better, and, as a result, the fatigue life of the specimens was improved.

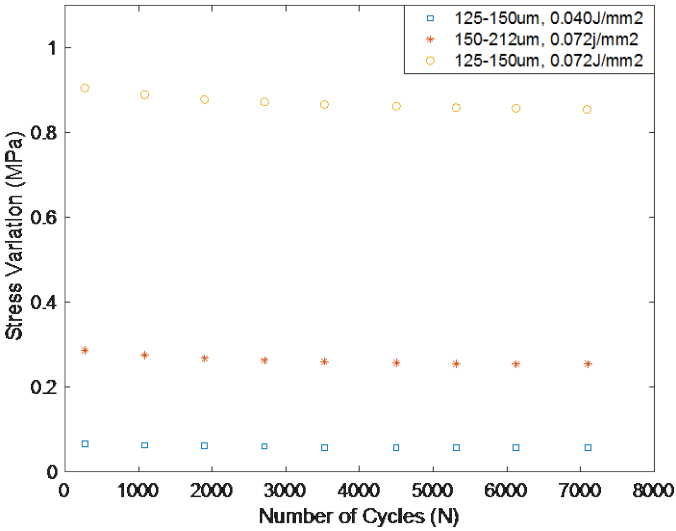

Figure 3.13: The results from [75] showing the stress variation vs. number of cycles for three different combinations of particle size and laser energy density. The smaller particles were between 125 and 150 µm, and the larger particles were between 150 and 212 µm. The smaller laser energy density was 0.040

J/mm2, while the larger energy density was 0.072 J/mm2. The blue squares had a combination of small particles and a large laser energy density, the red star curve had smaller particles and a smaller laser energy density, while the yellow circles had a combination of large particles with a large laser energy density.

The studies reported in [74] and [75], investigated how affinity between two particle types affected fatigue life. In the first study [74], rectilinear boxes (35x5x1.4 mm^3) were fabricated with a mixture of Polyamide 6 (PA6) and PA12. It was found that the 20/80 and 50/50 blends had the best fatigue life, but overall there was poor affinity between the two particles (Figure 3.14). Since the stress variation between the two particles was negative, it meant that the stiffness of the specimen was decreasing, leading to a poor fatigue life (Figure 3.14). Similarly, [75] fabricated rectilinear boxes of PA12 and BASF polybutylene terephthalate (PBT). The blend of 90/10 had the best fatigue life (Figure 3.14). The stress variation in the 90/10 blend stayed relatively constant, meaning that the specimen was neither hardening or softening under cyclic loading.

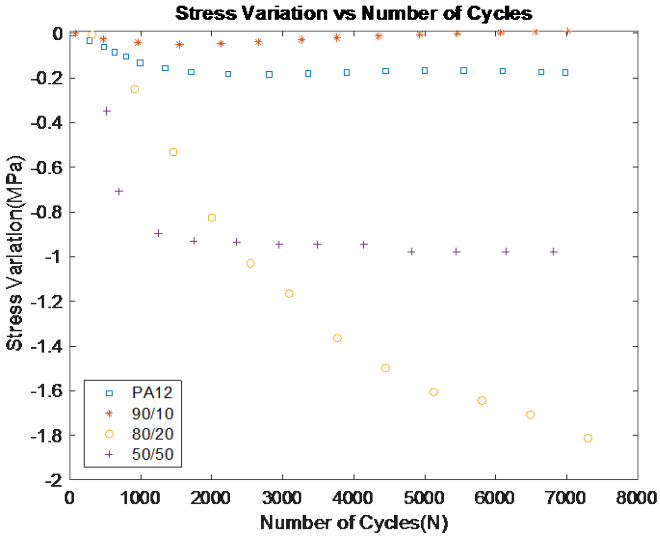

Figure 3.14: The results of the best combinations of powders from [76] and [77], showing stress variation vs. number of cycles. As a control, the curve with only PA12 is represented by blue squares. The combination of PA12/PBT at 90/10 is shown with the red stars. The yellow circle and purple cross curves are PA6/ PA12 blends of 80/20 and 50/50, respectively (For interpretation of the references to colour in this figure legend, the reader is referred to the web version of this article).

Fracture mechanical fatigue

Several studies investigated how different material properties affected fracture fatigue life by comparing 3D printed and injection-molded specimens, varying materials, and changing environments. In [76], compact tension specimens [77] made of PA12 were built with 3D printing and injection molding. The results found that the SLS parts had longer fatigue lives, with less deformation. In [78], compact tension specimens (50x48x10 mm^3), made of neat PA12 (PA12) and short glass fiber PA12 (PA12-f), were tested in a dry environment at 23 °C and -50 °C. At 23 °C, both materials had similar fatigue lives, but PA12-f had greatly improved fatigue life at -50 °C. In [79], compact tension specimens (50x48x10 mm^3) were fabricated of PA12 and PA11, a bio-based polymer, and tested in a dry environment at 23 °C, a dry environment at -50 °C, and a wet environment at 23 °C. Independent of the temperature and environment, PA11 showed improved fatigue crack propagation. Testing in water significantly reduced the fatigue life for both samples.

Table 3.2: A summary of fatigue testing parameters and results from the studies that used selective laser sintering.

Testing Method	Material	Specimen Geometry	Results	Study
Tension-compression fatigue	PA12	Hourglass	Orientation did not affect fatigue life, but notched specimens performed better than un-notched	Hooreweder and Kruth (2014)
Tension-tension fatigue Tension-compression fatigue	PA12	Dog Bone	Density and surface roughness did not affect fatigue life	Amel et al. (2014)
Tension-compression fatigue	PA12	Hourglass	Lower density samples led to more crack initiation	Hooreweder et al. (2010)
Tension-compression fatigue	PA12	Hourglass	3D-printed specimens had similar fatigue life to injection molded samples	Hooreweder et al. (2013)
Tension-tension fatigue Tension-compression fatigue	PA12	Dog Bone	Fatigue life increased with section thickness, and larger section thicknesses depended on density	Amel et al. (2016)
Rotating Bending Fatigue	PA12	Hourglass	Specimens had an endurance limit of 15 MPa	Munguia and Dalgarno (2014)
Rotating Bending Fatigue	PA12	Hourglass	Specimens showed isotropic material behavior	Munguia and Dalgarno (2015)
Bending Fatigue	PCL	Rectilinear Box	Smaller particles with a higher degree of sintering had better fatigue life	Salmoria et al. (2014)
Bending Fatigue	PA6/PA12	Rectilinear Box	There was poor affinity between PA6 and PA12	Salmoria et al. (2012)
Bending Fatigue	PA12/PBT	Rectilinear Box	The 90%/10% blend of PA12/PBT had the best fatigue life	Salmoria et al. (2018)
Fracture Mechanical Fatigue	PA12	Compact Tension	3D-printed specimens had a longer fatigue life than injection molded	Blattmeier et al. (2012)
Fracture Mechanical Fatigue	Neat PA12 and PA12-f	Rectilinear Box	PA12-f had better fatigue life at lower temperatures	Salazar et al. (2014a)
Fracture Mechanical Fatigue	PA12 and PA11	Rectilinear Box	Independent of environment and temperature, PA11 had better fatigue life than PA12	Salazar et al. (2014b)

3.6.3 Material jetting

Axial loading fatigue

In one study, [80], the effects of build orientation were investigated in parts printed with a material jetting printer. Veroclear 720 dog bone specimens [41] were fabricated parallel to the X and Y-axes (Figure 3.5), and cycled at 20 Hz. Veroclear 720 is a translucent, rigid acrylic-based photopolymer produced by Stratasys. The specimens that were fabricated parallel to the Y-axis (Figure 3.5) had better fatigue resistance, but more experimentation was required to have statistical validity.

Material properties, such as material interfaces and surface treatments, were investigated to see how they affect the fatigue life. In two studies reported in [81] and [82], dog bone specimens [83] were fabricated using TangoBlackPlus and VeroWhitePlus. The first study [81], examined the effects of no interface, a single interface, and a dual interface on the fatigue life. TangoBlackPlus is an elastomeric acrylic-based photopolymer fabricated by Stratasys. The results of the study indicated that interface specimens do not have a shorter fatigue life as compared with the pure material itself. In a continuation study [82], dual interface specimens were used to see how surface finish affects the fatigue life. It was found that smoother, “glossy” finish specimens had a longer fatigue life as compared to matte finish, though not statistically significant.

3.7 Discussion

3.7.1 Extrusion-based printing

Throughout the literature for fatigue of extrusion-based printing, it appeared that printing and material parameters all affect the fatigue life of specimens. Focusing on printing parameters, it was found that the raster orientation had the most influence on the fatigue life. All of the studies investigating raster orientation concurred that printing at 0° or 90° resulted in the worst fatigue life than printing at 45° or 45/45° (Figure 3.4A-D).

Table 3.3: A summary of fatigue testing parameters and results from the studies that used material jetting.

Testing Method	Material	Specimen Geometry	Results	Study
Tension-tension fatigue	Veroclear 720	Dog Bone	Build orientation affected fatigue life	Suresh et al. (2017)
Tension-relaxation fatigue	TangoBlackPlus	Dog Bone	Interface specimens had a higher fatigue life than no interface	Moore and Williams (2012)
Tension-relaxation fatigue	TangoBlackPlus	Dog Bone	"Glossy" finish specimens had a longer fatigue life than matte finish	Moore and Williams (2015)

One possibility as to why 45/45° had the best fatigue life is that in uniaxial loading shear tends to occur at an angle of 45°, but during loading it is constantly counteracted by the -45° configuration [47]. This development could delay or prevent a crack from fully propagating through the material. Another possibility is that as the specimens are cyclically loaded, the 45/45° configuration start to rotate into a 0/90° orientation, resulting in the structure being better aligned with the loading direction so strand strength becomes more prevalent [47]. Aside from raster orientation, other parameters such as the printing orientation, layer height, and infill all influence the fatigue life. Printing orientation determines the stress-carrying direction, layer height affects the cohesion between the layers, and infill affects the stiffness and density of the part, all of which impact how the material behaves during fatigue testing [60]. Due to the synergy between all of the parameters, it was challenging to characterize the best settings for maximizing the fatigue life. While the general consensus between studies was that printing with 45/45° (Figure 3.4D) results in the best fatigue life, the best settings for the remainder of the printing parameters remain inconclusive.

The material parameters did not seem to have as substantial of an influence as the printing parameters due to the inconclusive nature of the results. Examining whether or not injection molding or 3D printed parts had better fatigue life yielded two conflicting results. This may be due to the differing printing parameters chosen by each study, where changing printing parameters could generate a different outcome. Looking at the chosen materials throughout the literature seemed to be inconclusive as to whether ABS or PLA had the best fatigue resistance. This can be seen in Figures 3.6, 3.7, and 3.9, in which ABS specimens typically had the longest fatigue life, but there were also instances where PLA has the best fatigue resistance. This fluctuation in which material is better may be due to the different printing parameters each test has used, which affect the mechanical behavior of the specimen.

3.7.2 Selective laser sintering

As with extrusion-based printing, both printing parameters and material properties impacted the fatigue life of SLS parts. Looking at the printing parameters, several studies concluded that the printing orientation did not affect the fatigue life, since there was as an isotropic material response. This can been seen in Figures 3.11 and 3.12. This isotropic response may be due to the localized heating and deformation that cause a uniform microstructure at the eventual fracture site through *in situ* drawing and/or an annealing process [70]. Another printing parameter that affects fatigue is the laser energy density, which was tested in [73]. Laser energy density affects the mechanical properties, such as porosity and microstructure, of parts built using SLS. As the laser energy density is increased, the degree of sintering increases, which leads to a denser morphology in parts.

Unlike extrusion-based printing, the material properties seemed to have a larger impact on fatigue life of SLS polymers. Throughout the literature, there seemed to be a consensus in SLS parts that an increase in the density leads to better fatigue resistance. This can be seen in Figures 3.10 and 3.13. The density of the SLS parts influences the mechanical properties, and at lower densities, with more unfused powder particles, there is a higher chance of crack initiation [66]. Looking at the differences in the injection molded and 3D printed parts did not lead to a definitive conclusion of one method being better than the other, as seen in Figure 3.11. The fatigue lives of both parts were found to be similar, with neither one having significantly better fatigue resistance. The affinity of two powders was essential to the success of the part. As can be seen in Figure 3.14, when there is poor affinity between powders, the part begins to lose stiffness and fail sooner. Finally, the majority of the studies used PA12 due to its desirable mechanical properties. It is interesting to note that the PA12/PBT blend of 90/10 had a higher fatigue strength than pure PA12 due to the addition of 10% PBT, which leads to an increase in stiffness and resistance to plastic deformation.

3.7.3 Material jetting

Due to the limited number of studies on material jetting, only material properties were investigated. As previously mentioned, the studies found that interface specimens did not have shorter fatigue lives as compared with no interface specimens, and that although the 'glossy' surface had better fatigue resistance, it was not statistically relevant. This might be due to the lower roughness of the glossy surface as compared to the matt surface [84]. A lower roughness decreases the potential sites of crack initiation [86].

3.7.4 General remarks

As is clear from the previous chapters, there is no clear answer as to which 3D printing technique or set of printing parameters results in parts that are optimized for maximum fatigue performance. Many of the relevant parameters strongly depend on the 3D printing process and the polymer used. For every polymer, a set of specimens fabricated with different processing parameters should be tested for fatigue following experimental design techniques such as Taguchi that allow for fractional factorial designs [84]. Other optimization processes include the full factorial, gray relational, artificial neural network (ANN), fuzzy logic, genetic algorithm (GA), and response surface methodology (RSM) and have been used for different outputs like part strength, surface quality, dimension accuracy, etc. [85]. Most of these techniques have not been used for fatigue analyses but could also be considered. The slicing algorithm used is another parameter that has not been investigated thoroughly and could have a significant effect on the mechanical properties of the resulting parts.

3.8 Conclusion

In this literature review, the aim was to interpret all of the papers to see, whether there are trends in the data that could lead to conclusions about which printing parameters and material properties resulted in the best fatigue life. For extrusion-based printing, it was found that printing with a 45/45° raster orientation had the best fatigue life, while it was inconclusive as to if ABS or PLA was the most fatigue resistant material. The synergy between all of the printing

parameters such as printing orientation, raster orientation, layer height, and infill made it challenging to determine the best parameters. In selective laser sintering, the printing orientation did not have an impact on the fatigue life of the specimens, with the specimens showing isotropic behavior. Higher densities in the parts also led to better fatigue resistance. In both extrusion-based printing and selective laser sintering, there was not enough information to determine if 3D printing yielded better fatigue results as compared with injection molding. Due to the lack of testing of parts made by material jetting, no conclusions could be made. While some conclusions about the influence of the printing parameters and material properties were made, there still is a need for more fatigue testing of 3D printed polymers. Understanding the mechanical properties of 3D printed polymers could aid in predicting and preventing fatigue failure.

3.9 References

[1] J.R.C. Dizon, A.H. Espera, Q.Y. Chen, R.C. Advincula, Mechanical characterization of 3D-printed polymers, Addit Manuf 20 (2018) 44-67.
[2] E. Macdonald, R. Salas, D. Espalin, M. Perez, E. Aguilera, D. Muse, R.B. Wicker, 3D Printing for the Rapid Prototyping of Structural Electronics, Ieee Access 2 (2014) 234-242.
[3] S.E. Bakarich, R. Gorkin, M.I.H. Panhuis, G.M. Spinks, Three-Dimensional Printing Fiber Reinforced Hydrogel Composites, Acs Appl Mater Inter 6(18) (2014) 15998-16006.
[4] J.L. Ifkovits, J.A. Burdick, Review: Photopolymerizable and degradable biomaterials for tissue engineering applications, Tissue Eng 13(10) (2007) 2369-2385.
[5] S.J. Kalita, S. Bose, H.L. Hosick, A. Bandyopadhyay, Development of controlled porosity polymer-ceramic composite scaffolds via fused deposition modeling, Mat Sci Eng C-Bio S 23(5) (2003) 611-620.
[6] F.P.W. Melchels, J. Feijen, D.W. Grijpma, A review on stereolithography and its applications in biomedical engineering, Biomaterials 31(24) (2010) 6121-6130.
[7] V.B. Morris, S. Nimbalkar, M. Younesi, P. McClellan, O. Akkus, Mechanical Properties, Cytocompatibility and Manufacturability of Chitosan:PEGDA Hybrid-

Gel Scaffolds by Stereolithography, Annals of Biomedical Engineering 45(1) (2017) 286-296.
[8] S.V. Murphy, A. Atala, 3D bioprinting of tissues and organs, Nat Biotechnol 32(8) (2014) 773-785.
[9] F. Rengier, A. Mehndiratta, H. von Tengg-Kobligk, C.M. Zechmann, R. Unterhinninghofen, H.U. Kauczor, F.L. Giesel, 3D printing based on imaging data: review of medical applications, Int J Comput Ass Rad 5(4) (2010) 335-341.
[10] G.H. Wu, S.H. Hsu, Review: Polymeric-Based 3D Printing for Tissue Engineering (vol 35, pg 285, 2015), J Med Biol Eng 36(2) (2016) 284-284.
[11] R. Liu, Z. Wang, T. Sparks, F. Liou, J. Newkirk, Aerospace applications of laser additive manufacturing, Woodh Pub Ser Elect (88) (2017) 351-371.
[12] R. Melnikova, A. Ehrmann, K. Finsterbusch, 3D printing of textile-based structures by Fused Deposition Modelling (FDM) with different polymer materials, Iop Conf Ser-Mat Sci 62 (2014).
[13] R.H. Sanatgar, C. Campagne, V. Nierstrasz, Investigation of the adhesion properties of direct 3D printing of polymers and nanocomposites on textiles: Effect of FDM printing process parameters, Appl Surf Sci 403 (2017) 551-563.
[14] J.W. Stansbury, M.J. Idacavage, 3D printing with polymers: Challenges among expanding options and opportunities, Dent Mater 32(1) (2016) 54-64.
[15] J.Y. Lee, J. An, C.K. Chua, Fundamentals and applications of 3D printing for novel materials, Appl Mater Today 7 (2017) 120-133.
[16] J.V. Crivello, E. Reichmanis, Photopolymer Materials and Processes for Advanced Technologies, Chem Mater 26(1) (2014) 533-548.
[17] J.S. Mohammed, Applications of 3D Printing Technologies in Oceanography, Methods in Oceanography 17 (2016) 97-117.
[18] W. Gao, Y.B. Zhang, D. Ramanujan, K. Ramani, Y. Chen, C.B. Williams, C.C.L. Wang, Y.C. Shin, S. Zhang, P.D. Zavattieri, The status, challenges, and future of additive manufacturing in engineering, Comput Aided Design 69 (2015) 65-89.
[19] A.M. Forster, Materials Testing Standards for Additive Manufacturing of Polymer Materials: State of the Art and Standards Applicability, US Department of Commerce, National Institute of Standards and Technology 2015.
[20] L. Pruitt, L. Bailey, Factors affecting near-threshold fatigue crack propagation behavior of orthopedic grade ultra high molecular weight polyethylene, Polymer 39(8-9) (1998) 1545-1553.
[21] J.A. Sauer, M. Hara, Effect of Molecular Variables on Crazing and Fatigue of Polymers, Crazing in Polymers 2 (1990) 69-118.

[22] R.J. Crawford, P.P. Benham, Some Fatigue Characteristics of Thermoplastics, Polymer 16(12) (1975) 908-914.
[23] R.W. Hertzberg, R.P. Vinci, J.L. Hertzberg, Deformation and Fracture Mechanics of Engineering Materials, Wiley2012.
[24] I. Constable, J.G. Williams, D.J. Burns, Fatigue and Cyclic Thermal Softening of Thermoplastics, Journal of Mechanical Engineering Science 12(1) (1970) 20-29.
[25] R.J. Crawford, P.P. Benham, Cyclic Stress Fatigue and Thermal Softening Failure of a Thermoplastic, J Mater Sci 9(1) (1974) 18-28.
[26] J.A. Sauer, G.C. Richardson, Fatigue of Polymers, Int J Fracture 16(6) (1980) 499-532.
[27] M.T. Takemori, Polymer Fatigue, Annu Rev Mater Sci 14 (1984) 171-204.
[28] J. Schijve, Fatigue of structures and materials in the 20th century and the state of the art, Int J Fatigue 25(8) (2003) 679-702.
[29] P. Chowdhury, H. Sehitoglu, Mechanisms of fatigue crack growth - a critical digest of theoretical developments, Fatigue Fract Eng M 39(6) (2016) 652-674.
[30] J.M. Schultz, Fatigue Behavior of Engineering Polymers, Treatise on Materials Science and Technology 10 (1977) 599-636.
[31] W. Weibull, Fatigue Testing and Analysis of Results Elsevier2013.
[32] A.S.f. Metals, Atlas of Fatigue Curves, ASM International 1985.
[33] K.R. Chandran, Mechanical Fatigue of Polymers: A New Approach to Characterize the SN Behavior on the Basis of Macroscopic Crack Growth Mechanism, Polymer 91 (2016) 222-238.
[34] K.C. Ang, K.F. Leong, C.K. Chua, M. Chandrasekaran, Investigation of the mechanical properties and porosity relationships in fused deposition modelling-fabricated porous structures, Rapid Prototyping J 12(2) (2006) 100-105.
[35] A. Equbal, A.K. Sood, S.S. Mahapatra, Prediction of Dimensional Accuracy in Fused Deposition Modelling: a Fuzzy Logic Approach, International Journal of Productivity and Quality Management 7(1) (2010) 22-43.
[36] A.K. Sood, R.K. Ohdar, S.S. Mahapatra, Parametric appraisal of mechanical property of fused deposition modelling processed parts, Mater Design 31(1) (2010) 287-295.
[37] A.K. Sood, R.K. Ohdar, S.S. Mahapatra, Experimental Investigation and Empirical Modelling of FDM Process for Compressive Strength Improvement, Journal of Advanced Research 3(1) (2012) 81-90.

[38] H. Zarringhalam, N. Hopkinson, N.F. Kamperman, J.J. de Vlieger, Effects of processing on microstructure and properties of SLS Nylon 12, Mat Sci Eng a-Struct 435 (2006) 172-180.
[39] ASTM D7774-17 Standard Test Method for Flexural Fatigue Properties of Plastics, ASTM International West Conshohocken, PA, 2017.
[40] ASTM D3479/D3479M-12 Standard Test Method for Tension-Tension Fatigue of Polymer Matrix Composite Materials, ASTM International West Conshohocken, PA, 2012.
[41] ASTM D7791-12 Standard Test Method for Uniaxial Fatigue Properties of Plastics, ASTM International, West Conshohocken, PA, 2017.
[42] ISO 13003:2003 Fibre-reinforced plastics -- Determination of fatigue properties under cyclic loading conditions, ISO, Switzerland, 2003.
[43] ASTM D6115-97(2011) Standard Test Method for Mode I Fatigue Delamination Growth Onset of Unidirectional Fiber-Reinforced Polymer Matrix Composites, ASTM International West Conshohocken, PA, 2011.
[44] ISO 15850:2014 Plastics -- Determination of tension-tension fatigue crack propagation -- Linear elastic fracture mechanics (LEFM) approach, ISO, Switzerland 2014.
[45] ASTM E739-10 Standard Practice for Statistical Analysis of Linear or Linearized Stress-Life (S-N) and Strain-Life (ε-N) Fatigue Data, ASTM International, West Conshohocken, PA, 2015.
[46] C.W. Ziemian, M. Sharma, S. Ziemian, Anisotropic Mechanical Properties of ABS Parts Fabricated by Fused Deposition Modelling, Mechanical Engineering, InTech2012.
[47] S. Ziemian, M. Okwara, C.W. Ziemian, Tensile and fatigue behavior of layered acrylonitrile butadiene styrene, Rapid Prototyping J 21(3) (2015) 270-278.
[48] C.W. Ziemian, R.D. Ziemian, K.V. Haile, Characterization of stiffness degradation caused by fatigue damage of additive manufactured parts, Mater Design 109 (2016) 209-218.
[49] ASTM D638-10 Standard Test Method for Tensile Properties of Plastics, ASTM International West Conshohocken, PA, 2010.
[50] T. Letcher, M. Waytashek, Material Property Testing of 3d-Printed Specimen in Pla on an Entry-Level 3d Printer, Proceedings of the Asme International Mechanical Engineering Congress and Exposition, 2014, Vol 2a (2014).

[51] M.F. Afrose, S.H. Masood, P. Lovenitti, M. Nikzad, I. Sbarski, Effects of Part Build Orientations on Fatigue Behaviour of FDM-Processed PLA Material, Progress in Additive Manufacturing 1(1-2) (2016) 21-28.
[52] J. Lee, A. Huang, Fatigue analysis of FDM materials, Rapid Prototyping J 19(4) (2013) 291-299.
[53] UNI EN ISO 527-1 Plastics-Determination of Tensile Properties-General Principles, Italy 1977.
[54] T. Corbett, T. Kok, C. Lee, J. Tarbutton, Identification of Mechanical and Fatigue Characteristics of Polymers Fabricated by Additve Manufacturing Process, Proc. 2014 ASPE Spring Topical Meeting: Dimensional Accuracy and Surface Finish in Additive Manufacturing. (2014).
[55] M.M. Padzi, M.M. Bazin, W.M.W. Muhamad, Fatigue Characteristics of 3D Printed Acrylonitrile Butadiene Styrene (ABS), 2017 4th International Conference on Advanced Materials, Mechanics and Structural Engineering (4th Ammse 2017) 269 (2017).
[56] A.T. Miller, D.L. Safranski, K.E. Smith, D.G. Sycks, R.E. Guldberg, K. Gall, Fatigue of injection molded and 3D printed polycarbonate urethane in solution, Polymer 108 (2017) 121-134.
[57] M. Fischer, V. Schoppner, Fatigue Behavior of FDM Parts Manufactured with Ultem 9085, Jom-Us 69(3) (2017) 563-568.
[58] A.T. Miller, D.L. Safranski, C. Wood, R.E. Guldberg, K. Gall, Deformation and fatigue of tough 3D printed elastomer scaffolds processed by fused deposition modeling and continuous liquid interface production, J Mech Behav Biomed 75 (2017) 1-13.
[59] B.M. Gong, S.H. Cui, Y. Zhao, Y.T. Sun, Q. Ding, Strain-controlled fatigue behaviors of porous PLA-based scaffolds by 3D-printing technology, J Biomat Sci-Polym E 28(18) (2017) 2196-2204.
[60] G. Gomez-Gras, R. Jerez-Mesa, J.A. Travieso-Rodriguez, J. Lluma-Fuentes, Fatigue performance of fused filament fabrication PLA specimens, Mater Design 140 (2018) 278-285.
[61] H.Y. Zhang, L.L. Cai, M. Golub, Y. Zhang, X.H. Yang, K. Schlarman, J. Zhang, Tensile, Creep, and Fatigue Behaviors of 3D-Printed Acrylonitrile Butadiene Styrene, J Mater Eng Perform 27(1) (2018) 57-62.
[62] F. Arbeiter, M. Spoerk, J. Wiener, A. Gosch, G. Pinter, Fracture mechanical characterization and lifetime estimation of near-homogeneous components produced by fused filament fabrication, Polym Test 66 (2018) 105-113.

[63] B. Van Hooreweder, J.P. Kruth, High cycle fatigue properties of selective laser sintered parts in polyamide 12, Cirp Ann-Manuf Techn 63(1) (2014) 241-244.
[64] ISO 1352 Metallic materials - Torque-controlled fatigue testing, ISO, Switzerland, 2011.
[65] H. Amel, H. Moztarzadeh, J. Rongong, N. Hopkinson, Investigating the behavior of laser-sintered Nylon 12 parts subject to dynamic loading, J Mater Res 29(17) (2014) 1852-1858.
[66] B. Van Hooreweder, F. De Coninck, D. Moens, R. Boonen, P. Sas, Microstructural characterization of SLS-PA12 specimens under dynamic tension/compression excitation, Polym Test 29(3) (2010) 319-326.
[67] B. Van Hooreweder, D. Moens, R. Boonen, J.P. Kruth, P. Sas, On the difference in material structure and fatigue properties of nylon specimens produced by injection molding and selective laser sintering, Polym Test 32(5) (2013) 972-981.
[68] H. Amel, J. Rongong, H. Mortarzadeh, N. Hopkinson, Effect of section thickness on fatigue performance of laser sintered nylon 12, Polym Test 53 (2016) 204-210.
[69] J. Munguia, K. Dalgarno, Fatigue behaviour of laser-sintered PA12 specimens under four-point rotating bending, Rapid Prototyping J 20(4) (2014) 291-300.
[70] J. Munguia, K. Dalgarno, Fatigue behaviour of laser sintered Nylon 12 in rotating and reversed bending tests, Mater Sci Tech-Lond 31(8) (2015) 904-911.
[71] BS 3518-3 Methods of fatigue testing: Direct stress fatigue tests, British Standards Institution 1963.
[72] ASTM D671-93 Standard Test Method for Flexural Fatigue of Plastics by Constant-Amplitude-of-Force (Withdrawn 2002), ASTM International West Conshohocken, PA, 1993.
[73] G.V. Salmoria, D. Hotza, P. Klauss, L.A. Kanis, C.R.M. Roesler, Manufacturing of Porous Polycaprolactone Prepared with Different Particle Sizes and Infrared Laser Sintering Conditions: Microstructure and Mechanical Properties, Adv Mech Eng (2014).
[74] G.V. Salmoria, J.L. Leite, L.F. Vieira, A.T.N. Pires, C.R.M. Roesler, Mechanical properties of PA6/PA12 blend specimens prepared by selective laser sintering, Polym Test 31(3) (2012) 411-416.

[75] G.V. Salmoria, V.R. Lauth, M.R. Cardenuto, R.F. Magnago, Characterization of PA12/PBT specimens prepared by selective laser sintering, Opt Laser Technol 98 (2018) 92-96.
[76] M. Blattmeier, G. Witt, J. Wortberg, J. Eggert, J. Toepker, Influence of surface characteristics on fatigue behaviour of laser sintered plastics, Rapid Prototyping J 18(2) (2012) 161-171.
[77] ASTM E399-17 Standard Test Method for Linear-Elastic Plane-Strain Fracture Toughness KIc of Metallic Materials, ASTM International West Conshohocken, PA, 2017.
[78] A. Salazar, A. Rico, J. Rodriguez, J.S. Escudero, R. Seltzer, F.M.D. Cutillas, Fatigue crack growth of SLS polyamide 12: Effect of reinforcement and temperature, Compos Part B-Eng 59 (2014) 285-292.
[79] A. Salazar, A. Rico, J. Rodriguez, J.S. Escudero, R. Seltzer, F.M.D. Cutillas, Monotonic loading and fatigue response of a bio-based polyamide PA11 and a petrol-based polyamide PA12 manufactured by selective laser sintering, Eur Polym J 59 (2014) 36-45.
[80] J.A. Suresh, G.S. Kumar, P. Ramu, J. Rengaswamy, Fatigue Life Characterization of Additively Manufactured Acrylic like Poly-Jet Printed Parts, Advances in Structural Integrity (2018) 623-632.
[81] J.P. Moore, C.B. Williams, Fatigue Characterization of 3D Printed Elastomer Material, 19th Annual International Solid Freeform Fabrication Symposium (SFF) (2008).
[82] J.P. Moore, C.B. Williams, Fatigue properties of parts printed by PolyJet material jetting, Rapid Prototyping J 21(6) (2015) 675-685.
[83] ASTM D4482-11(2017) Standard Test Method for Rubber Property—Extension Cycling Fatigue, ASTM International West Conshohocken, PA, 2017.
[84] G. Taguchi, S. Chowdhury, Y. Wu, Taguchi's Quality Engineering Handbook, John Wiley & Sons, Hoboken, NJ, 2005.
[85] O.A. Mohamed, S.H. Masood, J.L. Bhowmik, Optimization of fused deposition modeling process parameters: a review of current research and future prospects, Adv Manuf 3(1) (2015) 42-53.

Chapter 4: Ten guidelines for the design of non-assembly mechanisms

The case of 3D printed prosthetic hands

Juan Sebastian Cuellar, Gerwin Smit, Amir A. Zadpoor and Paul Breedveld

Published as:

Ten guidelines for the design of non-assembly mechanisms: The case of 3D-printed prosthetic hands, Proc Inst Mech Eng H (2018) 954411918794734.

Abstract

In developing countries prosthetic workshops are limited, difficult to reach, or even non-existent. Especially fabrication of active, multi-articulated, and personalized hand prosthetic devices is often seen as a time-consuming and demanding process. An active prosthetic hand made through the fused deposition modelling (FDM™) technology and fully assembled right after the end of the 3D printing process will increase accessibility of prosthetic devices by reducing or bypassing the current manufacturing and post-processing steps. In this study, an approach for producing active hand prosthesis that could be fabricated fully assembled by FDM™ technology is developed. By presenting a successful case of non-assembly 3D-printing, this paper defines a list of design considerations that should be followed in order to achieve fully functional non-assembly devices. Ten design considerations for AM of non-assembly mechanisms have been proposed and a design case has been successfully addressed resulting in a fully functional prosthetic hand. The hand prosthesis can be 3D printed with an inexpensive FDM™ machine and is capable of performing different types of grasping. The activation force required to start a pinch grasp, the energy required for closing and the overall mass are significantly lower than body-powered commercial prosthetic hands. The results suggest that this non-assembly design may be a good alternative for amputees in developing countries.

4.1 Introduction

The World Health Organization (WHO) estimates that there are ≈40 million amputees in developing countries and that only ≈5% of them have access to prosthetic devices [1]. In low income countries, there are only a few big cities capable of providing reasonable healthcare conditions and transportation from rural areas is usually complicated, expensive, and may take several days. Amputees who come from villages either do not have access to prostheses whatsoever or they rarely go back for follow-up checks, maintenance, or repair [2-4]. In most of the cases, there is a general lack of trained personnel and materials making, prosthetic workshops limited, difficult to reach, or even non-

existent [5, 6]. In particular, fabrication of active, multi-articulated, and personalized hand prosthetic devices are often seen as a time-consuming and demanding process due to the large quantity of uncommonly shaped parts and long assembly times.

Non-assembly mechanisms are referred to as such mechanical systems whose fabrication is achieved without the need for post-manufacturing assembly [7]. Fabrication of non-assembly mechanisms is an attractive approach, because post-manufacturing steps are reduced or excluded when building multi-articulated mechanisms. Such a paradigm shift in manufacturing of mechanisms has been made possible thanks to the advent of additive manufacturing (AM) technologies, also referred to as 3D printing. AM creates 3D parts through sequential accumulation of material in a layer-by-layer process [8]. This manufacturing method enables fabrication of structures with unusual geometries without the need for any particular manual skill, elaborate tooling, or labour-intensive procedures. The inherent design versatility delivered by AM technologies is the core motivation for a significant change in the current approach of designing working mechanisms.

With the rapid development of AM technologies, many 3D printing techniques have become easily accessible and have opened a window for creating low-cost functional parts with very uncommon geometries. The case of the fused deposition modelling (FDM^{TM}) technique is a clear example of how AM technologies could reach the level required by producing accessible equipment and developing 3D printing materials suitable for many engineering applications. Several research groups and non-profit organizations have already demonstrated how various limitations of conventional manufacturing could be mitigated by FDM^{TM} to fabricate inexpensive and functional prosthetic hands [9]. A successful example is the Raptor Hand [10]. Many of the same organizations have also granted free on-line access to the digital drawings as open source files. However, extra post-assembly steps are still required to deliver fully functional prosthetic devices to users. For instance, the Raptor Hand consists of more than 20 parts that need to be assembled with hinge pins,

screws, elastic cords and braided line. Trained personnel and extra parts are necessary, thus reducing the overall accessibility of prostheses.

Non-assembly mechanisms have been successfully fabricated with different AM techniques including traditional rigid-body joints made out of polymers [7, 11, 12] and metals [13-15], compliant joints [16-18], soft robots [19, 20], and actuators [21]. However, no design processes based on FDM™ technology that could be followed to achieve fully functional non-assembly mechanisms have been reported so far. An active prosthetic hand made through the FDM™ technology and fully assembled right after the end of the 3D printing process will increase accessibility of prosthetic devices by reducing or bypassing the current manufacturing and post-processing steps. The goal of this study therefore was to develop an approach for producing an active hand prosthesis that could be fabricated fully assembled by FDM™ technology. By presenting a successful case of non-assembly 3D-printing, we aim to define a list of design considerations that should be followed in order to achieve fully functional non-assembly devices.

4.2 Case study: a non-assembly 3D printed hand prosthesis

The hand prosthesis should be specifically designed to be 3D-printed fully assembled and to meet the basic functional requirements listed below.

Body-powered control

Body-powered (BP) hand prostheses offer easy and intuitive control. The simple driving principle provides a straightforward way to use the prosthetic device to users while allowing them to benefit from proprioceptive force feedback. Such characteristics make BP prosthesis easy to implement in developing countries. The new prosthesis should also have voluntary closing control due to the direct relation between the pinch force and the driving force that is delivered to users [22].

Adaptive grasp

Grasping of a large variety of objects is simpler when fingers could adapt their grasping pattern. This could be achieved by introducing adaptability between the fingers inside the prosthetic hand [23]. Even when only a single driving force is available (due to the body-powered control), the finger links should perform motion differentials between themselves to achieve an adaptive grasp.

Cosmetics

A device that resembles a human hand is considered essential in some developing countries, because it contributes to the patient's acceptance in their community [3]. Moreover, a highly cosmetic prosthesis is commonly more accepted among users and according to Plettenburg [24] is part of the basic requirements. Therefore, the hand prosthesis should have the basic dimensions of an average human and resemble a real hand.

Low weight

Wearing comfort of prosthetic hands is directly related to the mass of the device. Since the prosthetic device is perceived as an extra load, mass should be taken to a minimum [25]. Considering the weight of a human hand (426 ± 62 g [26]), the prosthetic hand should weigh less than the average hand by one standard deviation (364 g).

Water proof and dust proof

Highly reliable prosthetic hands work properly under several environmental conditions. The hand should be manufactured from washable and corrosion resistant materials especially for developing countries where high moisture and dirt is commonly found.

4.2.1 Functioning principle

The main design concept of the hand prosthesis (Figure 4.1) consists of four moving fingers driven by a single link and a static thumb. All fingers are connected to the palm by a single hinge joint allowing full rotational motion. The fingers are coupled together following a whippletree configuration. This enables motion differentials between the fingers, thereby allowing adaptive

grasp. All moving fingers are pulled by a force transmission system consisting of a main driving link, the whippletree configuration, and the connecting links of the fingers. The fingers are driven by a Bowden cable connected to the main driving link and restricted to follow a linear motion along with the excursion of the cable. Restoring forces are achieved by springs connected to the base of the fingers.

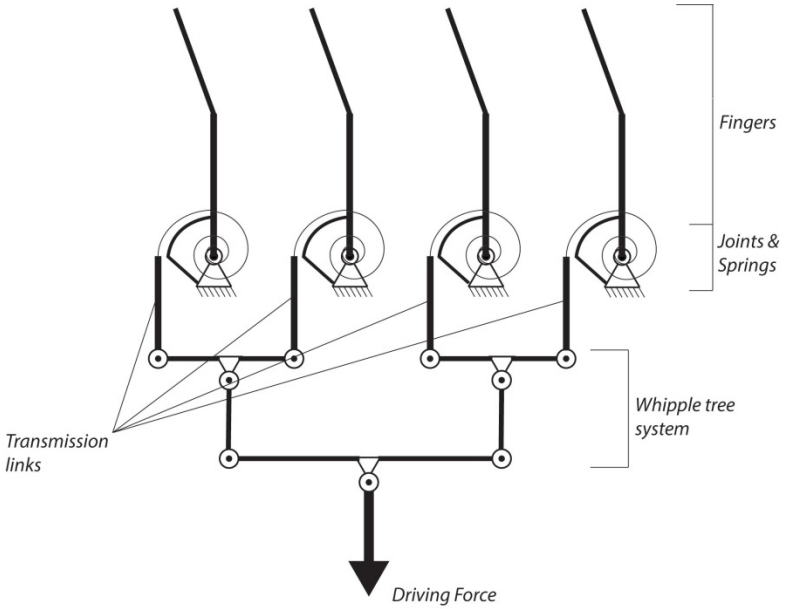

Figure 4.1: A schematic drawing of the design concept used for the hand prosthesis.

4.2.2 Design considerations applied in the hand prosthetic design.

General design considerations

Large play. AM achieves different fabrication accuracies depending on the technology and machine used. The minimum building feature varies amongst AM techniques and should be taken into consideration to set proper tolerance

values. Furthermore, there could be a considerable dimensional difference between the CAD design and the built object. Due to such differences, conservative values for clearances between the bodies should always be used. Although FDM™ machines have achieved fabrication accuracies of features as small as 0.1 mm, 3D-printing several bodies in a single step using such a small gap to distinguish between bodies does not always result in a successful outcome. There might also be small differences between different printing jobs even when the same FDM™ machine and printing parameters are used. These dimensional variances could cause fusion of printed parts. A minimum gap of 0.5 mm between the moving bodies guarantees non-fusion of plastic parts during the printing process. All mechanical parts should therefore be 3D printed with a minimum tolerance of 0.5 mm to ensure proper division of individual parts.

3D-printed surfaces. When building overhangs with FDM™, addition of support structures might be unavoidable. Non-soluble support structures need to be extracted manually and are undesired because the process contributes to a poor surface finish. Interacting surfaces requiring smooth motion should not be connected to support structures because the chances of high roughness and friction in the final parts are increased. In order to avoid this, such surfaces must be printed perpendicular to the printing plane and without any structural adhesion to the support structures.

Support removal. The removal of washable support structures requires open purge connections where solvent liquids can flow through. These openings can be as small as the minimum area required to provide constant flow of the liquid. On the other hand, as previously mentioned, non-washable structures need to be manually removed, thus, requiring wider openings. Such support structures must be easily reachable by hand or common tools. Given the printing direction, enclosed connections of links within the whippletree mechanism and the hinge joints of the fingers inevitably require support structures. Such enclosed configurations should be designed with proper openings to allow for easy access to the support structures. Bodies enclosing

the support structures are recommended to be separated minimally by 1 mm distance. This provides sufficient gap in where support structures could be manipulated and where, following extraction, occasional residuary material does not affect motion. Likewise, a minimum opening area of 4 mm^2 offering 1 mm distance between bodies provides a sufficient aperture for common pliers and is also recommended.

Integrated parts. Different standard part functions could be included directly into the design of 3D printed assemblies. Functions delivered by external components of traditional assemblies such as bolts, springs, washers, etc. could be provided through smart design of 3D printed parts. For example, working hinge joints and springs could be built from printing materials and be also integrated directly into the entire assembly. Here, transmission linkage from the whippletree mechanisms to the base of each finger is accomplished by semi-circle leaf springs. This compliant shape has two major advantages as compared to other force transmission designs. First, the semi-circle shape ensures constant moment arm transmission to the fingers for the complete range of positions. Second, following activation of fingers motion, as the leaf springs recovers from deformation, the resulting spring behaviour provides a clever way to return the moving parts to their neutral position.

Design considerations for mechanical play

Reduction of play. Due to the layer-by-layer process of AM, surfaces fabricated perpendicular to the printing plane present decreased dimensional accuracy (smoothness) due to the well-known "staircase effect" [27]. For instance, cross-sectional curved geometries are built with well-defined shapes when they are oriented parallel to the printing plane. Accurate curved shapes, like the hinge joints in the fingers, must be printed with their circular cross-section area oriented parallel to the building plate. In this way, contacting surfaces inside the hinge joints present smoother surfaces and, thus, reduced friction.

Re-accommodation of play. Due to building tolerances, undesired high play might be expected. Moving parts are estimated to shift contact points

continuously inside joints. However, to keep proper functionality, joints could be designed in such a way that they are automatically aligned under the effect of the driving force. Such configuration allows for fixation of joints when required. All mechanical components that are part of the whippletree configuration are connected with the presence of high play (Figure 4.2). In passive conditions, all joints are allowed to move freely inside the boundaries of the connection. Nevertheless, the curved structures designed in each connection permit an instant alignment of joints in the presence of the driving force. When the driving link (bottom link) is moved downwards by the activation force, all connected links move downwards to the edge of the curvature providing fixed connecting points (Figure 4.2).

Compliant parts. Considerable elastic deformation is achievable by many printing materials without the risk of failure [28]. Based on this fact, moving joints presenting small displacements could be fabricated in a compliant configuration. Compliant joints do not present friction and most importantly they could achieve motion out of a monolithic structure [29]. Compliant configurations facilitate non-assembly manufacturing and are therefore preferred when play inside joints is unacceptable and should be included when possible. Force transmission from the whippletree mechanism to each individual finger is achieved by compliant connections over the base of each finger (Figure 4.3). Such connections present relatively low displacement and help to provide spring behaviour due to the energy stored when deformed.

Design considerations for part strength

Cross-section of parts. Given the geometric freedom delivered by AM, all parts withstanding forces should be shaped to present sufficient cross-section area to evade the risk of material failure. All part connections should also present increased contact surface area and eliminate point and line contacts as well as sharp corners to exclude stress concentrations. All moving parts, from the driving link to the semi-circle leaf springs, should be smoothly in contact by rounded surfaces and be fully aligned to the line of action of the driving force to prevent unnecessary bending moments (Figure 4.3). Likewise, the leaf spring

connection with the base of the fingers should have a smooth transition in order to prevent stress concentrations (Figure 4.3). All links should present sufficient cross-section area, considering the equal division of the driving force amongst the fingers, to prevent the failure of the material due to high tensile stresses.

Density of parts. The building principles of some AM techniques allow control of material density in printed parts while keeping pre-set outer shapes. Such density control could be used to maximize part strength or reduce weight, time, and cost. Parts withstanding high stress should be printed with 70-100% of material infill whereas low stressed parts should be printed with lower densities in order to reduce overall mass and material cost. In our design, all moving parts from the driving link to the semi-circle leaf springs as well as the hinge joint connecting all fingers to the palm present 100% material density. Cosmetic parts presenting low forces like fingers and palm present 15% material density.

Part anisotropy. Nearly all AM technologies produce parts presenting anisotropic mechanical behaviour. In most of the cases, 3D printed parts are stronger along directions in the parallel with the printing plane (plane defined by the building plate) [30-33]. Poor interlayer bonding leads to weak tensile and torsional properties when the part is loaded along the perpendicular direction of the printing plane [28]. Parts like the whippletree system or the semi-circle leaf spring connections stand high tensile forces due to the actuation force. Furthermore, additional bending stress is present in the leaf spring due to its semi-circle configuration. The best mechanical performance, i.e. higher ultimate stress and higher ultimate strain, is also achieved by printing layers along the direction of the stress induced by the bending moments [34]. The corresponding critical cross-sectional areas under stress should therefore be built perpendicular to the printing plane. In other words, the prosthesis should be printed sideways.

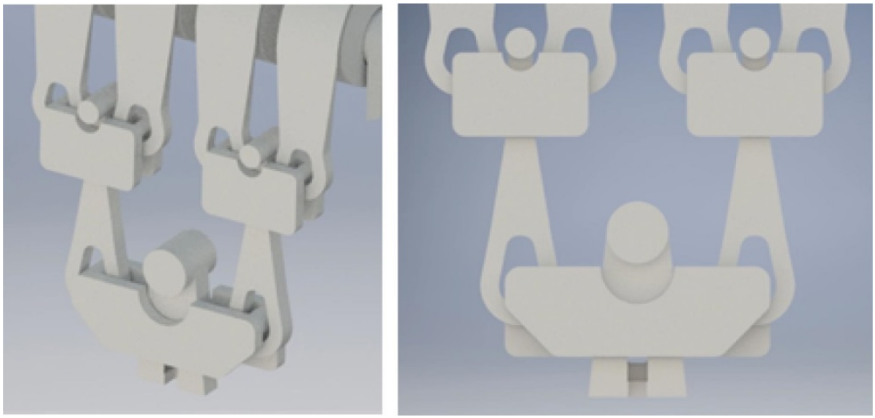

Figure 4.2: *(left)* isometric view of the whippletree mechanism. All connections are designed to be 3D printed with large play, *(right)* frontal view of the whippletree mechanism.

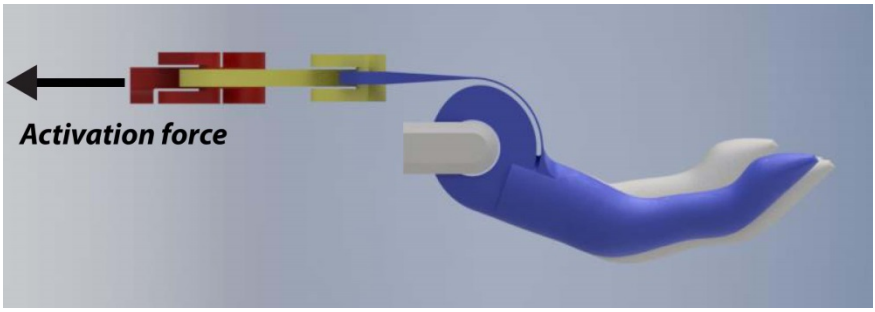

Figure 4.3: Force transmission system to the finger, (blue) semi-circle leaf spring connected from the base of the finger to the whippletree mechanism, (yellow) the first level of the whippletree mechanism and connecting links, (red) the second level of the whippletree mechanism and main driving link. The Bowden cable is connected to the main driving link.

4.3 The 10 guidelines of non-assembly design with 3D printing

Based on the analysis presented in the previous section regarding the design considerations, here we summarize the ten design guidelines for 3D printed hand prosthesis. The applicability of these guidelines to the different parts of prostheses is visualized using annotation in Figure 4.4.

General

1. Design in terms of large mechanical play.
2. Support moving parts perpendicular to their plane of interaction. Planes which require smooth surfaces (e.g. planes of interaction) should not be touched by the support material
3. Provide openings for removal of supports.
4. Integrate the functionality of standard parts (e.g. bolts, springs, washer, etc.) into the design.

Play

5. Reduce play by positioning the parts with high tolerances in parallel with the printing plane.
6. Remove play by pretension or actuation force.
7. Avoid play by replacing rigid contact by compliant interfaces.

Stress

8. Design the shape of various components according to the stress.
9. Choose the material density (when 3D printing) according to the stress.
10. Align the 3D-printing plane with the dominant load.

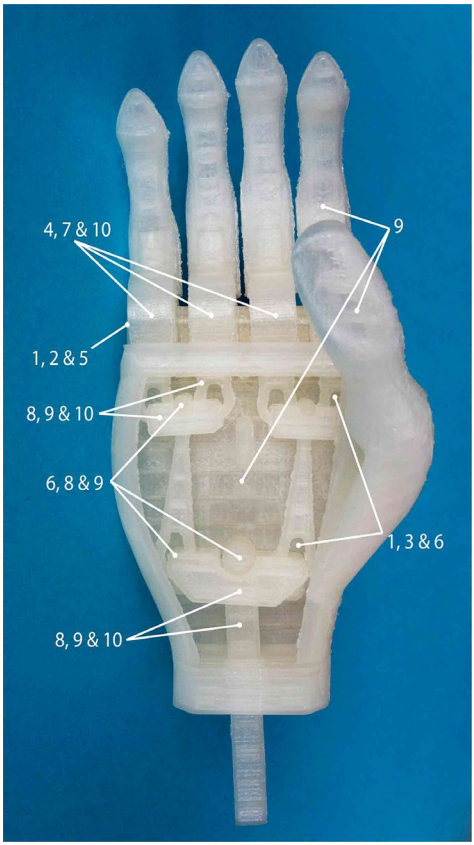

Figure 4.4: Non-assembly prosthesis prototype after support removal. Each number represents the corresponding design principle used to build the part.

4.4 Materials and methods

An Ultimaker 3 machine loaded with polylactic acid (PLA) material was used to print the prosthetic hand. A layer thickness of 0.2 mm and a printing speed of 70 mm/s were used as 3D printing parameters. The part dimensions are overall delimited by a building volume of 94.4 mm x 223.8 mm x 99.6 mm. Figure 4.5 shows the printing direction of the hand prosthesis.

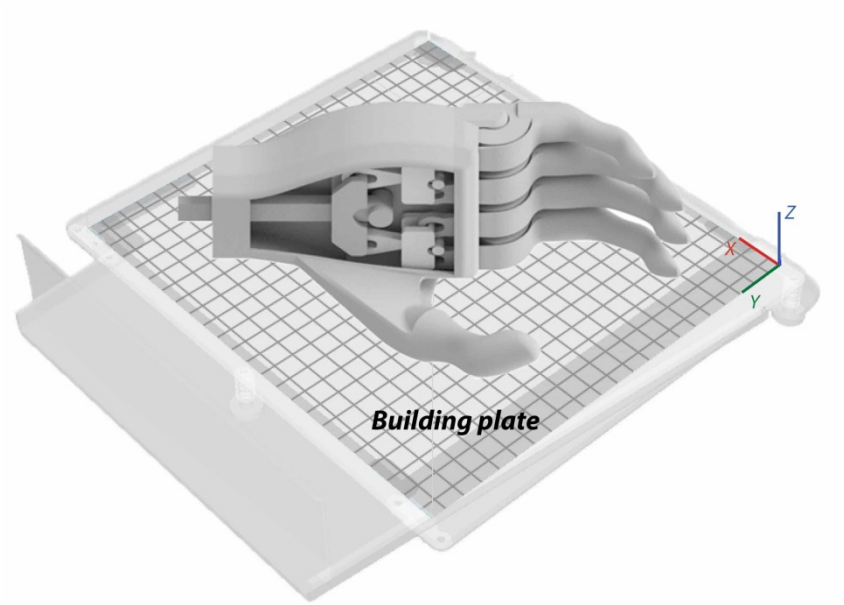

Figure 4.5: Printing direction of the hand prosthesis.

An experimental setup and protocol based on our previous work [35] was used to assess the mechanical performance of the device. The test setup measured (1) pinch force output given an activation input force and (2) the energy efficiency of the prosthesis for a closing-opening cycle. The test setup consisted of a load cell (Zemic: FLB3G-C3-50 kg-6B) to measure the input force, a custom-built 11 mm thick case housing, a FUTEK LLB130 force load cell placed on the thumb fingertip to measure pinch force, and a displacement sensor (Schaevitz: LCIT 2000) to measure the actuation displacements.

The mechanical efficiency of the prosthesis is obtained by measuring the energy employed to close the device and the energy delivered back to return the fingers to the open position. The energy employed in each event could be determined by integrating the forces along the displacements obtained. A measure of the energy dissipated by the device could be obtained as the

difference between the input energy and the returned energy. To measure the variables of interest, the following protocol has been followed

1. A full closing and opening cycle without pinching.
2. Closing and pinching the pinch load cell until an actuation force of 100 N was reached. The load cell is pressed against the thumb by the index and middle fingers of the prosthesis.

Data availability. The datasets generated during and/or analysed during the current study are available from the corresponding author on reasonable request.

4.5 Results

The hand prosthesis printed from polylactic acid (PLA) is shown in Figure 4.4. The prosthetic device could achieve adaptive grasping even though it was driven by a single force signal. A counter force was delivered by the compliant behaviour of the leaf springs to return the fingers to an open state during passive conditions. A driving link was fabricated with the hand prosthesis in order to manually activate the device and perform several grasping patterns (Figure 4.6). Pinch force – activation force relationship is presented in Figure 4.7. The prosthesis allows for body-powered control, its geometrical shape resembles a real human hand, it has a mass of 130 g and its building material makes it water and dust proof. Furthermore, the cost of the material lies around 10 US dollars. The energy for closing the device was calculated to be 0.104 Nm and the energy dissipated during a full closing-opening cycle was calculated as 0.048 Nm.

4.6 Discussion

A functional multi-articulated hand prosthesis was designed and manufactured using 3D-printing. The design procedure has concluded in a concept that reduces manufacturing requirements to a single 3D printer and its building material. Extra material, supplies, or laborious post-manufacturing steps have been eliminated. In addition to fulfilling the functional requirements listed here,

the material cost of this prosthetic hand is low as compared to commercial prosthetic devices as well as similar 3D-printed prosthetic hands [9].

Figure 4.6: Grasping patterns. Pinch grasping *(Top left & right)*, power grasping *(Middle left & right)*, spherical grasping *(Bottom left),* and tripod grasping *(Bottom right)*.

The activation force required to start a pinch grasp on the 11 mm load cell (16-18 N) and the energy required for closing (0.104 Nm) are significantly lower

than other BP commercial prosthetic hands (Figure 4.7a,b) [35]. The force transmission ratio is, however, lower and is clear from the slope between the input and output forces. Pinch force was measured only by the gripping action of the index and middle fingers. Equal distribution of the activation force between every finger suggests similar pinching forces for the ring and little fingers. By extrapolating the pinch force measurements, one could argue that gripping forces during power grasp could be at least doubled if all fingers are used at the same time. Despite relatively low pinch forces, the hand prosthesis is capable of reaching reasonable pinching forces and different grasping patterns in order to execute various daily activities [36]. According to ten-Kate et al. [9], only one 3D printed hand prosthesis has been tested for gripping forces, reporting similar fingertip force measurements (3.9 – 11.5 N) [37]. For activities requiring more than 15 N grasping force, the corresponding input force needed (>100 N) might be unacceptable for many users [38]. Design alternatives such as increased transmission moment arms to the fingers, unequal distribution of force favouring index and middle fingers, and merging the ring and little finger into a single driving link could increase the force delivered by the index and middle fingers into precision grasps.

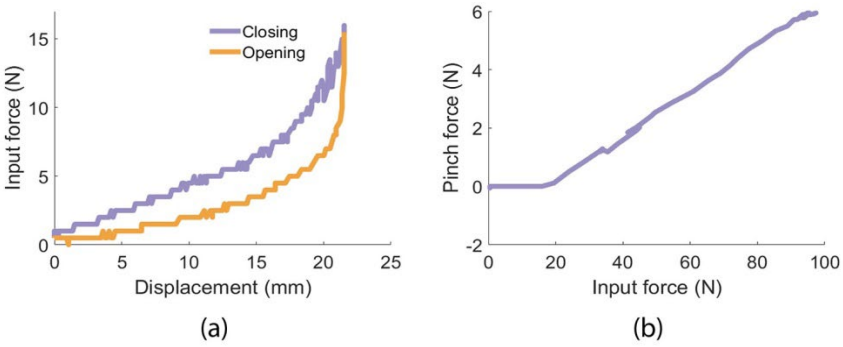

Figure 4.7: The mechanical assessment of the prosthesis. (a) Input force vs. pinch force and (b) cable displacement vs. the input force of a closing-opening cycle.

The design considerations conceived here should be followed as guidelines to circumvent many of the limitations commonly found when using AM to build non-assembly mechanisms. This guideline was followed to build a prosthetic hand with the most accessible AM technology, i.e. FDM™. Reference values employed to fulfil the design considerations proposed are therefore based on the characteristics of FDM™. Considering the AM machine used here (i.e. Ultimaker 3) and its relatively low building accuracy, dimensions employed in the case presented here are an appropriate starting point for building non-assembly mechanisms with all AM techniques. Lower tolerance values and the use of washable support structures could be set to solve mechanical problems arising from high play between joints, if the corresponding AM technology and equipment are available.

Although large mechanical play is often seen as a significant concern in traditional mechanical design, it is usually necessary in FDM™-based mechanical design and is addressed using the advantages of AM. AM characteristic of geometrical freedom allows for design of mechanical linkages that conveniently remove mechanical play when actuated or reconfigured. Driving forces can reposition moving components into desired locations when needed. Furthermore, extra components that could remove mechanical play by manually reconfiguring their position inside the device are the other options. Compliant components might be also considered when mechanical play is unwanted and the range of motion is suitable for the deformation limits of 3D-printing materials. Compliant configurations could be also included when a spring behaviour is required as shown by the fabrication of the semi-circle leaf springs. Here compliancy was achieved by manipulating the geometry of the constructs even though the mechanical behaviour of 3D-printed parts of all materials compatible with FDM™ are unknown to their full extent, especially reflecting on their response to large deformations. 3D printing thin sheets of PLA as curved shapes allowed relatively small deformations and sufficient spring behaviour even for a material such as PLA that is usually considered brittle.

Despite successful fabrication of non-assembly mechanisms using PLA, little attention was paid to the building materials during the design process

employed and presented here. This study was focused on exploiting the advantages of AM when designing non-assembly mechanisms while maximizing design versatility. We found that given one particular material (PLA), the preferred mechanical response could be achieved by manipulating the geometry of parts. In this way, compliant and rigid body parts are created out of a single material. Undoubtedly, the intrinsic mechanical properties of every 3D-printing material differ between each other, which in consequence open a window for different design opportunities. For instance, when large deformation is required, other FDM™ materials such as Nylon present better resistance for large bending strain and should be considered as well. Nevertheless, as mentioned before, 3D-printed parts are highly anisotropic and their mechanical behaviour, including their compliant behaviour, strongly depends on the 3D-printing direction. Based on previous research we have built critical parts depositing the fibres parallel and longitudinally to the loading direction in order to provide best mechanical performance. Still, a thorough study regarding compliant design properties of all 3D-printing materials compatible with FDM™ and 3D-printing parameters should be conducted in order to provide better tools when choosing a more suited combination of material and design concepts to solve a specific engineering problem.

Despite achieving different grasping patterns, a more in depth quantitative study of this prosthetic design including mechanical performance and capabilities, should be considered in order to provide a thorough comparative analysis on the functionality of the alternatives found in literature. Furthermore, activities requiring high grasping forces might be unrealizable for most users. Further design steps should be geared towards increased force transmission ratio. That being said, most of daily activities require low gripping force [39]. The low material costs and the reduced post-processing assembly steps suggest that this non-assembly design may be a good alternative for amputees in developing countries.

4.7 Conclusion

Ten design considerations for AM of non-assembly mechanisms have been proposed and a design case has been successfully addressed resulting in a fully functional prosthetic hand. The hand prosthesis was 3D printed with an inexpensive FDM™ machine and is capable of performing different types of grasping as a result of the adaptive grasp provided by its inner mechanism. Furthermore, the prosthesis has been fabricated under a process that reduces manufacturing requirements to a single 3D printer and its building material. Extra material, supplies or laborious post-manufacturing steps have been eliminated, hence introducing the first non-assembly hand prosthesis manufactured by FDM™. Given the characteristics of FDM™, such non-assembly process will increase the accessibility of prosthetic devices in developing countries by producing cheap and customized parts regardless of any specialized workshops and tools and highly skilled personnel. We encourage the use of the design considerations recommended here as a guideline for future design and manufacturing of fully assembled mechanisms.

4.8 References

[1] W.H. Organization, Standards for P&O Service Provision | ISPO, (2015).

[2] M. Marino, S. Pattni, M. Greenberg, A. Miller, E. Hocker, S. Ritter, K. Mehta, Access to prosthetic devices in developing countries: Pathways and challenges, 2015 IEEE Global Humanitarian Technology Conference (GHTC), 2015, pp. 45-51.

[3] L. Magnusson, G. Ahlström, Experiences of providing prosthetic and orthotic services in Sierra Leone – the local staff's perspective, Disability and Rehabilitation 34(24) (2012) 2111-2118.

[4] R.A. Gosselin, The Increasing Burden of Injuries in Developing Countries: Direct and Indirect Consequences, Techniques in Orthopaedics 24(4) (2009) 230-232.

[5] I. Grobler, G.J. van Schalkwyk, C. Wagner, The Application of Critical Psychology to Facilitate Reflective Clinical Practice in Orthotics/Prosthetics, Prosthet Orthot Int 30(3) (2006) 237-245.

[6] D. Wyss, S. Lindsay, W.L. Cleghorn, J. Andrysek, Priorities in lower limb prosthetic service delivery based on an international survey of prosthetists in low- and high-income countries, Prosthet Orthot Int 39(2) (2015) 102-111.
[7] C. Mavroidis, K.J. DeLaurentis, J. Won, M. Alam, Fabrication of Non-Assembly Mechanisms and Robotic Systems Using Rapid Prototyping, Journal of Mechanical Design 123(4) (2000) 516-524.
[8] I. Gibson, D.W. Rosen, B. Stucker, Introduction and Basic Principles, Additive Manufacturing Technologies, Springer US2010, pp. 20-35.
[9] J.t. Kate, G. Smit, P. Breedveld, 3D-printed upper limb prostheses: a review, Disability and Rehabilitation: Assistive Technology 12(3) (2017) 300-314.
[10] e-NABLE, The Raptor Hand, Enabling The Future, 2014.
[11] J. Calì, D.A. Calian, C. Amati, R. Kleinberger, A. Steed, J. Kautz, T. Weyrich, 3D-printing of Non-assembly, Articulated Models, ACM Trans. Graph. 31(6) (2012) 130:1-130:8.
[12] K.J. De Laurentis, F.F. Kong, C. Mavroidis, Procedure for Rapid Fabrication of Non-Assembly Mechanisms With Embedded Components, (2002) 1239-1245.
[13] F. Calignano, D. Manfredi, E.P. Ambrosio, S. Biamino, M. Pavese, P. Fino, Direct Fabrication of Joints based on Direct Metal Laser Sintering in Aluminum and Titanium Alloys, Procedia CIRP 21 (2014) 129-132.
[14] Y. Chen, J. Lu, Minimise joint clearance in rapid fabrication of non-assembly mechanisms, International Journal of Computer Integrated Manufacturing 24(8) (2011) 726-734.
[15] X. Su, Y. Yang, D. Wang, Y. Chen, Digital assembly and direct fabrication of mechanism based on selective laser melting, Rapid Prototyping Journal 19(3) (2013) 166-172.
[16] M.W.M. Groenewegen, M.E. Aguirre, J.L. Herder, Design Of a partially compliant, three-phalanx underactuated prosthetic finger, Proceedings of the ASME Design Engineering Technical Conference, 2015.
[17] E.G. Merriam, L.L. Howell, Lattice flexures: Geometries for stiffness reduction of blade flexures, Precision Engineering 45 (2016) 160-167.
[18] J.A. Mirth, An examination of trispiral hinges suitable for use in ABS-based rapid prototyping of compliant mechanisms, Proceedings of the ASME Design Engineering Technical Conference, 2014.
[19] B.N. Peele, T.J. Wallin, H. Zhao, R.F. Shepherd, 3D printing antagonistic systems of artificial muscle using projection stereolithography, Bioinspiration & Biomimetics 10(5) (2015) 055003.

[20] R. MacCurdy, R. Katzschmann, K. Youbin, D. Rus, Printable hydraulics: A method for fabricating robots by 3D co-printing solids and liquids, 2016 IEEE International Conference on Robotics and Automation (ICRA), IEEE, 2016, pp. 3878-3885.
[21] Y. Wei, Y. Chen, Y. Yang, Y. Li, Novel Design and 3-D Printing of Nonassembly Controllable Pneumatic Robots, IEEE/ASME Transactions on Mechatronics 21(2) (2016) 649-659.
[22] C.L. Taylor, The Biomechanics of Control in Upper-Extremity Prostheses, Artificial Limbs 2(3) (1955) 4-25.
[23] L. Birglen, C.M. Gosselin, Force analysis of connected differential mechanisms: Application to grasping, Int J Robot Res 25(10) (2006) 1033-1046.
[24] D.H. Plettenburg, Basic requirements for upper extremity prostheses: the WILMER approach, Proceedings of the 20th Annual International Conference of the IEEE Engineering in Medicine and Biology Society. Vol.20 Biomedical Engineering Towards the Year 2000 and Beyond (Cat. No.98CH36286), Hong Kong, 1998, pp. 2276-2281 vol.5.
[25] E. Biddiss, T. Chau, Upper-limb prosthetics: critical factors in device abandonment, Am J Phys Med Rehabil 86(12) (2007) 977-87.
[26] R.F. Chandler, C.E. Clauser, J.T. McConville, H.M. Reynolds, J.W. Young, Investigation of Inertial Properties of the Human Body, AIR FORCE AEROSPACE MEDICAL RESEARCH LAB WRIGHT-PATTERSON AFB OH, AIR FORCE AEROSPACE MEDICAL RESEARCH LAB WRIGHT-PATTERSON AFB OH, 1975.
[27] W. Oropallo, L.A. Piegl, Ten challenges in 3D printing, Eng Comput-Germany 32(1) (2016) 135-148.
[28] J.R.C. Dizon, A.H. Espera, Q. Chen, R.C. Advincula, Mechanical characterization of 3D-printed polymers, Additive Manufacturing 20 (2018) 44-67.
[29] A. Midha, T.W. Norton, L.L. Howell, On the Nomenclature, Classification, and Abstractions of Compliant Mechanisms, J. Mech. Des 116(1) (1994) 270-279.
[30] S.-H. Ahn, M. Montero, D. Odell, S. Roundy, P.K. Wright, Anisotropic material properties of fused deposition modeling ABS, Rapid Prototyping Journal 8(4) (2002) 248-257.
[31] B. Caulfield, P.E. McHugh, S. Lohfeld, Dependence of mechanical properties of polyamide components on build parameters in the SLS process, Journal of Materials Processing Technology 182(1) (2007) 477-488.

[32] A. Takaichi, Suyalatu, T. Nakamoto, N. Joko, N. Nomura, Y. Tsutsumi, S. Migita, H. Doi, S. Kurosu, A. Chiba, N. Wakabayashi, Y. Igarashi, T. Hanawa, Microstructures and mechanical properties of Co–29Cr–6Mo alloy fabricated by selective laser melting process for dental applications, Journal of the Mechanical Behavior of Biomedical Materials 21(Supplement C) (2013) 67-76.
[33] A.R. Torrado, C.M. Shemelya, J.D. English, Y. Lin, R.B. Wicker, D.A. Roberson, Characterizing the effect of additives to ABS on the mechanical property anisotropy of specimens fabricated by material extrusion 3D printing, Additive Manufacturing 6(Supplement C) (2015) 16-29.
[34] T. Letcher, M. Waytashek, Material Property Testing of 3D-Printed Specimen in PLA on an Entry-Level 3D Printer, ASME 2014 International Mechanical Engineering Congress and Exposition, Montreal, Quebec, Canada, 2014, p. V02AT02A014.
[35] G. Smit, D.H. Plettenburg, Efficiency of Voluntary Closing Hand and Hook Prostheses, Prosthet Orthot Int 34(4) (2010) 411-427.
[36] L.A. Jones, S.J. Lederman, Human Hand Function, Oxford University Press, Oxford, New York, 2006.
[37] K. Andrianesis, A. Tzes, Development and Control of a Multifunctional Prosthetic Hand with Shape Memory Alloy Actuators, J Intell Robot Syst 78(2) (2015) 257-289.
[38] M. Hichert, A.N. Vardy, D. Plettenburg, Fatigue-free operation of most body-powered prostheses not feasible for majority of users with trans-radial deficiency, Prosthet Orthot Int 42(1) (2018) 84-92.
[39] J.T. Belter, J.L. Segil, A.M. Dollar, R.F. Weir, Mechanical design and performance specifications of anthropomorphic prosthetic hands: A review, J Rehabil Res Dev 50(5) (2013) 599-617.

Chapter 5: Functional evaluation of a non-assembly 3D printed hand

Juan Sebastian Cuellar , Gerwin Smit , Paul Breedveld, Amir A. Zadpoor and Dick Plettenburg

Published as:

Functional evaluation of a non-assembly 3D-printed hand prosthesis, Proc Inst Mech Eng H 233(11) (2019) 1122-1131.

Abstract

In developing countries the access of amputees to prosthetic devices is very limited. In a way to increase accessibility of prosthetic hands we have recently developed a new approach for the design and 3D printing of non-assembly active hand prostheses using inexpensive 3D printers working on the basis of Material Extrusion technology. This paper describes the design of our novel 3D-printed hand prosthesis and also shows a mechanical and functional evaluation in view of its future use in developing countries. We have fabricated a hand prosthesis using 3D printing technology and a non-assembly design approach that reaches certain level of functionality. The mechanical resistance of critical parts, the mechanical performance, and the functionality of a non-assembly 3D-printed hand prosthesis were assessed. The mechanical configuration used in the hand prosthesis is able to withstand typical actuation forces delivered by prosthetic users. Moreover, the activation forces and the energy required for a closing cycle are considerably lower as compared to other body-powered (BP) prostheses. The non-assembly design achieved a comparable level of functionality with respect to other body-powered alternatives. We consider this prosthetic hand a valuable option for people with arm defects in developing countries.

5.1 Background

The most frequent causes of upper limb amputations are traumas, malignancy, vascular disease, congenital deformities and infection [1]. Recent estimations by the World Health Organization (WHO) indicate that out of the nearly 40 million people around the globe that require prosthetic and orthotic devices just 5-15% have access to them [2]. In developing countries, reasonable healthcare services are usually merely available in a small number of big cities, while transportation from rural regions to the major healthcare hubs may be expensive and difficult. Under such circumstances, the access of amputees to prosthetic devices is very limited and maintenance and follow-up checks are very rare [3-5]. The lack of treatment centres for amputees can be explained by a broad absence of trained workforce and materials, leading to limited availability of prosthetic workshops

[6, 7]. In particular, active, multi-articulated, and personalized prosthetic hands are mostly inaccessible.

Due to the recent developments in additive manufacturing (AM) technologies, also known as 3D printing, many research groups and non-profit institutions have already produced affordable prosthetic devices (e.g. [8-10]) by reducing the production costs to a few hundreds or even tens of Euros. Furthermore, according to Phillips et al. [11] 3D printing technology is also more suited for developing countries as compared to other manufacturing techniques because of its relatively low start-up costs and minimal skill required. Little information is however available regarding whether basic user requirements are met for short- or long-term use by prosthetic hands produced this way [12]. Moreover, additional post-printing assembly actions are yet necessary to provide functional prostheses to users. Those assembly steps usually need to be performed by skilled personnel and may necessitate extra tools, thereby reducing the overall accessibility of prostheses. The design versatility offered by AM allows for production of mechanisms that do not require additional assembly steps (non-assembly mechanisms), e.g. [13-16]. While a functional prosthetic device still requires an activation system and proper fitting to the residual limb, an active prosthetic hand that is printed in a fully assembled state will increase the accessibility of such prosthetic devices through elimination of a number of post-processing steps. In low resource-settings, the prosthetic hand can be 3D-printed in the closest centers in large cities where reasonable technical conditions can be found and 3D printers are available. The prosthetic hand can be transported to the end-user using local distribution networks.

Based on a study on 3D-printed mechanisms and joints [17], we have recently developed a new approach for the design and 3D printing of non-assembly active hand prostheses [18] using inexpensive printers working on the basis of fused deposition modeling (FDM^{TM}) (i.e., polymer extrusion) [19]. This paper describes the design of our novel 3D-printed hand prostheses with a focus on a mechanical and functional evaluation in view of its future use in developing countries.

5.2 The 3D printed hand prosthesis

Our 3D-printed hand prosthesis was designed to be the first 3D-printed fully assembled prosthesis that meets the following basic (functional) requirements: body-powered (BP) control, cosmetic appearance, light weight, and water/dirt resistant (materials do not fail in contact with water and dirt) [20].

A detailed explanation of the 3D-printed prosthetic design (Figure 5.1) can be found in [18], however a brief description is given in order to contextualize the current study. The design is made up of four individual fingers and a stationary thumb. All fingers are coupled to the palm through one hinged joint permitting a one degree of freedom (DoF) rotating motion. The fingers are joined through a whippletree arrangement. This permits relative movement amongst the fingers equalizing the pinching force on each finger as they adjust to the geometry of the object being grasped (adaptive grasping) [21]. All fingers in motion are activated by a force transmission scheme which is made out of a main driving link, the whippletree arrangement, and the links that connect the four fingers. The hand is actuated by a Bowden cable attached to the main driving link that is allowed to go on a linear motion following the movement of the cable. Return forces that permit hand opening are generated by leaf springs connected on one end to the base of the fingers and on the other end to the whippletree mechanism. The leaf spring configuration is designed as a series of curved thin 3D-printed plastic sheets that allow elastic bending and work at the same time as pulling elements. When the fingers are activated, the pulling forces drive the leaf springs to unbend and deform to a straight configuration. As the leaf springs return and recover from the deformation, spring-like behaviour is provided, combining actuation and a return spring in one non-assembly 3D-printed element.

In order to achieve non-assembly fabrication of the concept, a number of design guidelines [18] were used using the advantages of 3D printing for design versatility while circumventing many of its shortcomings. The prosthetic hand was 3D-printed from polylactic acid (PLA) using an Ultimaker 3 3D printer.

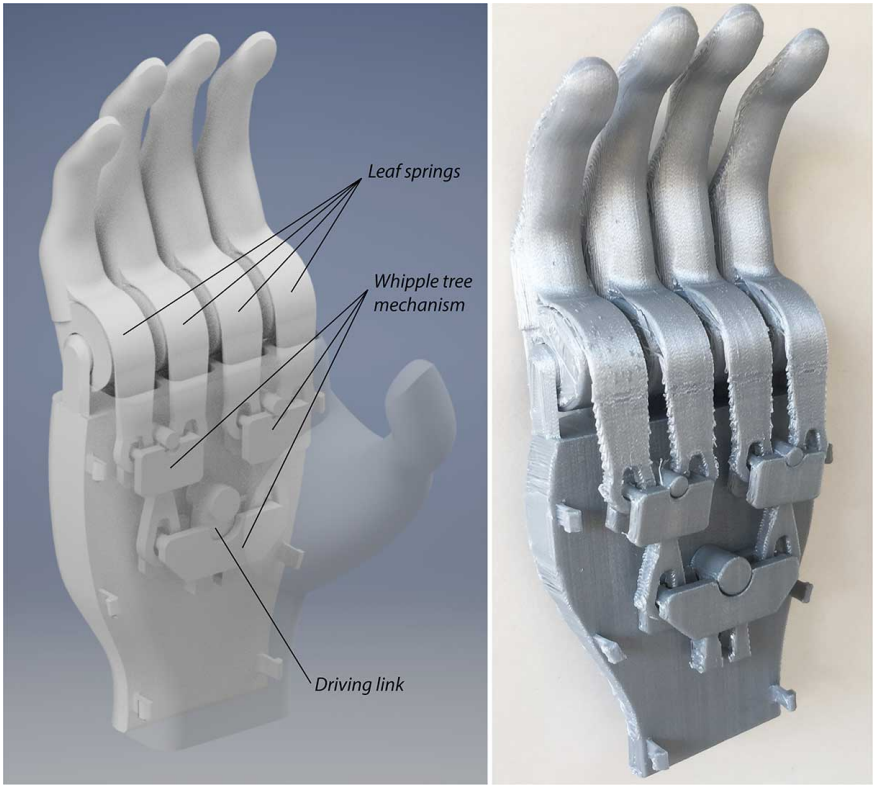

Figure 5.1: Design of our 3D-printed prosthetic hand. The palm in the left picture is translucent to show the inner mechanisms (from top to bottom: leaf springs, whippletree mechanisms, and driving link) (*Left*). The 3D-printed prosthetic hand without the palm (*Right*).

This machine is relatively an affordable alternative compared to other 3D printing technologies allowing for the production of low-cost parts. A cover encasing the whippletree mechanism and forming the palm of the prosthetic hand was printed separately and was assembled using snap-fit joints. The entire mechanisms were 3D-printed assembled as to avoid elaborated post assembly steps. Only one simple additional snap-fit step is needed to cover the

mechanism with the prosthetic palm which can be easily done by the user. The hand was 3D-printed with the circular cross-section area of the hinges of the fingers parallel to building plate of the 3D printer. In this way, the layers that form the leaf springs, the whippletree mechanism and the driving link are deposited along the perpendicular direction of their moving direction during the hand prosthesis activation. To visualize the printing direction of the prosthesis please refer to [18].

5.3 Methods

5.3.1 Leaf spring ultimate strength and fatigue life

In the prosthetic hand the moving part that has the lowest cross-sectional area (most prone to failure) is the leaf spring. Furthermore, the leaf springs experience a combination of tensile and bending loads as the prosthetic hand activates. This loading condition is worrisome since it can be more critical to the structural integrity of the part than any other in the prosthetic hand. Tensile stress vs. strain experiments have been conducted previously on a number of 3D-printed PLA samples [22]. However, a combination of tensile and bending loads has never been explored. It is therefore unclear whether the leaf spring configuration is able to withstand the maximum input force delivered by a regular prosthetic user via a Bowden cable. According to [23] the maximum input force registered by a prosthetic user is 538 N. Due to the distribution of the force given by the whippletree mechanism that divides the force equally over the four fingers, with this maximum input force, each leaf spring should be able to withstand a tensile load of 134.5 N (538 N/4). An experimental set-up consisting of an ElectroPlus^{TM} E10000 (Instron, USA) electrodynamic testing machine and customized 3D-printed PLA samples designed to fit into the testing clamps were used in order to measure the failure force of a leaf spring under the corresponding loading and motion conditions. The 3D-printed samples were designed to have the same dimensions as the leaf springs in the prosthetic hand, with a bent initial shape (Figure 5.1 and Figure 5.2, left) and to fully restrict the motion at both extremes once the leaf spring has been manually

uncurled to a straight configuration (Figure 5.2, right), equivalent to their full closing function (90 deg. flexion) in the prosthetic hand. In the straight configuration, the sample was loaded with a strain rate of 0.01 mm/s until failure. The experiment was repeated five times using samples fabricated with the same 3D printing parameters as the prosthetic hand.

Similarly to the ultimate strength, the number of cycles that the leaf spring can be used before it breaks is unknown. A similar experimental setup using the same equipment and materials as the previous experiment was used. The testing samples were modified to allow free rotation at one of the clamping ends to simulate the activation of one finger. The clamped end of the sample that is connected to the finger is able to move from the extended (0 deg.) to the flexed position (90 deg.). Note that the leaf spring goes from the bent (curved) configuration to the straight configuration during one cycle. Five samples were cyclically loaded at 0.5 Hz until failure.

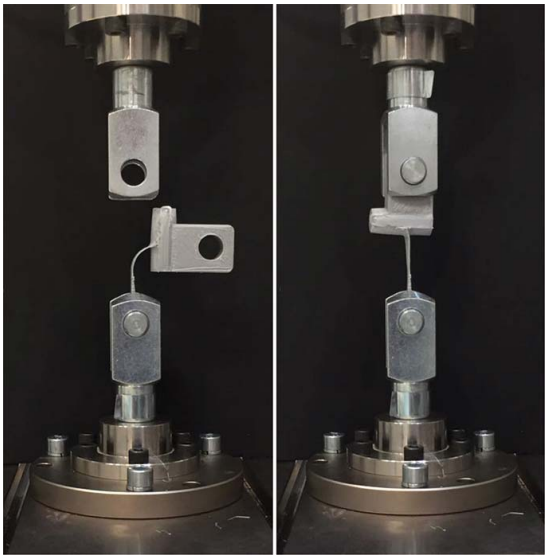

Figure 5.2: The experimental set-up for the leaf spring ultimate strength test. The leaf spring is in its neutral configuration *(left)*. 3D-printed sample under tensile and bending loading conditions during experiment. Note that the leaf

spring is bent to a straight configuration, corresponding with a 90 degrees flexion of the finger *(right).*

5.3.2 Pinch force and mechanical work

To study the mechanical performance of the prosthetic hand, a previously established test setup was employed [18, 24]. The test setup measured the input force using a load cell (Zemic: FLB3G-C3-50 kg-6B), the pinch force of the prosthetic hand using a 11 mm-thick cover encasing a FUTEK LLB130 load cell positioned on the tip of thumb, and the actuation displacements of the driving cable using a displacement sensor (Schaevitz: LCIT 2000). The variables of interest are (1) pinch force output, delivered by the contact between the thumb and the index and middle fingers, given a driving input force and displacement and (2) the energy used to close and open the prosthesis for one cycle.

The measurements of the energy input to close the device and the energy returned to move the fingers back to the straight configuration were used to calculate the mechanical efficiency of the hand prosthesis. The energy utilized in each opening-closing cycle could be calculated as the integration of the cable loads along the measured driving cable displacements. A calculation of energy dissipation can be acquired as the subtraction of the input energy minus the returned energy. Figure 5.3 shows the test setup. In order to quantify the concerning variables, the subsequent procedure was used. First, a cycle of closing and opening with no pinch force measurements was repeated five times. Second, closing and holding into a pinch grasp the load cell until an activation force of 100 N was attained. The index and middle fingers pressed the load cell against the thumb as they were moved towards the thumb by activation of the prosthetic hand. Note that the ring finger and little finger moved until they met the maximum closing angle (90 degrees), at which point the whole system was in equilibrium.

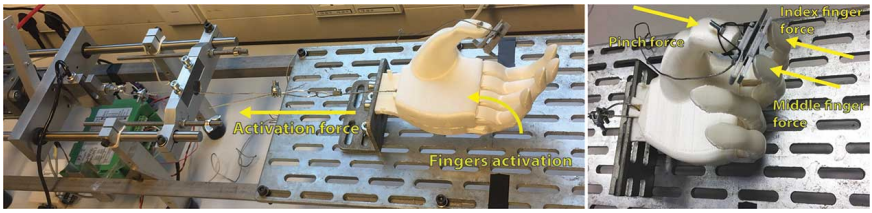

Figure 5.3: The experimental setup to measure the activation and pinch forces (*left*). The index and middle fingers push the load cell against the thumb. The ring and little fingers meet the maximum closing angle (90 degrees) (*right*).

5.3.3 Functional testing

The prosthesis design was assessed using the Box and Blocks Test (BBT) [25] and the Southampton Hand Assessment Procedure (SHAP) test [26], which are well-established tests for evaluation prosthetic designs with prosthetic users [27, 28]. The BBT consists of 25 mm wooden square cubes and a container separated in two areas by a wall in the middle. The subject must transfer as many blocks as possible from one area into the other. The score is registered as the number of blocks the subject is able to transfer within 1 minute. The SHAP test consists of a first part in which the user has to move abstract items with different shapes and weights, and a second part in which some activities of daily living (ADL) have to be completed by the user. This test measures the ability of the user to perform spherical, power, tip, tripod, lateral and extension grasping. The times to perform all activities are measured and uploaded to the online SHAP test center [29] in order to obtain the SHAP index of function (IOF).

Twenty able-body and right-handed students or employees of the Delft University of Technology (8 males and 12 females; age: 22-32) were recruited. Ten (4 males and 6 females; age: 27 ±5) were assigned to perform both tests. During the tests, our 3D-printed prosthesis was attached to a strapped cuff that fits around the user's forearm (TRS Inc.) in order to use it as a prosthesis simulator. The fingers were driven by pulling a Bowden cable attached to a figure-of-nine shoulder harness (Figure 5.4). The simulator was placed at the dominant arm of the subject. The study was approved by the human research

ethics committee of the Delft University of Technology. Written informed consent to participate in the study was obtained for all subjects.

The subjects were allowed to perform two practice sessions of BBT to get familiarized with the test setup before being scored. Afterwards, the BBT was repeated four times followed by one implementation of the SHAP test given the inherent long testing time (45-60 min for one test of the SHAP). The first results suggested poor friction properties over the interacting surfaces used for grasping (i.e., finger pads), as the objects tended to slip away during testing. To assess the effects of such friction properties on the performance of the prosthesis, the other ten subjects (4 males and 6 females; age: 27.5 ±2.5) were assigned to perform the BBT with our 3D-printed hand prosthesis enhanced by sticking strips of gaffer tape over the surface of the finger pads to increase the friction to a level that objects did not slip out of the fingers anymore during the tests (Figure 5.5). The subjects were again allowed to perform two practice sessions of BBT and then four sessions of BBT were performed and recorded. The median score of the last trial of all subjects was calculated and used as a functional metric of the BBT to compare with other BP prostheses. The median of the last trial of all subjects is more consistent because of the effects of a learning curve. Using the average of means for all subjects would include trials where the subject is still not fully familiarized with the device and thus evidencing not low functionality of the device but rather inexperience of the subject when using it. The median is also less susceptible to the occurrence of outliers than the average.

5.4 Results

5.4.1 The ultimate tensile strength of the leaf springs and fatigue life

Figure 5.6 shows the mechanical behavior of the leaf spring design under tension and bending loading. The ultimate load to failure of the five tests was 316 N ± 22.7 (mean ±SD) which is significantly larger than the required

maximum of 134.5 N. The number of cycles to failure of the five leaf spring samples was 2446 cycles ± 499 (mean ±SD).

Figure 5.4: Our 3D printed prosthetic hand attached to the simulator and a figure-of-nine shoulder harness. The cable tension that is delivered by the harness and activates the prosthetic hand is depicted *(left).*

Figure 5.5: Our 3D-printed prosthetic hand attached to the simulator and used by the participating subjects *(left)* for the Box and Blocks test *(top right)* and the

SHAP test *(bottom right).* Gaffer tape strips were put over the thumb, the index, and middle fingers to increase grip *(right)*.

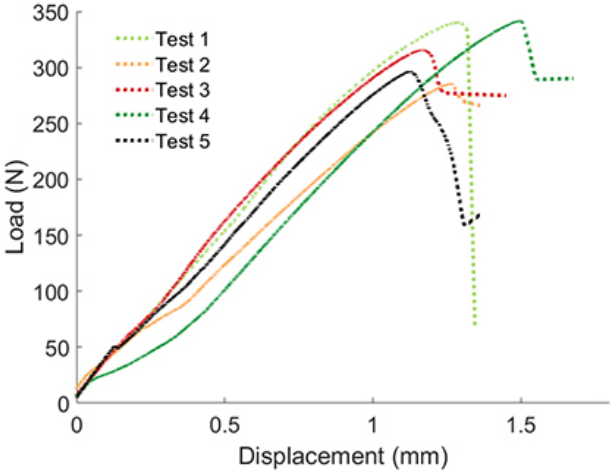

Figure 5.6: A Load vs. displacement response for five samples of the leaf spring configuration.

5.4.2 Pinch force and mechanical work

The five closing-opening cycles are shown in Figure 5.7 (left). A full closing-opening cycle and the relationship between the input force and output pinch force over the index and middle fingers is shown in Figure 5.7 (right). The energy used to close the prosthetic hand was computed as $0.104 \pm 6 \times 10^{-3}$ Nm and the energy dissipated for one cycle of closing and opening motion was computed as $0.048 \pm 3 \times 10^{-3}$ Nm.

5.4.3 Functional testing

The scores of the box and blocks test and the IOF of the SHAP test are shown in Table 1 and Table 2. For the prosthetic device without further modifications the median score of the last trial (4^{th}) of the BBT among all subjects is 14 blocks and the average IOF for the SHAP is 33.1. For the prosthetic device with enhanced

friction properties the median score of the last trial (4^{th}) of the BBT among all subjects is 21 blocks (Figure 5.8).

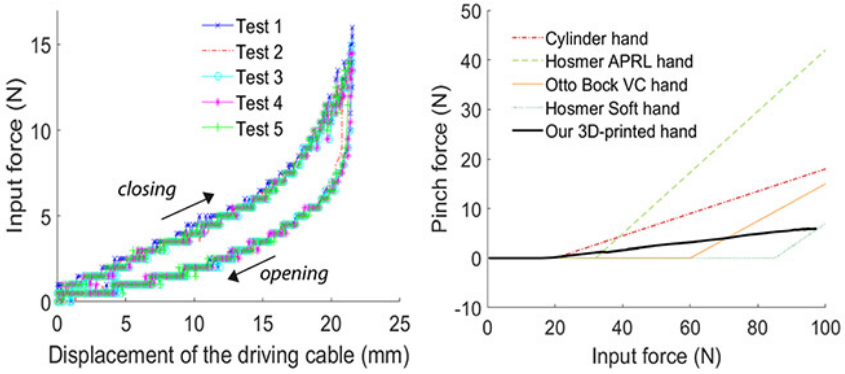

Figure 5.7: The results of the mechanical assessment of the prosthesis. Cable displacement vs. the input force for five closing-opening cycles *(left)* and a representative trial of the input force vs. pinch force including commercially available prostheses subjected to the same testing protocol (adapted from [24] and [21]) *(right)*.

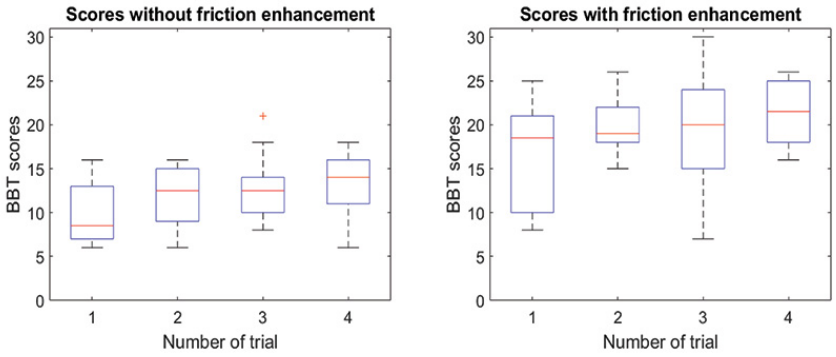

Figure 5.8: Scores during the BBT in four trials for the 3D-printed hand without any modifications *(left)* and the 3D-printed hand with friction enhancement *(right)*.

Table 5.1. Scores of the box and blocks tests and Index of function (IOF) from SHAP test.

Subject	*1*	*2*	*3*	*4*	*5*	*6*	*7*	*8*	*9*	*10*
Mean # of blocks	**7.8**	**11**	**17.5**	**11.5**	**12.8**	**8**	**12**	**15**	**13**	**12.3**
(Std. deviation)	**(±2.4)**	**(±2.9)**	**(±2.6)**	**(±4.9)**	**(±1.9)**	**(±0.8)**	**(±3.7)**	**(±1.2)**	**(±3.7)**	**(±1.7)**
Median of the last (4^{th}) trial	**14**									
IOF	**31**	**13**	**37**	**40**	**31**	**14**	**36**	**48**	**40**	**41**
Average	**33.1**									

Table 5.2. Scores of the box and blocks tests for the prosthetic hand with increased friction properties over the finger pads.

Subject	*1*	*2*	*3*	*4*	*5*	*6*	*7*	*8*	*9*	*10*
Mean # of blocks	**26.8**	**18.3**	**17.8**	**15.8**	**13**	**14**	**21.5**	**20**	**23.5**	**22.3**
(Std. deviation)	**(±2.2)**	**(±3.9)**	**(±1.3)**	**(±4.8)**	**(±5.8)**	**(±4.2)**	**(±2.4)**	**(±2.2)**	**(±1.3)**	**(±3.4)**
Median of the last (4^{th}) trial	**21**									

5.5 Discussion

We have fabricated a prosthetic hand with reduced post-assembly requirements using 3D printing technology. Apart from the removal of support structures and a single snap-fit step the hand was successfully designed following a non-assembly approach. The hand achieves adaptive grasping even though is made out of only two parts. We argue that such a design and fabrication approach can increase accessibility of hand prostheses since easy accessible low cost equipment (an Ultimaker 3 3D printer) was used together with low-cost material (PLA).

The leaf spring strength requirement has been met. The measurements show a significantly larger load to failure (316 N ± 22.7) than required (134.5 N). The thin sheet of PLA material fabricated to serve as a spring component is able to work under the static loading conditions proposed in this prosthetic design. On the other hand, the fatigue life experiments show that the leaf spring is not able to withstand cyclic loading for a prolonged period. The material used for the leaf spring is therefore not suitable to ensure long-term durability and reliability of the prosthetic hand. The use of other materials suitable for 3D printing might provide better fatigue life properties for such compliant configurations like the leaf spring. Further investigations aimed to study the fatigue life of compliant mechanisms fabricated with 3D-printed polymers should be conducted.

The design choices made for the mechanisms led to a prosthetic hand that needs considerable lower energy (0.104 Nm ± 6 x 10^{-3}) to close as compared to other BP prosthetic hands (1.1–2.3 Nm or J [24]). Additionally, the activation force (16-18 N) needed for the onset of a pinch grasp on the 11 mm pinch load cell is considerably lower as compared to other alternatives [24] (Figure 5.7). This indicates that the user has to put less energy in order to close our hand prosthesis. The force transmission (Pinch force/Input force) to the fingertips is lower than other BP prosthetic hands as indicated by the slopes shown in Figure 5.7 (right). The pinch force achieved by the index and middle fingers given a force input of 100 N is low (6 N) in comparison to other BP prostheses (10-60 N) [24].

The results of the box and blocks test (median 14 blocks) and the SHAP (average overall IOF of 33.1) indicate lower functionality of the device compared to other BP alternatives (median 17-30 blocks [27] [30]; average overall IOF of 65.75-66.05 [31] and 64-65 [32]). This could be explained partly by the low pinch forces and the lack of friction between the fingertips (made of PLA material) and the objects involved in the test. An increase of the friction coefficient of the finger pads led to better performances of the box and blocks test (median 21 blocks), reaching comparable scores to that of other BP hands. This highlights the importance of friction of the fingertips for improving the performance of 3D-printed prosthetic hands and indicates that new finger designs providing high friction surfaces should be developed. These high friction surfaces should be considered in other parts of the hand that are also involved in daily grasping, these include the anterior side of: the rest of each finger, the rest of the thumb and the palm. Moreover, a learning curve effect can be considered as the scores of the BBT tend to be higher on the 4^{th} trial (Figure 5.8). It is likely, yet unproven, that scores could improve if the subjects had repeated the test more times since learning curve effects have been demonstrated in BP prosthetic users at least up to the 9^{th} trial in BBT [27].

Our design is one of the few entirely 3D printed and BP hands that has been assessed by mechanical and user testing. Only one 3D printed hand reports comparable force measurements over the fingertips (3.9-11.5 N) [33] and only one study presents results of a SHAP test on a 3D printed hand [34], not reporting, however, IOF scores. Just another study performs a BBT on a 3D printed hand (Cyborg beast) (13 ± 12.7 blocks) scoring similarly to our 3D printed non-assembly hand [35], although our design performs better in comparison when using friction enhancements over the finger pads. Interestingly Zuniga et al. is one of the few that provide other clinical metrics like range of motion or wrist strength [35, 36]. Apart from prosthesis for partial hand amputation [37-39], little is known about the performance and reliability of most 3D printed hand prostheses. Most studies of fully 3D printed hand prostheses do not present any kind of evaluation on the short or long term use [12] or use other different metrics making a direct comparison with the

prosthetic hand presented here very limited. The data acquired during this study can be used as a basis for future developments on 3D printed prosthetic hands.

The prosthetic design assessed in this work shows functional characteristics (Box and Blocks and SHAP scores) that are not yet matching the traditional BP prosthetic devices. Nevertheless, the 3D-printed hand evaluated in this study shows a comparable performance with just a small friction enhancement on the finger pads. Yet, grasping and functionality can be improved by increasing the pinch force. Moreover, it is worth noting that most activities of daily living require low grip forces [40]. This suggests that with such level of functionality and considering that this hand was mainly designed to reduce manufacturing requisites to just one 3D printer and its fabrication material, we can consider the design and manufacturing strategies used for this prosthetic hand as valuable approaches that could aid in improving the access to prosthetic devices in developing countries. To finally demonstrate the usefulness of the prosthetic hand, further usability studies involving end-users with upper limb absence should be conducted including close follow-up checks and questionnaires.

5.6 Conclusion

We have fabricated a hand prosthesis using 3D printing technology and a non-assembly design approach that reaches certain level of functionality. The mechanical resistance of critical parts (leaf spring), the mechanical performance, and the functionality of a non-assembly 3D-printed hand prosthesis were assessed. The leaf spring configuration used in the hand prosthesis is able to withstand typical actuation forces delivered by prosthetic users. Moreover, the activation forces and the energy required for a closing cycle are considerably lower as compared to other BP prostheses. Conversely, the achievable pinch force and the functionality scores are in comparison significantly lower. The results also suggest that increased friction over the finger pads is highly beneficial for the prosthesis functionality. Direct comparison with other existing 3D-printed hands was not possible given the

lack of data in the literature. The results presented in this study can be used as a starting point for future developments on 3D-printed prosthetic hands.

The non-assembly design achieved a comparable level of functionality with respect to other BP alternatives. Taking into consideration that most activities of daily living require low gripping forces and adding an increased accessibility provided by the advantages of the non-assembly and 3D printing approach, we consider this prosthetic hand a valuable option for people with arm defects in developing countries.

5.7 References

[1] M.P. Fahrenkopf, N.S. Adams, J.P. Kelpin, V.H. Do, Hand Amputations, Eplasty 18 (2018) ic21.

[2] W.H. Organization, Standards for P&O Service Provision | ISPO, (2015).

[3] M. Marino, S. Pattni, M. Greenberg, A. Miller, E. Hocker, S. Ritter, K. Mehta, Access to prosthetic devices in developing countries: Pathways and challenges, 2015 IEEE Global Humanitarian Technology Conference (GHTC), 2015, pp. 45-51.

[4] L. Magnusson, G. Ahlström, Experiences of providing prosthetic and orthotic services in Sierra Leone – the local staff's perspective, Disabil Rehabil 34(24) (2012) 2111-2118.

[5] R.A. Gosselin, The Increasing Burden of Injuries in Developing Countries: Direct and Indirect Consequences, Tech Orthop 24(4) (2009) 230-232.

[6] I. Grobler, G.J. van Schalkwyk, C. Wagner, The Application of Critical Psychology to Facilitate Reflective Clinical Practice in Orthotics/Prosthetics, Prosthet Orthot Int 30(3) (2006) 237-245.

[7] D. Wyss, S. Lindsay, W.L. Cleghorn, J. Andrysek, Priorities in lower limb prosthetic service delivery based on an international survey of prosthetists in low- and high-income countries, Prosthet Orthot Int 39(2) (2015) 102-111.

[8] K.F. Gretsch, H.D. Lather, K.V. Peddada, C.R. Deeken, L.B. Wall, C.A. Goldfarb, Development of novel 3D-printed robotic prosthetic for transradial amputees, Prosthet Orthot Int 40(3) (2016) 400-3.

[9] J. Zuniga, The Cyborg Beast, 2014. https://www.unomaha.edu/college-of-education/biomechanics-core-facility/research/cyborg-beast/index.php. (Accessed 19/07/2018 2018).

[10] e-NABLE, The Raptor Hand, 2014. http://enablingthefuture.org/upper-limb-prosthetics/the-raptor-hand/. (Accessed 19/07/2018 2018).
[11] B. Phillips, G. Zingalis, S. Ritter, K. Mehta, A Review of Current Upper-Limb Prostheses for Resource Constrained Settings, Proceedings of the Fifth Ieee Global Humanitarian Technology Conference Ghtc 2015 (2015) 52-58.
[12] J. ten-Kate, G. Smit, P. Breedveld, 3D-printed upper limb prostheses: a review, Disabil Rehabil Assist Technol 12(3) (2017) 300-314.
[13] C. Mavroidis, K.J. DeLaurentis, J. Won, M. Alam, Fabrication of Non-Assembly Mechanisms and Robotic Systems Using Rapid Prototyping, Journal of Mechanical Design 123(4) (2000) 516-524.
[14] F. Calignano, D. Manfredi, E.P. Ambrosio, S. Biamino, M. Pavese, P. Fino, Direct Fabrication of Joints based on Direct Metal Laser Sintering in Aluminum and Titanium Alloys, Procedia CIRP 21 (2014) 129-132.
[15] M.W.M. Groenewegen, M.E. Aguirre, J.L. Herder, Design Of a partially compliant, three-phalanx underactuated prosthetic finger, Proceedings of the ASME Design Engineering Technical Conference, 2015.
[16] Y. Wei, Y. Chen, Y. Yang, Y. Li, Novel Design and 3-D Printing of Nonassembly Controllable Pneumatic Robots, IEEE/ASME Transactions on Mechatronics 21(2) (2016) 649-659.
[17] J.S. Cuellar, G. Smit, D. Plettenburg, A. Zadpoor, Additive manufacturing of non-assembly mechanisms, Addit Manuf 21 (2018) 150-158.
[18] J.S. Cuellar, G. Smit, A. Zadpoor, P. Breedveld, Ten guidelines for the design of non-assembly mechanisms: The case of 3D-printed prosthetic hands, Proc Inst Mech Eng H (2018) 954411918794734.
[19] S.S. Crump, Apparatus and method for creating three-dimensional objects, in: S. United (Ed.) Stratasys Inc, 1992.
[20] D.H. Plettenburg, Basic requirements for upper extremity prostheses: the WILMER approach, Proceedings of the 20th Annual International Conference of the IEEE Engineering in Medicine and Biology Society. Vol.20 Biomedical Engineering Towards the Year 2000 and Beyond (Cat. No.98CH36286), Hong Kong, 1998, pp. 2276-2281 vol.5.
[21] G. Smit, D.H. Plettenburg, F.C.T. van der Helm, The Lightweight Delft Cylinder Hand: First Multi-Articulating Hand That Meets the Basic User Requirements, Ieee T Neur Sys Reh 23(3) (2015) 431-440.
[22] J.R.C. Dizon, A.H. Espera, Q. Chen, R.C. Advincula, Mechanical characterization of 3D-printed polymers, Addit Manuf 20 (2018) 44-67.

[23] M. Hichert, A.N. Vardy, D. Plettenburg, Fatigue-free operation of most body-powered prostheses not feasible for majority of users with trans-radial deficiency, Prosthet Orthot Int 42(1) (2018) 84-92.
[24] G. Smit, D.H. Plettenburg, Efficiency of Voluntary Closing Hand and Hook Prostheses, Prosthetics and Orthotics International 34(4) (2010) 411-427.
[25] V. Mathiowetz, G. Volland, N. Kashman, K. Weber, Adult norms for the Box and Block Test of manual dexterity, Am J Occup Ther 39(6) (1985) 386-91.
[26] C.M. Light, P.H. Chappell, P.J. Kyberd, Establishing a standardized clinical assessment tool of pathologic and prosthetic hand function: normative data, reliability, and validity, Arch Phys Med Rehabil 83(6) (2002) 776-83.
[27] L. Haverkate, G. Smit, D.H. Plettenburg, Assessment of body-powered upper limb prostheses by able-bodied subjects, using the Box and Blocks Test and the Nine-Hole Peg Test, Prosthet Orthot Int 40(1) (2016) 109-16.
[28] L. Resnik, M. Borgia, B. Silver, J. Cancio, Systematic Review of Measures of Impairment and Activity Limitation for Persons With Upper Limb Trauma and Amputation, Arch Phys Med Rehab 98(9) (2017) 1863-1892.
[29] C.M. Light, P.H. Chappell, P.J. Kyberd, SHAP: Southampton Hand Assessment Procedure, 2002. http://www.shap.ecs.soton.ac.uk/entry.php. (Accessed 23/05/2018.
[30] T.R. Farrell, R.F. Weir, The optimal controller delay for myoelectric prostheses, IEEE Trans Neural Syst Rehabil Eng 15(1) (2007) 111-8.
[31] I.A. Ramirez, C.P. Lusk, R. Dubey, M.J. Highsmith, M.E. Maitland, Crossed four-bar mechanism for improved prosthetic grasp, J Rehabil Res Dev 46(8) (2009) 1011-20.
[32] J.T. Belter, M.T. Leddy, K.D. Gemmell, A.M. Dollar, Comparative Clinical Evaluation of the Yale Multigrasp Hand, P Ieee Ras-Embs Int (2016) 528-535.
[33] K. Andrianesis, A. Tzes, Development and Control of a Multifunctional Prosthetic Hand with Shape Memory Alloy Actuators, J Intell Robot Syst 78(2) (2015) 257-289.
[34] C. Dally, D. Johnson, M. Canon, S. Ritter, K. Mehta, Characteristics of a 3D-Printed Prosthetic Hand for Use in Developing Countries, Proceedings of the Fifth Ieee Global Humanitarian Technology Conference Ghtc 2015 (2015) 66-70.
[35] J.M. Zuniga, J.L. Peck, R. Srivastava, J.E. Pierce, D.R. Dudley, N.A. Than, N. Stergiou, Functional changes through the usage of 3D-printed transitional prostheses in children, Disabil Rehabil Assist Technol 14(1) (2019) 68-74.

[36] J.M. Zuniga, J.L. Peck, R. Srivastava, D. Katsavelis, A. Carson, An open source 3D-printed transitional hand prosthesis for children, J Prosthet Orthot 28(3) (2016) 103-108.
[37] P. Alvial, G. Bravo, M.P. Bustos, G. Moreno, R. Alfaro, R. Cancino, J.C. Zagal, Quantitative functional evaluation of a 3D-printed silicone-embedded prosthesis for partial hand amputation: A case report, J Hand Ther 31(1) (2018) 129-136.
[38] J.M. Zuniga, 3D Printed Antibacterial Prostheses, Appl Sci-Basel 8(9) (2018).
[39] K.H. Lee, S.J. Kim, Y.H. Cha, J.L. Kim, D.K. Kim, S.J. Kim, Three-dimensional printed prosthesis demonstrates functional improvement in a patient with an amputated thumb: A technical note, Prosthet Orthot Int 42(1) (2018) 107-111.
[40] J.T. Belter, J.L. Segil, A.M. Dollar, R.F. Weir, Mechanical design and performance specifications of anthropomorphic prosthetic hands: A review, J Rehabil Res Dev 50(5) (2013) 599-617.

Chapter 6: 3D printed hand prosthesis featuring bio-inspired fingers

Juan Sebastian Cuellar, Dick Plettenburg, Amir A. Zadpoor, Paul Breedveld and Gerwin Smit

Published as:

Design of a 3D-printed hand prosthesis featuring articulated bio-inspired fingers, Proc Inst Mech Eng H. Preprint (2020). DOI: https://doi.org/10.1177/0954411920980889

Abstract

Various upper-limb prostheses have been designed for 3D printing but only a few of them are based on bio-inspired design principles and many anatomical details are not typically incorporated even though 3D printing offers advantages that facilitate the application of such design principles. We therefore aimed to apply a bio-inspired approach to the design and fabrication of articulated fingers for a new type of 3D printed hand prosthesis that is body-powered and complies with basic user requirements. We first studied the biological structure of human fingers and their movement control mechanisms in order to devise the transmission and actuation system. A number of working principles were established and various simplifications were made to fabricate the hand prosthesis using a fused deposition modelling (FDM) 3D printer with dual material extrusion. We then evaluated the mechanical performance of the prosthetic device by measuring its ability to exert pinch forces and the energy dissipated during each operational cycle. We fabricated our prototypes using three polymeric materials including PLA, TPU, and Nylon. The total weight of the prosthesis was 92 g with a total material cost of 12 US dollars. The energy dissipated during each cycle was 0.380 N.m with a pinch force of ≈16 N corresponding to an input force of 100 N. The hand is actuated by a conventional pulling cable used in BP prostheses. It is connected to a shoulder strap at one end and to the coupling of the whiffle tree mechanism at the other end. The whiffle tree mechanism distributes the force to the four tendons, which bend all fingers simultaneously when pulled. The design described in this manuscript demonstrates several bio-inspired design features and is capable of performing different grasping patterns due to the adaptive grasping provided by the articulated fingers. The pinch force obtained is superior to other fully 3D printed body-powered hand prostheses, but still below that of conventional body powered hand prostheses. We present a 3D printed bio-inspired prosthetic hand that is body-powered and includes all of the following characteristics: adaptive grasping, articulated fingers, and minimized post-printing assembly. Additionally, the low cost and low weight make this

prosthetic hand a worthy option mainly in locations where state-of-the-art prosthetic workshops are absent.

6.1 Introduction

The demand for prosthetic limbs is rising as the number of amputations is increasing worldwide. In the United States alone, it is estimated that 185.000 amputations are performed every year [1]. The demand for upper limb prostheses is important since a relevant percentage of all limb loss cases are related to the upper limb(s). In the United States a total of 41.000 cases of trans-radial and trans-humeral amputations were estimated in 2005 [2]. The after-effects of an upper limb loss can be devastating both for the mental and physical well-being of the amputee. Designing and fabricating an upper limb prosthesis is therefore essential in order to help amputees to recover functionality and increase their quality of life [3].

The ultimate goal of prosthetic devices is to mimic the functionality of a missing body part. Unfortunately, the complexity of anatomic structures in a real hand is such that prosthetic designs have to be simplified to facilitate fabrication with current technologies. In this context, designers tend to disregard biological principles, instead opting for existing conventional design methods that they are confident would work and provide partial functionality of the missing body part. These conventional approaches guide the design process of most of the prosthetic hands found in the literature. The designers will, in most cases, use standard parts and mechanisms such as helical springs, screws, cables, *etc*. Examples of such designs are reviewed in the work of Belter *et al*. [4] including descriptions of a number of mechanical specifications. Many working principles of a number of anatomical structures, like finger pads, ligaments, tendons or skin that could improve the performance of current hand prostheses, are usually not present in their designs [4, 5]. One simple example is to include sliding joints similar to the ones found in the human finger instead of conventional hinged joints.

3D printing is a relatively new, rising technology that facilitates the manufacturing of parts with irregular and uncommon geometric shapes [6]. The form-freedom offered by 3D printing techniques has paved the way for the application of new design approaches; for example the non-assembly design approach [7, 8]. Current 3D-printed hands are based on a mechanical inspired design, rather than a biological inspired design. Previous hand prostheses produced by 3D printing are typically articulated by hinged joints, are assembled with screws and driven and stabilized by cables or mechanical linkages, e.g. [9-14]. Others have rather opted for 3D printed compliant mechanisms such as joints and/or extensors of the fingers [8, 15-17], but still using conventional driving mechanisms. Bio inspiration then serves as design alternative founded on the idea that biological designs are different, and that in this difference new and smart solutions can be found that we do not find in conventional technical approaches. By studying something that is entirely different, gateways to other worlds of solutions can be opened expanding creativity. Bio-inspiration is not about simply copying these other worlds, but about using this knowledge to find new combinations of solutions that could be better as compared to solutions just drawn from pure technical backgrounds. A few examples originating from this include biarticular actuators by Sharbafi *et al.* [18], a rolling robot by Lin *et al.* [19], a micro air vehicle by Nguyen *et al.* [20] and a surgical steerable needle by Scali *et al.* [21]. In the same way, following a design approach inspired by human anatomy could improve the performance of prosthetic hands.

The advantages of 3D printing could be used to fabricate advanced, yet simple to print, prosthetic hands based on the biological design principles in human hands. A bio-inspired design approach could be a more practical way of incorporating new beneficial features into a prosthetic hand instead of mimicking the biological structures with synthetic materials. In this study, we therefore aimed to identify working principles in the human hand that can be included in a new prosthetic hand using 3D printing technology. We then applied a bio-inspired approach to the design and fabrication of articulated fingers that allows for the execution of multiple grasping patterns.

Our bio-inspired design approach started with the study of the biological assembly of the human finger: the bones (links) and the structures that connect them (joints). We then continued with an analysis of the anatomic elements for force and motion control in order to devise the transmission and actuation system (*i.e.*, muscles, tendons, anatomical pulleys, and tendon sheaths). Structures such as the nerves and veins are out of the scope of this study, because their function is not directly related to the mechanical performance of the finger. A human finger consists of four rigid bones, starting from proximal to distal, the metacarpal (MC), proximal phalanx (PP), middle phalanx (MP), and distal phalanx (DP). The interconnecting joints are the metacarpophalangeal (MCP) joint, the proximal inter-phalangeal (PIP) joint, and the distal inter-phalangeal (DIP) joint. Two different forms of joints can be distinguished in this regard: hinged joints that permit flexion/extension and ellipsoid joints that also allow for adduction/abduction (rotation around the dorsal-palmar direction). This corresponds to 1 degree of freedom (DoF) at the PIP and DIP joints (hinged) and 2 DoF at the MCP joint (ellipsoid), respectively. More distinctively, in the hinged joints, there is a tongue along the convex surface and a groove along the concave surface of the joint, this helps to prevent lateral translation (Ulnar-Radial directions, see Figure 6.1) [22].

Ligaments connect the bones of the hand to one another. Their main role is to stabilize the joints and constrain the range of motion of the bones. The *collateral ligaments* are found on the lateral sides of the joints, see Figure 6.1; the proper ligament is attached eccentrically with the shape of a cord and the accessory ligament initiates from the center of rotation of the proximal side of the joint and is fixed to the palmar plate in a fan shape. These two ligaments restrict translation of the bones to the distal direction of the finger and also movement to the Ulnar-Radial direction[22], see Figure 6.1.

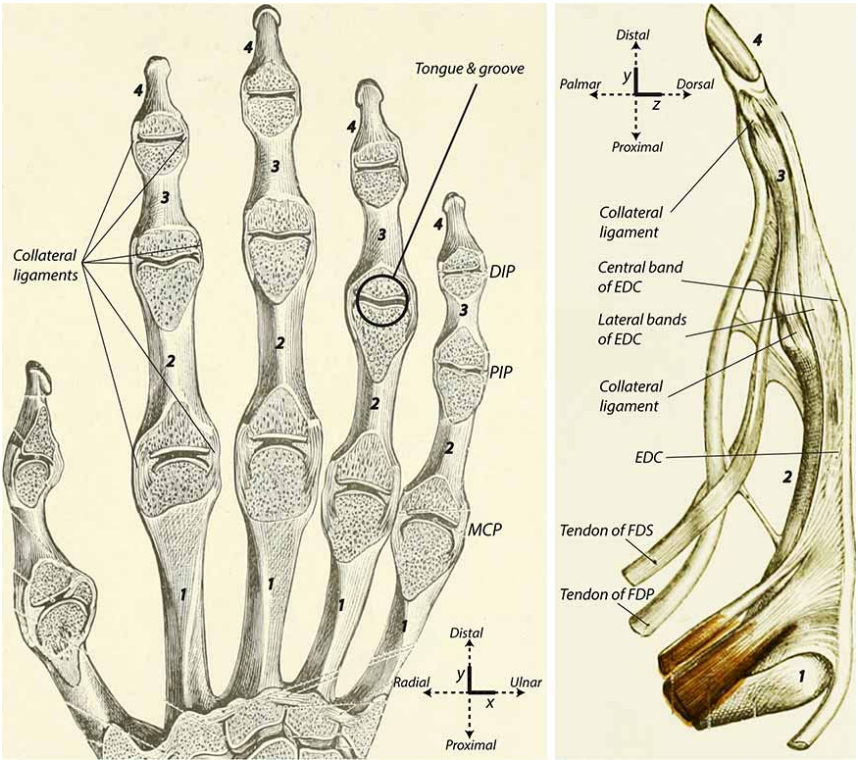

Figure 6.1: Anatomy of the finger. *(Left)* Dorsal aspect of the bones of the human hand. The metacarpophalangeal (MCP) joint, the proximal inter-phalangeal (PIP) joint, the distal inter-phalangeal (DIP) joint, the tongue and groove configuration inside the joints and collateral ligaments are shown. *(Right)* Ulnar aspect of the middle finger of the human hand. Also shown: The tendons of the flexor digitorum profundus (FDP) and the flexor digitorum superficialis (FDS), the central and lateral bands of the extensor digitorum comunis (EDC) and collateral ligaments. For both images: 1) Metacarpal bone (MC), 2) Proximal phalanx (PP), 3) Middle phalanx (MP) and 4) Distal phalanx (DP) are identified; anatomical directions can be seen at the bottom right corner *(left)* and upper left corner *(right)*. Modified and reprinted from [23] under a CC BY license.

The muscles can be considered to be the actuators of the finger, while the tendons are the structures that transmit the force of the muscles to the bones. Two groups of muscles and tendons are primarily used for the flexion of the fingers, namely the flexor digitorum profundus (FDP) and the flexor digitorum superficialis (FDS), see Figure 6.1. The FDP is the main flexor. The FDS contributes to exert larger forces when the FDP is not providing sufficient force. The mechanical configuration of the finger is therefore underactuated (more DoF than actuators) during the flexion of the human finger (3 DoF, 2 actuators). The central band of the extensor digitorum comunis (EDC) has the principal role of extending the MCP joint. The lateral bands of the EDC have two functions depending on the position of the bands with respect to the center of rotation of the joint: they can either aid to extend or flex the PIP and DIP joint. As the phalanges move, the bands of the EDC move to the other side of the center of rotation providing a moment to the opposite direction and favoring the flexion of the joints [22]. Interestingly, the flexor and extensor tendons inside the hand have different cross-sectional area shapes depending on the function and location. For example, the tendons of the FDS have an oval shape over the region of the MCP joint, they flatten close to the middle of the PP and then splits into halves [24].

The sheaths and pulleys form a kind of 'tunnel' that keeps the tendons in place and constrains their excursion. They fulfil the role of keeping the force delivered by the flexor muscles perpendicular to the center of rotation of the joint [25]. Sheaths are located over the anterior side of the finger and prevent the dislocation of the extensor tendon. On the palmar side, fibrous sheaths enclose the finger along its full length. A sequence of flexible bands strengthens the fibrous sheaths at intervals forming the pulleys [26].

6.2 Design of the prosthetic hand

6.2.1 Simplifications for applications in body powered (BP) hand prostheses

We continued our design by establishing a number of basic (*i.e.*, functional) requirements for the hand prosthesis based on the work by Plettenburg [27]: body-powered (BP) control, cosmetic appearance, light weight, and water/dirt resistance (materials resisting any contact with water and dirt). A number of simplifications as compared to the human hand are therefore considered in order to fulfil these criteria.

BP hand prostheses use a single driving input to activate the grasper. Individual finger control or multi-degree of freedom thumb control are thus not feasible; to comply with this requirement we decided for a static thumb and four active fingers for the grasping action. The movement of the active fingers can then be controlled by a single driving link. This means that there is one movement available, which is the simultaneous closing of the four fingers. Furthermore, natural underactuation during the flexion of the human finger (3 DoF, 2 actuators) must be simplified to a single actuator as well. Moreover, the number of DoF per finger in the human hand is problematic from a mechanical design standpoint, as every joint adds a force loss associated with friction. We therefore decided to reduce the number of DoF per finger from three to two by combining the distal and medial phalanges into a single link. As a result, each finger can be driven by a single tendon-based transmission system guided by two rigid pulleys connected at the end of each joint. In this way, the FDP and FDS are merged into a single muscle-tendon system. At the same time, force can be distributed to all fingers using a whiffle tree configuration similar to our previous design [8]. The pulley system is simplified to only three annular pulleys per finger (one per joint and one over the MC bone), since extra guiding elements would increase the contact points of the driving tendon and thus the friction associated with its activation. In contrast with the biological counterpart, lubricant fluids are not considered. The complex structure of

tissues that holds the joints in position is also reduced to spring-like elements that constrain the motion to only one rotational DoF, i.e. flexion/extension.

6.2.2 Working principles

The shape of the links and joints is based on the shape of the human bone phalanges. The joints are designed as circular hinged joints including a tongue and groove contact at the centre of the lateral plane along the radial line of the joint (Figure 6.2), thereby restricting the lateral motion. The MCP joint is larger compared to the PIP joint. The moment arm that can be exerted with the driving cable is therefore larger at the MCP joint. A reduction of the cross–sectional area of the phalanges can be seen towards the centre, allowing for additional space where parts of the driving mechanism can be placed. The nominal size of the links is set to the average size of human bones of a sample of 253 males in the USA, as described in the work of Vicinus [28]. The size of the palm and thumb are also based on this work. The total weight of the prostheses must be below 400 g, which is below the average weight of a human hand [29].

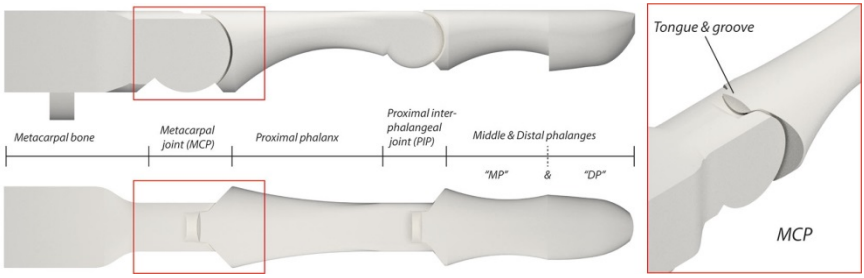

Figure 6.2: The design of the links of the prosthetic finger.

The parts that return the phalanges to a straight position are flexible strips that provide a spring-like behavior. These elements can be easily bent and stretched within the elastic region of the material and are designed similar to the biological configuration of the EDC tendons over the PIP joint, one central strip running above the dorsal side of the bones and two lateral strips, one along the ulnar direction and the other along the radial direction of the bones (Figure 6.3,

top). As the phalanges bend, the lateral flexible strips stretch, following a trajectory that reduces the moment arm to the centre of rotation (Figure 6.3, *bottom left & right*). Following the biological example, this creates less opposing moment, which favors the grasping force as the fingers bend. The range of closure is resisted for the 90 degrees bending at both joints. As the joints exceeds the 90 degrees bending the lateral bands move beyond the centre of rotation and start assisting the flexion. This is not the case in this design since the fingers are never meant to bend more than 90 degrees. Note that these flexible elements also have the role of stabilizing the joint for translation and adduction/abduction. The joint stabilizes for hyperextension once the driving system (tendons and whiffle tree mechanism) is assembled.

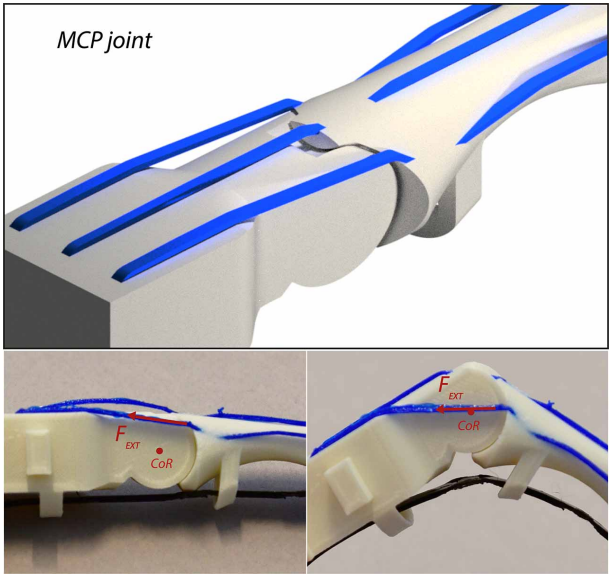

Figure 6.3: The design of the links and the connections. *(Top)* The design of the MCP joint with strip elements ("EDC tendons") in blue. *(Bottom left)* Note that in the straight configuration, the line of action of the extension force (Fext) is above the center of rotation (CoF) of the MCP joint. *(Bottom right)* The MCP joint in a flexed configuration; note that the line of action of Fext is closer to the CoF.

The mathematical formula describing friction in belt drives (Eq. 1) describes the case of cables moving around fixed circular surfaces. The ratio between the pulling tension in the direction of the moving cable T_2 and the tension at the other end of the surface T_1 depends on the coefficient of friction between the cable and the surface μ_s and the angle of contact Θ. On this basis, a tendon-based driving system that provides a smooth change between the inlet and outlet directions of the pulleys of the phalangeal joints reduces the force loss associated to friction. In other words, the angle Θ should be kept close to 0 degrees (Figure 6.4, *right*); this can be achieved by designing a driving "tendon" that bends over predefined points located in the space between pulleys. In these spaces the tendon can bend and follow the shape of the flexing finger while the segments of the tendon in contact with the pulleys remain stiff (difficult to deform), thus preventing sharp bending angles over the pulleys. The dashed lines in Figure 6.4, *right* show a tendon with no predefined bending points forming the angle Θ'. Note that angle Θ' is larger than Θ, indicating less friction force involved. The tendon bending points can be defined by modifying the geometry of the cross-sectional area of the tendon at certain segments (points identified with A and B in Figure 6.4, *left*) similar to the flexor tendons in the human hand. These segments have flatter cross-section while the nominal value of the cross-sectional area is kept identical to the rest of the tendon, i.e. the tendon is flatter but wider at those points. This provides low bending resistance of the cable at those flat points but maintains the same tensile strength at every point of the cable. To reduce the friction even further, the contact surfaces between the cable and the pulleys are rounded to reduce sharp interactions. The pulley therefore has a circular profile to the dorsal direction of the finger (where the pulley is in contact with the tendon), reducing the action of the normal forces on the contacting surfaces.

$$T_2 = T_1 e^{\mu_s \theta} \tag{6.1}$$

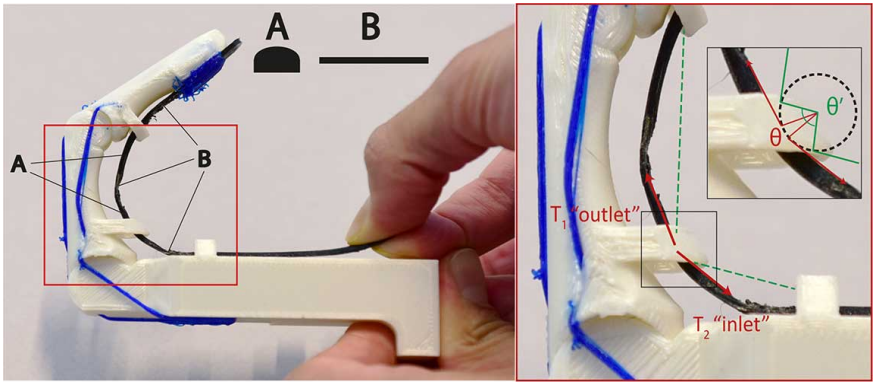

Figure 6.4: The design of the driving tendon. *(Left)* A and B represent the corresponding cross-section area at the points indicated by the lines. B is significantly flatter. However, both A and B have the same area. *(Right)* A close-up view of the pulley at the MCP joint. The angle of contact Θ between the cable and the circular surface (pulley) is shown. The dashed points in green indicate the lines of action of T1 and T2 if the tendon had the same cross-section area along its full length. The tendon would bend around the shape of the pulley. Note that Θ' is larger than Θ.

6.2.3 Design choices for 3D printing using the material extrusion technology.

An Ultimaker 3 FDM printer utilising multi-material extrusion technology was used to fabricate the design proposed in this study. This type of FDM process permits the deposition of materials with different mechanical properties. In this way, a material with a low elastic modulus can be 3D printed together with a material with a high elastic modulus. For the manufacturing of each finger, the phalanges (i.e., stiff "bony" parts) were 3D printed using Ultimaker® polylactic acid (PLA) (Ultimaker B.V., Utrecht, The Netherlands), while the connecting parts that keep the joints together (i.e., flexible "ligament" parts) were printed using Ultimaker® TPU 95A thermoplastic polyurethane (TPU) (Ultimaker B.V., Utrecht, The Netherlands). The design was prepared in such a way that the TPU parts were embedded into the PLA parts during the 3D printing process,

thereby creating fully assembled structures. Similarly, the finger pads were also fabricated in TPU together with the phalanges, embedding parts of the finger pads to the distal part of the fingers and thumb. As a soft material, TPU is able to deform elastically around an object's shape when pressed against it, increasing the friction over the finger pads and thereby enhancing grasping.

The parts fabricated in TPU are designed to stretch during maximum flexion before yielding. This elastic deformation provides spring-like behavior that returns the fingers to an extended position. A relatively low cross-section area (1.2 mm^2) is chosen to facilitate bending and tensional deformation. This is an important decision, because the force needed to achieve the flexion of the fingers should be relatively low in order to minimize user fatigue. Furthermore, the lengths of the TPU parts are selected such that sufficient elongation is provided for the full range of motion, while preventing extensions beyond the yield point , i.e. an extension of less than 55% [30].

The tendons that comprise the transmission system are 3D printed in Nylon in a second printing job. This material is both strong and ductile, allowing relatively high bending angles without failure, and has a low coefficient of friction [31]. The nominal cross-section area is set to 4 mm^2, ensuring sufficient strength to prevent yielding below a tensile load of 110 N per finger (taking the yield stress as 27.8 MPa [31]). The transmission system can then hold a total activation force of 440 N without risk of failure. This is beyond the average operational forces reported in [32]. Additionally, each tendon has a geometrical profile that reduces the interaction with the pulleys to round contacts in order to reduce the friction. The tendons are assembled manually by inserting them through the tip of the finger pads and the pulleys. Once the insertion is completed, the tendon is fixed by mechanical contact between the PP and the head of the tendon. The whiffle tree mechanism is 3D printed in PLA and assembled by manually inserting the four fixation points into the holes at the end of each tendon.

6.3 Evaluation methods

The mechanical performance of the hand prosthesis was evaluated using two criteria: (1) the energy employed to execute a pinch grasp and the energy dissipated when the prosthesis opens, and (2) pinch force output due to contact between the thumb, index, and middle fingers. These variables explain how easy it is to operate the prosthetic hand in terms of the user's energy demand and how functional the grasping function is in terms of the maximum magnitude of the force that can be exerted to an object. For this reason, an experimental setup based on previous work was used [8, 33]. It consists of two load cells and a displacement sensor. A Zemic FLB3G-C3-50 kg-6B (Zemic Europe B.V., Etten-Leur, The Netherlands) load cell was used to measure the input (pulling) force and a FUTEK LLB130 (FUTEK Advanced Sensor Technology Inc, Irvine (CA), USA) load cell housed by a 11 mm-thick cover was used to measure the pinch force. The displacement sensor measures the movement of the cable associated with the activation force of the prosthesis. The hand prosthesis was mounted on the test bench by fixing the palm to the frame and connecting the displacement sensor and the load cells. One load cell was fixed to the thumb's finger pad and the other load cell was connected together with the displacement sensor to the whiffle tree mechanism's driving link via a steel cable. An input force was then exerted to the prosthesis by pulling from the cable. No human subjects were involved to test the hand prosthesis.

The energy dissipated by the prosthesis is obtained by measuring the energy used to close (E_c) the device and the energy returned (E_r) when the fingers open to the initial state. The energy dissipated is then the difference E_c - E_r. The energy utilized in each event could be calculated as the integration of the cable forces along their related values of cable excursion. The procedure to measure the variables of interest is described as follows. First a full closing and opening cycle for a pinch grasp (until the index and middle fingers meet the thumb); and second, closing and pinching the pinch load cell until an actuation force of 100 N was reached. Each experiment was repeated five times. An average and a standard deviation were calculated for each variable. Note that

the 100 N is applied to the whiffle tree mechanism, which equally divides the force to each moving finger (25 N per finger).

6.4 Results

The 3D printed prosthetic hand was fabricated using three materials (i.e., PLA, TPU, and Nylon). The total weight of the device is 92 g and its total material price is ≈ 12 US dollars. The neutral pose of the hand is with the fingers fully extended. The hand is actuated by a conventional pulling cable used in BP prostheses that is connected to the coupling of the whiffle tree mechanism. The whiffle tree mechanism distributes the force to the four tendons which bend all fingers simultaneously as pulled. The hand can perform power, pinch, and tripod grasps as shown in Figure 6.5. The force vs. displacement curve and the pinch force measurements are presented in Figure 6.6. The energy used to close the prosthesis is 0.380 Nm ± 0.053 (mean ±SD) and the energy dissipated is 0.324 Nm ± 0.055 (mean ±SD). The pinch force measured for a 100 N input force is 16.84 N ± 0.88 (mean ±SD).

6.5 Discussion

The design described in this manuscript demonstrates several bio-inspired design features and was successfully produced using 3D printing. The device is capable of executing different grasping patterns due to the adaptive grasping provided by the articulated fingers and the whiffle tree mechanism. The assembly of the hand was minimized to two post-processing operations besides the usual support removal after 3D printing: 1. the insertion of the Nylon tendons and 2. the assembly of the force distribution system (i.e., the whiffle tree mechanism). No extra parts or tools were required. The main body of the hand, the phalanges and the connecting elements are 3D printed simultaneously with PLA and TPU taking 20 hours of printing time. The four driving tendon elements and the whiffle tree mechanism take 4 hours and 3.5 hours respectively. The 3D printer was used with the following settings: nozzle diameter: 0.4 mm, layer height: 0.15 mm, and infill: 15 %. Assuming a peak power consumption of 221 W (from the technical datasheet of the

manufacturer) the total energy usage can be estimated as 5.97 kWh for a total running time of 27 hours. The average electricity price in the Netherlands is 23 cents of euro per kWh, which at the current exchange rate yields a total energy cost of 1.5 US dollars for producing the hand.

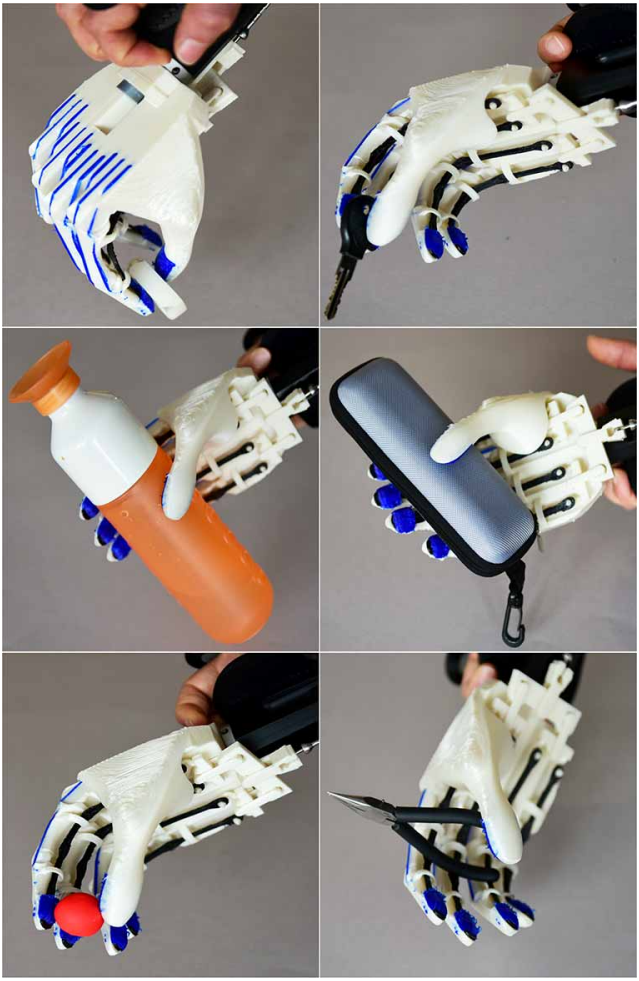

Figure 6.5: The grasping patterns. *(Top left & right)* Pinch grasping, *(middle left & right)* power grasping, *(bottom left & right)* and tripod grasping.

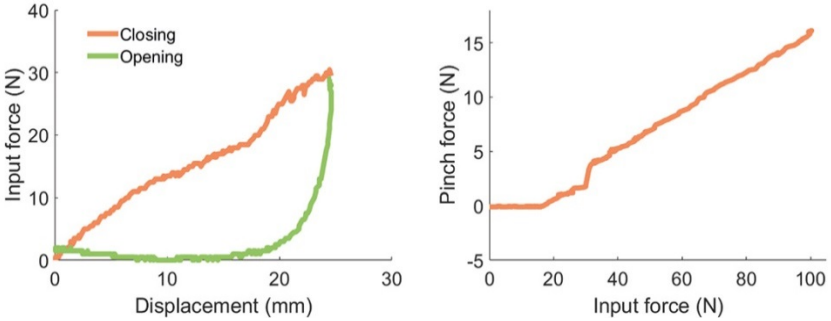

Figure 6.6: The mechanical test. *(Left)* Cable displacement vs. the input force for a closing-opening cycle. *(Right)* Input force vs. pinch force.

The manufacturing advantages of the 3D printing technology were conveniently used to fabricate an assembled mechanical device. Multi-material printing has proven to be particularly advantageous when building parts that are required to present different mechanical properties at different areas. It is worth noting that different combinations can be 3D printed, even if the materials are not bonding properly onto one another during their deposition. In our design two materials (PLA and TPU) can be 3D printed simultaneously, by embedding one of the materials into the other, thereby creating mechanical interlocking. This interlocking can withstand enough loads for the intended purpose because a high stress is never applied to these structures during normal actuation of the hand (less than 90 degrees bending per joint). These embedded parts are only subjected to the load of the TPU strips stretching during the flexion of the finger, which compared to the load at the PLA sliding joints is very low. On the other hand, the mechanical properties of these interlocked structures are mostly unknown. We encourage a study of the mechanical properties of the embedded TPU parts in PLA given different geometrical and 3D printing parameters because the mechanical behaviour could be optimized and used in future designs and applications.

Surprisingly almost all research describing 3D printed BP hand designs do not report pinch forces, e.g. [5, 10, 11, 13, 16, 17]. Just one other paper

reports grasping force measurements of a 3D printed hand (0.5 – 1 N for precision grasping), but without their corresponding activation forces [34]. In our design the pinch force achieved (16.84 N @ 100 N activation force) is superior to other fully 3D printed BP prosthetic hand (~6 N @ 100 N activation force) [8] (Chapter 5) but still below that of conventional BP hand prostheses (20-58 N @ 100 N) [33, 35]. The bio-inspired hand had a larger lever arm at the point of rotation of the PP as compared to the hand in Chapter 5. Also, the configuration of the lateral strips of each finger aids the pinch force as the gripping action is executed. The commercial BP hands that are usually produced in a factory or a specialized workshop with conventional production processes have a higher pinch force at the same activation force, but are accordingly more expensive and usually heavier and/or have no articulated fingers [35]. Due to lack of data regarding the mechanical evaluation of other 3D printed BP hands in the literature, it is impossible to establish direct comparisons [5]. The increase in the pinch force (>100%) compared to the current status of a 3D printed prosthesis is, nevertheless, noteworthy. This suggests better grasping and implies superior performance for the activities of daily life. The input force needed to start a pinch grasp (~30 N) and the energy required (0.380 Nm) are however higher than that of the other 3D printed hand (16-18 N, 0.104 Nm, respectively) [8], but nonetheless lower than most of the conventional BP prosthetic hands (~30-85 N, 0.720 Nm-2.292 Nm, respectively) [33, 35]. This data indicates that this bio-inspired prosthetic hand is capable of reaching a more suitable pinch force for activities of daily living at the expense of a higher energy cost. Our prosthesis might then be difficult to use for a significant part of the users although our prosthesis requires less activation force and shows better pinch force/actuation force ratio than other conventional prostheses already in the market [32, 33]. The increase of force required compared to the current status of 3D printed hands is therefore problematic and requires further development. A key challenge for the future is then to reduce the activation force and improving the pinch force/actuation force ratio. More testing would be required to evaluate user fatigue, as even though it requires less energy to use than conventional prosthetics, it does require more energy than other 3D

printed hands. The implications of this are also user-dependent; contractions up to 15-20% of a muscle's peak force can be largely fatigue-free [36], meaning the user's physical strength plays a large role in the rate of fatigue. To provide a deeper understanding of the limitations of this design, a functional evaluation involving prosthetic users would be highly desirable.

The amount of energy dissipated (0.324 Nm) suggests a damping-like dynamic of the joint, i.e. most of the energy is dissipated rather than returned (Figure 6.6, left). This can be explained partly by the friction still remaining in the system and by the nonlinear and/or viscoelastic response of the TPU to strain perturbation. In other words, the motion of the joints depends on the strain rate experience by the TPU strips and thus by the activation velocity of the fingers. As described earlier, the joint is stabilized by TPU strips and the returning forces are provided by their elastic deformations. During the experiment, the tension over the fingers was completely released almost instantly after the pinch grasp was achieved. For different releasing and tension speeds, the response could be significantly different. While the nonlinear mechanical behavior of industrial TPU is well understood [37, 38], in 3D-printed TPU it is mainly unknown. As manifested in several investigations, 3D printed parts are highly anisotropic and important differences can be found between the standard material and the one used for 3D printing [39]. Further investigations on the influence of 3D printing parameters in the mechanical behaviour of TPU can provide more understanding of its nonlinear behaviour and give better tools to design improved joint connections that reduce the energy dissipation for the current application. Ideally the TPU connecting parts should behave like a spring without damping. Alternatively, other soft material suitable for FDM 3D printing could be explored.

We identified new bio-inspired elements, based on anatomical parts of the human finger, that were successfully incorporated into a prosthetic hand design and manufactured entirely by 3D printing technology. The resulting prosthetic hand is body-powered and has the following features: anthropomorphic shape, light weight, adaptive grasping, articulated fingers, and minimized post-printing assembly. The prosthetic hand is also an accessible

option due to its low production cost and is therefore potentially suitable for places where state-of-the-art prosthetic workshops are absent.

6.6 Conclusion

A BP prosthetic hand featuring bio-inspired articulated fingers was designed and manufactured via multi-material FDM 3D printing from three materials. The pinch force measurements demonstrate that the prosthetic hand achieves higher forces as compared to other 3D printed prosthetic hands but do not match other BP prosthetic devices. Nevertheless, other advantageous features were included using the unique characteristics of 3D printing technology. This prosthetic hand incorporates new bio-inspired features, is body-powered and has the following characteristics: anthropomorphic shape, light weight, adaptive grasping, articulated fingers, and minimized post-printing assembly. Summing the relatively low price of the materials, these characteristics make the prosthesis presented in this work a feasible alternative for current solutions in low-income countries.

6.7 References

[1] M.F. Owings, L.J. Kozak, Ambulatory and inpatient procedures in the United States, 1996, Vital Health Stat 13 (139) (1998) 1-119.
[2] K. Ziegler-Graham, E.J. MacKenzie, P.L. Ephraim, T.G. Travison, R. Brookmeyer, Estimating the prevalence of limb loss in the United States: 2005 to 2050, Arch Phys Med Rehabil 89(3) (2008) 422-9.
[3] C. Murray, Amputation, Prosthesis Use, and Phantom Limb Pain, Springer2010.
[4] J.T. Belter, J.L. Segil, A.M. Dollar, R.F. Weir, Mechanical design and performance specifications of anthropomorphic prosthetic hands: A review, J Rehabil Res Dev 50(5) (2013) 599-617.
[5] J. ten-Kate, G. Smit, P. Breedveld, 3D-printed upper limb prostheses: a review, Disabil Rehabil Assist Technol 12(3) (2017) 300-314.
[6] I. Gibson, D.W. Rosen, B. Stucker, Additive Manufacturing Technologies, Introduction and Basic Principles, Springer US2010, pp. 20-35.
[7] J.S. Cuellar, G. Smit, D. Plettenburg, A. Zadpoor, Additive manufacturing of non-assembly mechanisms, Addit Manuf 21 (2018) 150-158.

[8] J.S. Cuellar, G. Smit, A. Zadpoor, P. Breedveld, Ten guidelines for the design of non-assembly mechanisms: The case of 3D-printed prosthetic hands, Proc Inst Mech Eng H (2018) 954411918794734.
[9] K. Andrianesis, A. Tzes, Development and Control of a Multifunctional Prosthetic Hand with Shape Memory Alloy Actuators, J Intell Robot Syst 78(2) (2015) 257-289.
[10] M.S. Bahari, A. Jaffar, C.Y. Low, R. Jaafar, K. Roese, H. Yussof, Design and Development of a Multifingered Prosthetic Hand, Int J Soc Robot 4(1) (2012) 59-66.
[11] T. Laliberte, M. Baril, F. Guay, C. Gosselin, Towards the design of a prosthetic underactuated hand, Mech Sci 1(1) (2010) 19-26.
[12] K.F. Gretsch, H.D. Lather, K.V. Peddada, C.R. Deeken, L.B. Wall, C.A. Goldfarb, Development of novel 3D-printed robotic prosthetic for transradial amputees, Prosthetics and Orthotics International 40(3) (2016) 400-403.
[13] J.M. Zuniga, J.L. Peck, R. Srivastava, D. Katsavelis, A. Carson, An open source 3D-printed transitional hand prosthesis for children, J Prosthet Orthot 28(3) (2016) 103-108.
[14] e-NABLE, The Raptor Hand, 2014. http://enablingthefuture.org/upper-limb-prosthetics/the-raptor-hand/. (Accessed 19/07/2018 2018).
[15] M.W.M. Groenewegen, M.E. Aguirre, J.L. Herder, Design Of a partially compliant, three-phalanx underactuated prosthetic finger, Proceedings of the ASME Design Engineering Technical Conference, 2015.
[16] F. Alkhatib, E. Mahdi, J.J. Cabibihan, Design and Analysis of Flexible Joints for a Robust 3D Printed Prosthetic Hand, IEEE Int Conf Rehabil Robot 2019 (2019) 784-789.
[17] R. Mutlu, G. Alici, M. in het Panhuis, G.M. Spinks, 3D Printed Flexure Hinges for Soft Monolithic Prosthetic Fingers, Soft Robotics 3(3) (2016) 120-133.
[18] M.A. Sharbafi, C. Rode, S. Kurowski, D. Scholz, R. Mockel, K. Radkhah, G.P. Zhao, A.M. Rashty, O. von Stryk, A. Seyfarth, A new biarticular actuator design facilitates control of leg function in BioBiped3, Bioinspir Biomim 11(4) (2016).
[19] H.T. Lin, G.G. Leisk, B. Trimmer, GoQBot: a caterpillar-inspired soft-bodied rolling robot, Bioinspir Biomim 6(2) (2011).
[20] Q.V. Nguyen, W.L. Chan, Development and flight performance of a biologically-inspired tailless flapping-wing micro air vehicle with wing stroke plane modulation, Bioinspir Biomim 14(1) (2019).

[21] M. Scali, T.P. Pusch, P. Breedveld, D. Dodou, Ovipositor-inspired steerable needle: design and preliminary experimental evaluation, Bioinspir Biomim 13(1) (2018).
[22] S.R. Flinn, L. DeMott, Functional Anatomy, in: Elsevier (Ed.), Fundamentals of Hand Therapy, Elsevier2014, pp. 15-34.
[23] C. Toldt, A. Dalla Rosa, E. Paul, An atlas of human anatomy for students and physicians, Rebman Company, New York, 1919.
[24] M.M. Shrewsbury, K. Kuczynski, Flexor digitorum superficialis tendon in the fingers of the human hand, Hand 6(2) (1974) 121-33.
[25] M. Benjamin, E. Kaiser, S. Milz, Structure-function relationships in tendons: a review, J Anat 212(3) (2008) 211-228.
[26] O. Hauger, C.B. Chung, N. Lektrakul, M.J. Botte, D. Trudell, R.D. Boutin, D. Resnick, Pulley system in the fingers: Normal anatomy and simulated lesions in cadavers at MR imaging, CT, and US with and without contrast material distention of the tendon sheath, Radiology 217(1) (2000) 201-212.
[27] D.H. Plettenburg, Basic requirements for upper extremity prostheses: the WILMER approach, Proceedings of the 20th Annual International Conference of the IEEE Engineering in Medicine and Biology Society. Vol.20 Biomedical Engineering Towards the Year 2000 and Beyond (Cat. No.98CH36286), Hong Kong, 1998, pp. 2276-2281 vol.5.
[28] J.H. Vicinus, X-ray anthropometry of the hand, Aerospace Medical Research Laboratories, Wright-Patterson AFB, Ohio, 1962.
[29] R. Chandler, C. Clauser, J. McConville, H. Reynolds, J. Young, Investigation of Inertial Properties of the Human Body, (1975) 171.
[30] Ultimaker, Technical data sheet, TPU, 2018. https://ultimaker.com/download/74605/UM180821%20TDS%20TPU%2095A%20RB%20V10.pdf. (Accessed 27/02/2019 2019).
[31] Ultimaker, Technical data sheet, Nylon, 2018. https://ultimaker.com/download/74969/UM180821%20TDS%20Nylon%20RB%20V11.pdf. (Accessed 27/02/2019 2019).
[32] M. Hichert, A.N. Vardy, D. Plettenburg, Fatigue-free operation of most body-powered prostheses not feasible for majority of users with trans-radial deficiency, Prosthet Orthot Int 42(1) (2018) 84-92.
[33] G. Smit, D.H. Plettenburg, Efficiency of Voluntary Closing Hand and Hook Prostheses, Prosthetics and Orthotics International 34(4) (2010) 411-427.
[34] F. Alkhatib, J.J. Cabibihan, E. Mahdi, Data for benchmarking low-cost, 3D printed prosthetic hands, Data Brief 25 (2019) 104163.

[35] G. Smit, D.H. Plettenburg, F.C.T. van der Helm, The Lightweight Delft Cylinder Hand: First Multi-Articulating Hand That Meets the Basic User Requirements, Ieee T Neur Sys Reh 23(3) (2015) 431-440.
[36] H. Monod, Contractility of Muscle during Prolonged Static and Repetitive Dynamic Activity, Ergonomics 28(1) (1985) 81-89.
[37] BASF, Thermoplastic Polyurethane Elastomers, Elastollan®–Material Properties, 2017. http://www.polyurethanes.basf.de/pu/solutions/en/function/conversions:/publish/content/group/Arbeitsgebiete_und_Produkte/Thermoplastische_Spezialelastomere/Infomaterial/elastollan_material_uk.pdf. (Accessed 27/02/2019 2019).
[38] H.J. Qi, M.C. Boyce, Stress-strain behavior of thermoplastic polyurethanes, Mech Mater 37(8) (2005) 817-839.
[39] J.R.C. Dizon, A.H. Espera, Q. Chen, R.C. Advincula, Mechanical characterization of 3D-printed polymers, Addit Manuf 20 (2018) 44-67.

Chapter 7: Automatic 3D anthropometry for prosthetic applications

Juan Sebastian Cuellar, Matthijs Mazereeuw, Dick Plettenburg, Amir A. Zadpoor, Paul Breedveld, Gerwin Smit and Toon Huysmans

Abstract

7.1 Introduction

The comfort and functionality of a hand prosthesis is highly dependent on its interface with the residual limb (*i.e.*, the prosthetic socket). The design of the socket is crucial, because it is one of the main factors determining the acceptability of the prosthetic device [1]. Prosthetic sockets are often custom made, given the fact that every residual limb is unique. The socket must, therefore, be fabricated accordingly and precisely fit the user's anatomy. The conventional method of socket manufacturing starts with a model of the residual limb in the form of a plaster cast. The prosthetic socket is then designed according to the shape of the plaster model. This process is executed by trained prosthetists who also require a suitable workshop, tooling, and materials [2, 3]. The conventional fitting procedure of a trans-radial prosthetic socket is, therefore, expensive and inaccessible for a considerable part of the population living in developing countries.

The emerging 3D printing technology, also known as additive manufacturing (AM), has provided new ways to create functional parts. In the field of prosthetics, 3D printing holds great potential, because it enables the accessible production of custom-made parts at relatively low prices. As a cost-efficient production process, 3D printing can compensate for the lack of supply of prostheses in developing countries [4]. In fact, many affordable hand prostheses [5-7] and prosthetic sockets have been fabricated this way. Most designs of prosthetic sockets have been created using 3D printing techniques based on material extrusion, in particular fused deposition modeling (FDM^{TM}) [8-11]. The relatively low costs of the FDM^{TM} technology, its widespread use, and good product properties, appear to be the main motivations. Although a reasonable number of trans-radial 3D printed sockets exist, their strength and long-term usability remains largely unproven with qualitative and quantitative evaluation generally missing in the scientific literature. A 3D printed socket for trans-radial arm defect that can be recommended with sufficient evidence for use in developing countries is, therefore, yet to be established.

3D scanning technology has gained significant traction in the field of wearable products, because it can be used to create reliable 3D computer models of various parts of the human body [12]. These 3D models can be used to extract anatomical measurements and facilitate the labor-intensive task of a custom-made fitting [13]. In the same way, a prosthetic socket can be designed with a geometry that fits the user's anatomy by using 3D models of the residual limbs in a virtual environment. Unfortunately, current scanning systems are mostly expensive and difficult to set-up/operate, rendering them unsuitable for applications in low-resource settings. One promising solution is to use alternative 3D scanning techniques that require more accessible hardware, such as the camera of a smartphone. Recent research has shown the potential of smartphones as a 3D scanning tool for medical applications [14-16]. The most commonly used technique utilizing smartphone cameras is known as photogrammetry, which uses a number of 2D images to obtain information about the physical shape of an object [17]. Despite the satisfactory performance of photogrammetry techniques, certain concerns still remain regarding the usability and practicality of the process [15]. Some of them are the high level of computational data transfer and data storage requirements. Furthermore, there is no scientific literature regarding the use of the smartphone-scanned stumps, sockets, or limbs to directly benefit the design process of prosthetic devices. Specifically, no reports of a trans-radial socket produced with the assistance of a smartphone camera could be found.

We propose an approach for the creation of 3D computer models of anatomical parts, based on statistical shape Models (SSM). SSM offer a mathematically rigorous way of describing the main modes of shape variation in a statistical population. SSM have a potential for the 3D modelling of surfaces, because the geometries can be predicted only based on shape cues and other partial inputs with reasonable accuracy. For other applications, 3D models of feet [18] and full bodies [19] have been produced this way using only a small set of silhouette images. Although promising, the feasibility of this approach, specifically for the 3D modelling of limbs with trans-radial defects, has never been explored.

The goal of this research is to develop a 3D modelling process based on 2D photos and SSM and to combine it with a method of automatic 3D anthropometry and a new parametric design for trans-radial sockets that can be 3D printed. This combination of techniques aims to facilitate the fitting process of prosthetic arms for users with trans-radial defects. It should eliminate the need for elaborate tooling and/or equipment, while drastically reducing the required level of expertise of the involved prosthetists, potentially improving the accessibility of trans-radial prosthetic sockets in low-resource settings.

7.2 Prosthetic socket design

In the first phase of this research, a trans-radial prosthetic socket was designed which could be printed using FDM. After considering different available solutions, we decided to adapt the WILMER Open Socket described in Plettenburg and Walta *et al.* [1, 20] as a basis for our research due to its known advantages, such as leaving ~75% of the skin uncovered. This not only prevents perspiration-related problems, but also saves raw material and time during the 3D print process. Moreover, minimal contact with the skin should make the socket more forgiving of design (scanning) imperfections. The current WILMER Open Socket design, however, is made of sturdy metal bars, a locking mechanism, and a large amount of open space, which do not lend themselves well to the 3D printing technique. In other words, significant changes had to be made to the design. We therefore decided to go back to the WILMER Open Socket's basic shape that , as explained by Walta (1989) [20] and Lake (2008) [21], includes 1) a distal ring that enables weight bearing on the distal part of the residual limb, 2) a proximal ring that utilizes bony prominences, such as the antecubitis and olecranon and enhances the anterior-posterior stability, and (3) a condyle brace running over the cubital fold that ensures the prosthesis cannot slip off distally. The latter also ensures rotational stability.

The requirements imposed by the FDM method were fully incorporated into the design process [7]. While 3D printing can manufacture almost any form, clear benefits, drawbacks, and limitations exist depending on the designed shape. Material extrusion-based 3D printers build parts by

stacking layers of material perpendicular to the plane of the building plate. The bond between these layers is relatively weak, which leads to anisotropic characteristics [22]. Another inherent weakness of the FDM technique is that support structures are required for overhanging sections. Supporting structures can be hard to remove, require post-processing, increase the printing time and material, and can cause dimensional inaccuracies. In our trans-radial prosthetic socket design, both z-direction load (direction perpendicular to the building plate) and support structures were avoided by creating a completely flat 2D print, which could subsequently be formed into its desired shape. The concept of a flat design was conceived as follows. When stripped to its core, the WILMER Open Socket envelops the residual limb with material strips, two rings, and a condyle brace. If these strips are flexible and cut open at one side, then the socket will be almost flat on a surface. Figure 7.1 illustrates this design concept. When the flat print is 3D printed, it can be reassembled and bent around the residual limb.

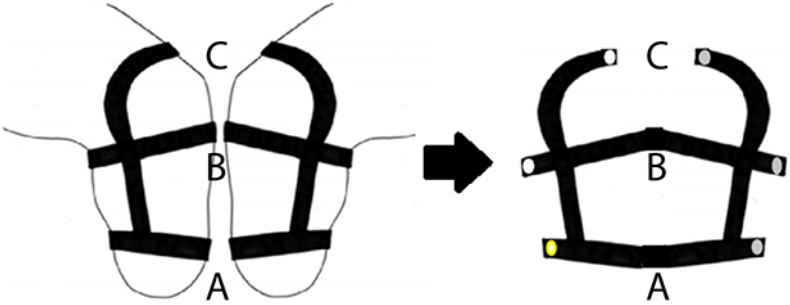

Figure 7.1: An early concept of flat fabrication of the WILMER-based open socket design including (A) a distal ring that promotes weight bearing on the distal part of the residual limb, (B) a proximal ring that utilizes bony prominences, such as the antecubitis and olecranon, enhances anterior-posterior stability, and (C) a condyle brace running over the cubital fold to ensure the prosthesis cannot slip off distally. Images are adopted from Lake (2008) [21].

Three options were considered to achieve low bending stiffness including the use of a flexible filament, printing micro-architectures to achieve high ductility [23], and limiting the material thickness along the z-axis. The latter limits the durability of the interface and the possible design dimensions. On the other hand, micro-architectures are highly challenging to print with most FDM printers. We therefore chose for the flexible filament approach. Thermoplastic polyurethane (TPU 95A) is wear and tear resistant, exhibits more ductility than other widely available alternatives compatible with FDM [24], and is superior in terms of print reliability. To guarantee that the socket could be printed perfectly flat, we decided to select shape our socket as a truncated oblique cone that a suitable approximation of the shape of the residual limb and can be easily unrolled and flattened. Figure 2 illustrates the design steps from an oblique cone to the socket.

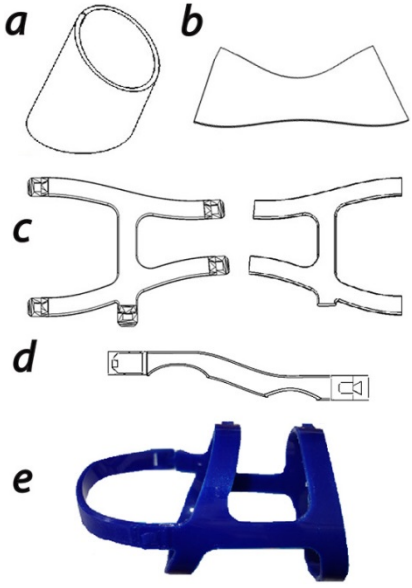

Figure 7.2: The design steps and separate pieces of the transradial socket. 2a) the truncated oblique cone, 2b) the flattened cone, 2c) the cutouts that

together form the proximal and distal rings, 2d): the condyle brace, and 2e) the assembled transradial socket.

An Ultimaker 3 machine was chosen for the manufacturing of the socket. As the dimensions of the flattened socket interface exceeded those of the Ultimaker 3's build plate, we decided to print the interface in three separate smaller pieces (Figures 2-4). Those pieces included two H-shaped pieces (Fig 2c) that together form the proximal and distal rings and a condyle brace (Fig 2d).

Assembly was achieved through two different locking mechanisms, each designed for their intended load bearing conditions. To print the interface perfectly flat, the locking mechanisms had to be printed in a flat orientation as well, requiring again no support structures. Two types of locks were designed (Figure 3): one to be used in the rings for assembly (type A) and another connected to the condyle brace, which was primarily used for donning and doffing (type B). Lock A combines a dovetail joint with a loop that catches behind an inclined block. A thin layer of material prevents skin getting caught between both sides. Lock B is a loop that slides over an hexagonal shaped block and has a rectangular pin that fits into a rectangular opening located inside the block. Cut-outs were implemented around the epicondyles to promote medial/lateral and rotational stability. Both mechanisms require very little printing support material and can be operated with one hand.

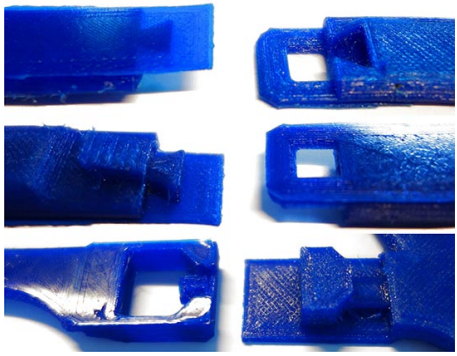

Figure 7.3: Lock designs for the assembly of the socket. Lock A is shown in the top two pictures while Lock B can be found in the bottom picture.

The design of the socket can be produced as a parametric design that can be resized according to the anatomical measurements of the residual limb. Once the measurements described by lines A, B, C, and D in Figure 4 are obtained, they can be used as parameters in a CAD software to produce a socket design that properly fits the residual limb. The circumference at the end of the oblique cone was based on the circumference required for the distal ring (line A), whose center was defined 1.5 cm proximally from the tip of the stump. The circumference at the base of the oblique cone was based on the circumference required for the proximal ring (line B). The distance from one side of the proximal ring to the other, running just above the cubital fold, determined the length of the condyle brace (line C). The distance between the center points of both proximal and distal rings (line D) can also be determined once the rings are positioned. The inclination angle between line B and line D is initially set at 110° (same as line A and line D), though that could be changed according to the size and shape of the residual limb.

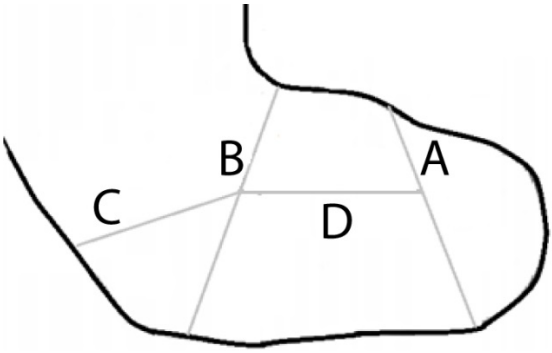

Figure 7.4: The required residual limb dimensions for the design of the socket. (A) the circumference required for the distal ring; (B) the circumference required for the proximal ring; (C) the length of the condyle brace, and (D) the distance between the center points of both rings.

7.3 Modelling of the shapes and the socket

7.3.1 Statistical Shape Model (SSM)

A training database made out of digital models of different residual limb shapes is required to create an SSM. Building such a database poses a challenge, because the number of subjects willing to participate is limited and a proper number of scans cannot be obtained easily. An artificial database was, therefore, created based on 40 full body scans of healthy humans from the CAESAR database [25, 26]. The scans of the arm were prepared by separating the right arm and shoulder from the rest of the body and cutting the scans at certain points between the wrist and the cubital fossa (*i.e.*, the elbow pit). For every scan, the 3D model was cut at four different cutoff planes aligned parallel to the line between the wrist and the cubital fossa. The four cutoff planes were defined by the length proportion of this line at the wrist level as well as at 75%, 50%, and 25% of the length, respectively. In this way, the database represents different amputation cases that can occur at different levels of the forearm. The training database, thus, consisted of N = 160 different 3D surfaces (40 body scans x 4 different cuts). Note that each cut of the four lengths of residual limb is represented by one SSM. We therefore created four different SSM.

In order to build the SSM, all the surfaces were required to have the same number of points and every point had to correspond to the same location of the surface across all the cuts (point #1 in surface 1 relates to point #1 in surface 2 and so on). To achieve this, a surface registration process was implemented. The surfaces were aligned using a rigid transformation and the points of every surface were rearranged to establish a point-to-point correspondence using a non-rigid transformation [27]. The process was implemented using a MATLAB® script as follows:

1. One first random surface was selected as the source and a second surface as the target.
2. The method performed a rigid transformation based on the General Procrustes Analysis (GPA) [28] that minimizes the distance between

the source and the target. The source underwent iterative rotation and translation to match the target. This process was continued until the root mean square error between the source and the target reached a certain threshold.

3. The method then used the non-rigid iterative closest point (ICP) algorithm based on Li *et al.* [29] to deform the source locally until it matched the shape of the target. The new shape was saved as a new .ply file.
4. A third surface was selected as the new target and the rigid and non-rigid transformation processes were repeated using the first surface as the source.
5. The process was repeated until the last surface (surface N = 160) was used as the target. The new training database was created with the 160 updated surfaces.

The surfaces in the training database were aligned under a common coordinate system using the same GPA algorithm as described above. In this case, all the surfaces were aligned to the first surface selected in the previous step as the "source". The SSM was then created using principal component analysis (PCA) [30]. With PCA, the main modes of shape variation causing the highest levels of statistical variance among the point distributions of the previously generated surfaces can be obtained as the eigenvectors of the covariance matrix. While the eigenvectors are a set of orthogonal axes describing the principal directions of variation, their corresponding eigenvalues are the numbers describing how widely spread the data is in the direction of the eigenvector. Given a set of shapes $M = [x_1, x_2, \dots, x_n]$ containing the coordinates of every surface (x_i), the PCA can be performed via singular value decomposition (SVD) [27]. First, the mean shape is defined as:

$$\bar{x} = \frac{1}{n}\sum_{i=1}^{n} x_i \tag{7.1}$$

The mean is then subtracted from each shape to solely focus on the variance. This results in a zero row-centered matrix of shapes:

$$X_c = [x_1 - \bar{x},\ x_2 - \bar{x},\ x_3 - \bar{x}, \dots, x_n - \bar{x}\ ] \tag{7.2}$$

The eigenvectors and eigenvalues can then be extracted from the covariance matrix of X_c. The covariance matrix is a symmetric matrix, so it can be diagonalized:

$$C = PLP^T \tag{7.3}$$

where C is the covariance matrix of the data X_c , P is an orthogonal matrix consisting of only eigenvectors, and L is a diagonal matrix with eigenvalues λ in the decreasing order on the diagonal [30]. The resulting eigenvectors are also referred to as shape modes. These statistical parameters can now be used to create a 3D adjustable model. A new surface x_a can be obtained following the linear equation:

$$x_a = \bar{x} + Pb \tag{7.4}$$

where b is a vector with the weight values $b = [b_1, b_2, b_3, \dots, b_{m-1}]^T$ and m can be equal or smaller than the number of surfaces for the training set but never larger. The vector b determines the contributions of the different shape modes P to the shape of any specific surface, x_a. The values in vector b are constrained to keep the shape within the normal distribution of shapes from the training dataset:

$$-3\sqrt{\lambda_i} \leq b_i \leq 3\sqrt{\lambda_i} \tag{7.5}$$

The resulting morphable 3D model is called a statistical shape model (SSM) can be used for approximating any other surface, which is obtained through adjustment of the weight values in b as described in equation 7.4.

7.3.2 3D modelling based on silhouettes and a SMM

The 3D modelling method used the segmented pictures of a residual upper limb and created a digital 3D shape of the residual upper limb. The method is described as follows and is illustrated in Figure 5.

1. A commercial smartphone (iPhone 6(c)) was used to take three pictures of a residual upper limb from different angles. The three different view planes (sagittal, transversal and frontal) can be seen in Figure 6. The three photos were taken 0.5 m away from the center of the residual limb while using a distinctive background color to facilitate segmentation.
2. The silhouettes of the residual limb were created by segmenting the photos based on color contrast. The obtained images were defined as I_p.
3. The SSM was manually chosen according to the level of limb amputation (at the wrist level, 75%, 50% or 25%). The mean shape of the SSM ($\bar{x}$) was projected on one of the 2D planes defined by the location of one of the cameras using the pinhole camera model [31]. The pinhole camera model transforms the 3D coordinates of the world into 2D coordinates using certain mathematical parameters that are intrinsic and extrinsic to the camera. The intrinsic parameters were those pertaining to the smartphone camera (e.g. focal length) and the extrinsic parameters were defined assuming that the optical center was aligned with the center of the coordinate system of the residual limb and that those two centers were 0.5 m away from each other. In this way, the extrinsic parameters were set using the virtual location of the camera with respect to the location of the residual limb.
4. The mean shape of the SSM was projected on both other planes defined by the location of the other cameras. The extrinsic parameters, namely the rotational matrix, were redefined to project the residual limb onto both other planes. The resulting projections were defined as I_{SSM}.
5. The difference between the silhouettes obtained from the subject (I_p) and their respective projection (I_{SSM}) was obtained and a mean error

was calculated based on the average of the three different view planes. For the error calculation, the images were converted to binary values were the pixels representing the limb had a value of "1" while the background pixels were all "0".

6. An optimizing algorithm was used to minimize the mean error. The algorithm took as an input the first 21 shape modes of the SSM and the initial location and orientation of the mean shape of the SSM ($\bar{x}$), namely the three translations and the three angles of rotation. The 21 first shape models are sufficient to explain the most important variances of the shape. The initial location of the SSM was included in the minimizing algorithm because perfect alignment of the residual limb with the optical center of the camera is very unlikely and a large error could be introduced. In other words, the algorithm tries to find the location and orientation of the SSM and the values of b such that the mean error is minimized.
7. The digital 3D shape of the residual upper limb was defined as the linear combination of the average of the SMM with the optimal variations of the shape modes found and the optimal location.

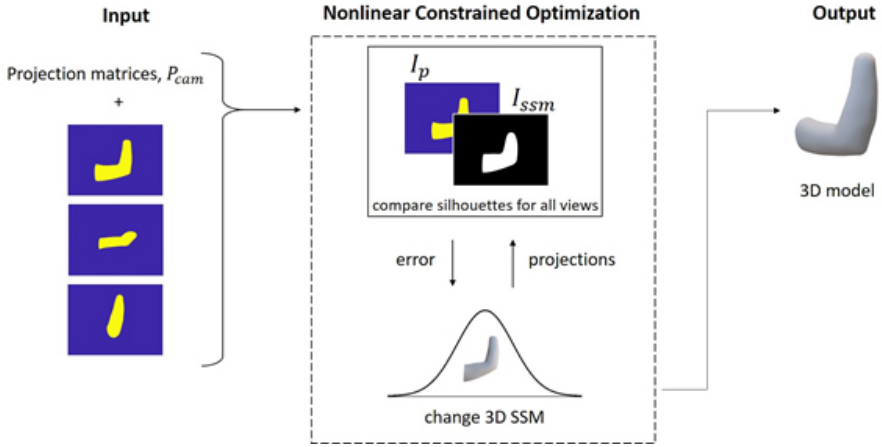

Figure 7.5: The 3D modelling process. Three silhouette images are used as the input and a 3D model of the residual limb constitutes the output. An

optimization algorithm iteratively compares the silhouettes with the projections of the SSM.

Figure 7.6: The photos taken from the three different view angles (planes). From left to right: sagittal plane, transversal plane and frontal plane.

7.3.3 Automatic anthropometry

3D anthropometry was performed once the fitting of the projections of the SSM onto the silhouettes produced a new model of the residual limb. The average surface of the SSM was marked manually before with the important landmark points. The landmarks include the tip of the stump, olecranon, antecubital fossa, and the position of the distal and proximal belt that were based on our socket design (Figure 4). As the SSM morphed to fit the target, the landmark points also relocated generating new positions that represented the important anatomical locations of the target. The new landmarked points were then used to define the anatomical measurements of interest. The circumferences were calculated based on the method proposed by Wasenmüller *et al.* [32]. The new marked points were used to define a regression plane that best fitted along the points of the distal and proximal belts. The intersection lines between the two fitted planes and the morphed SSM were obtained and both center points were calculated. A line was created from these two points, defining a line along the axis of the forearm and new regression planes were created that were required to be perpendicular to this line. The corrected planes were then used to obtain the measurements by finding their intersection with the morphed SSM. The output measurements were finally calculated by finding the Euclidian distance between the points identified as a part of the intersection. The entire process is summarized and depicted in Figure 7.7.

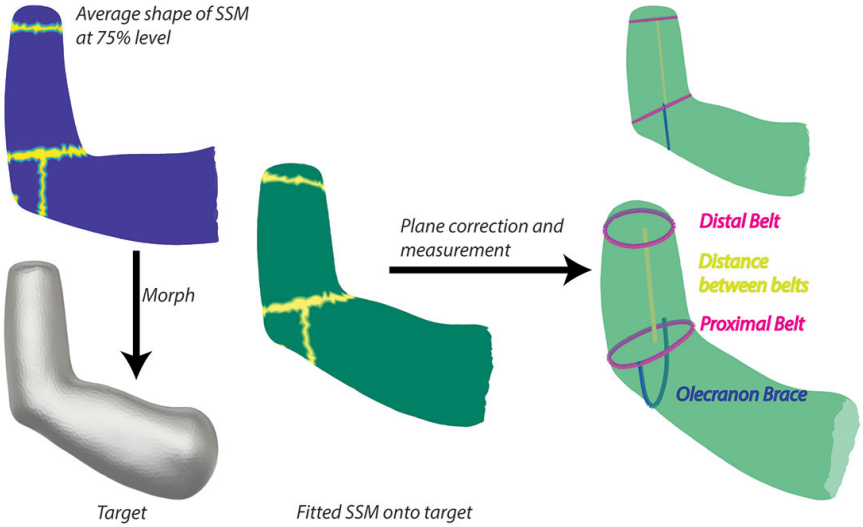

Figure 7.7: The morphing process of the SSM into the target surface and the 3D anthropometry. On the right, the measurements of interest are shown (i.e., distal belt, proximal belt, distance between belts and olecranon brace).

7.3.4 Evaluation: Error calculation and socket manufacturing

Three subjects with arm defects up to the trans-radial level were recruited in order to test our 3D modelling and anthropometry methods. The subjects were positioned in the photography setup, which consisted of an iPhone 6(c), a tripod holder, and a distinctive green background. The smartphone was used to take three different pictures from the view planes established with our modelling method focusing on the residual limb of each subject (Figure 6). Each subject had to move its upper limb accordingly. The above-described method was then used to process the photographs, build the digital models, and performing 3D anthropometry on the digital models resulting in four different measurements. The same measurements were taken on the limbs of the subjects by performing manual anthropometry using a measuring tape. The differences between the manual measurements and the measurements calculated by our method were

calculated as an indication of the error of our anthropometry method. We resized our socket design according to the distances taken manually with the measuring tape. The sockets were then 3D-printed using an Ultimaker 3 3D printer (Ultimaker, The Netherlands) and TPU material and were later fitted to the user.

7.4 Results

We created four training datasets of the residual upper limb 3D models and four corresponding SSMs. Using those SSMs, we created the 3D models of the residual limb for each subject. The distances measured using both techniques are presented in Table 1 while the measurement errors are listed In Table 2. The smallest absolute error measurement is 13 mm and the largest is 70 mm. No clear trends can be observed between dimensions or between subjects. Both positive and negative errors can be found per dimension and per subject. The dimension that presents the largest error on average is the distance between belts.

The total manufacturing time of the sockets was between 7 and 9.5 hours. They weighed 57-70 g, which translates to a material cost of 5.5 - 6.7 Euros. Once in position, the locks maintain the assembly stable.

Table 7.1. The measurements obtained using the automated (A) and manual (M) techniques. All distances are presented in mm.

	Subject 1 (JJR)		**Subject 2 (AM)**		**Subject 3 (LFT)**	
	A	M	A	M	A	M
Distal Belt (circ.)	188	175	162	120	174	160
Proximal Belt (circ.)	280	265	244	174	174	200
Distance bw Belts	80	111	105	75	79	45
Olecranon Brace	204	230	141	180	108	130

Table 7.2. The error associated with the automated measurement technique in % and absolute.

	Subject 1 (JJR)		Subject 2 (AM)		Subject 3 (LFT)	
	%	Abs (mm)	%	Abs (mm)	%	Abs (mm)
Distal Belt (circ.)	7.4	+13	35	+42	8.7	+14
Proximal Belt (circ.)	5.7	+15	40.2	+70	13	-26
Distance between Belts	27.9	-31	40	+30	75.6	+34
Olecranon Brace	11.3	-26	21.7	-39	16.9	-22

7.5 Discussion

The residual limb of subjects was 3D modeled and the digital outcome was introduced in the process of automatic anthropometry based on an SSM. The outcome was later used for determining the parameters of a parametric design of a trans-radial socket that can be 3D printed and fitted onto the user's residual limb. The automatic anthropometry process was proven to be fast and easy to use, only required an easy-to-build photo shoot set, which consisted of an A0-sized green background and a smartphone.

Sources of error of the automatic measurement

As the first 3D printed version of the WILMER socket it is challenging to establish a minimum acceptable dimensional error to ensure both comfort and proper suspension. Nevertheless, the error of the automatic measurement can be considered large (13 – 70 mm) and lies outside the acceptable boundaries for the design of the socket. Similar research has used more accurate scanning methods to produce sockets [9, 10], although the hardware is less accessible than a smartphone.

The dimensional errors in the digital models obtained with our SSM based method may have originated from multiple possible sources. First, the process of generating the training database for the SSM can introduce small

errors at different stages. The surface registration process ideally repositions the points to match the same location across surfaces. However, when the source and target shapes are significantly different, the reposition is not entirely accurate and the new locations will not truly represent a match between both surfaces. This can lead to an SSM that does not describe the shape variations accurately. The outcome could be improved by manually aligning the points. This is, however, a long and time-consuming process. Second, the pictures were assumed to be taken from a specific location and with a specific orientation, which in reality is challenging to realize, as precise positioning of the limb for photo shooting is difficult to achieve. This can influence the outcome considerably, because the projections of the SSM using the pinhole camera model are based on cameras positioned orthonormal to each other. Obtaining photographs of the limb from those exact positions is very challenging and the differences can lead to imprecise 3D models. An attempt was made to reduce this source of error by placing the smartphone in a fixed position with respect to the position of the limb and moving the limb to perform the photo shooting for all the view planes. This modification reduced the effects of moving the smartphone between the photo shoots, which can cause imprecise camera positioning. For that reason, we also used an optimization algorithm to find the position of the SSM that minimized the error of the comparisons between the projections and the silhouettes (Section 3.2). A jig for holding the arm in the three poses desired could be considered. Nonetheless, this could interfere visually in the camera, compromising the segmentation of the residual arm. Third, the landmarks used for the automatic 3D anthropometry method were annotated manually using visual cues, which makes the process somewhat subjective. Finally, an artificial database based on healthy subjects was constructed. An early assumption was that the shape of a residual limb could be directly derived from healthy limb shapes with no significant modifications. This may not be entirely true for some special cases of trans-radial defects where the shape is significantly different due to specific arm conditions. An extended SSM trained with a larger database including actual surfaces of limbs with trans-radial defects would, therefore, be desirable. In addition, we have used a

relatively small number of shapes to train the SSM (40 models were used to train each SSM). The 3D modelling of the test setup could be better performed, if the training dataset of the residual limb models was larger. In related research, a SSM was created from a database of 761 scans [19], 700 scans [18], and more [33, 34]. In that case, the SSM covers a larger variety of shapes and might, therefore, perform better.

During this research, we acquired the photos using an average quality camera (iPhone's 6 camera) but under controlled conditions. While it is expected that the conditions for the photo shooting could be easily met due to the low level of hardware requirements, the photo shooting process could pose some challenges, because three orthonormal photographs are required. This may be difficult to arrange for all users particularly those living in remote, disconnected areas. While the proposed methodology, makes the whole 3D modelling process faster, it leads to less accurate measurements in comparison to other scanning methods. While the proposed way of processing images is promising, its accuracy needs to be improved considerably and its practicality is yet to be proven both for the prosthetist and the user. A study of the usability of the scanning method proposed in this research and a comparison with other methods will clarify this aspect.

Prosthesis fitting

The socket was designed based on the assumption that it would fit perfectly on the user. To keep the design and manufacture complexity to the minimum the option of an adjustable socket was not considered. We fitted three subjects with personalized sockets that were created with the design methodology described here and the manual measurements taken on the stump. The sockets were produced relatively quickly and were adjusted easily onto the subjects. Fortunately, both the arm and the socket are relatively soft and malleable, which allows for some level of flexibility at the interface. This can help to compensate for the errors associated with the manual measuring method to a certain degree. The sockets are also lightweight (~57-70 g) and easy to don and doff, which are important characteristics that increase the general acceptance

of prosthetic devices by users [35]. Although the sockets were fitted, some functional characteristics, such as comfort or the maximum suspension loads were not investigated. Further investigation involving continuous follow-up of actual users wearing the socket in regular conditions (together with the prehensor and the control scheme) and grasping different objects with different weights should be conducted.

7.6 Conclusion

A semi-automatic procedure for the anthropometry of upper limbs with trans-radial defects based on 2D pictures was proposed, implemented, and tested. The resulting anatomical measurements were less accurate than manual measurements and need to be further improved before the application of this technique in actual practice can be realized. In particular, considerable improvements of the SSM and the photo shooting process are required. Manual measurements were used instead to design a socket that properly fits the residual limb of the users. The socket was then successfully manufactured using a 3D printer from a soft material. The resulting socket was lightweight and was easy to put on and put off, which increases the general acceptability of the device, and was affordable, which increases its accessibility to users living in low-resource settings.

7.7 References

[1] D.H. Plettenburg, Basic requirements for upper extremity prostheses: the WILMER approach, Proceedings of the 20th Annual International Conference of the IEEE Engineering in Medicine and Biology Society. Vol.20 Biomedical Engineering Towards the Year 2000 and Beyond (Cat. No.98CH36286), Hong Kong, 1998, pp. 2276-2281 vol.5.

[2] B. Curran, R. Hambrey, The prosthetic treatment of upper limb deficiency, Prosthet Orthot Int 15(2) (1991) 82-7.

[3] R.K. Chen, Y.-a. Jin, J. Wensman, A. Shih, Additive manufacturing of custom orthoses and prostheses—A review, Additive Manufacturing 12 (2016) 77-89.

[4] B. Phillips, G. Zingalis, S. Ritter, K. Mehta, A Review of Current Upper-Limb Prostheses for Resource Constrained Settings, Proceedings of the Fifth Ieee Global Humanitarian Technology Conference Ghtc 2015 (2015) 52-58.
[5] J.t. Kate, G. Smit, P. Breedveld, 3D-printed upper limb prostheses: a review, Disabil Rehabil Assist Technol 12(3) (2017) 300-314.
[6] J.M. Zuniga, 3D Printed Antibacterial Prostheses, Appl Sci-Basel 8(9) (2018).
[7] J.S. Cuellar, G. Smit, A. Zadpoor, P. Breedveld, Ten guidelines for the design of non-assembly mechanisms: The case of 3D-printed prosthetic hands, Proc Inst Mech Eng H (2018) 954411918794734.
[8] K.F. Gretsch, H.D. Lather, K.V. Peddada, C.R. Deeken, L.B. Wall, C.A. Goldfarb, Development of novel 3D-printed robotic prosthetic for transradial amputees, Prosthet Orthot Int 40(3) (2016) 400-3.
[9] N. Herbert, D. Simpson, W.D. Spence, W. Ion, A preliminary investigation into the development of 3-D printing of prosthetic sockets, J Rehabil Res Dev 42(2) (2005) 141-146.
[10] A. Radosh, W. Kuczko, R. Wichniarek, F. Gorski, Prototyping of Cosmetic Prosthesis of Upper Limb Using Additive Manufacturing Technologies, Adv Sci Technol-Res 11(3) (2017) 102-108.
[11] J.M. Zuniga, J.L. Peck, R. Srivastava, J.E. Pierce, D.R. Dudley, N.A. Than, N. Stergiou, Functional changes through the usage of 3D-printed transitional prostheses in children, Disabil Rehabil Assist Technol 14(1) (2019) 68-74.
[12] N. Magnenat-Thalmann, H. Seo, F. Cordier, Automatic modeling of virtual humans and body clothing, J Comput Sci Tech-Ch 19(5) (2004) 575-584.
[13] P. Apeagyei, Application of 3D body scanning technology to human measurement for clothing Fit, JDCTA 4 (2010) 58-68.
[14] O. Ciobanu, G. Ciobanu, M. Rotariu, Photogrammetric Scanning Technique and Rapid Prototyping Used for Prostheses and Orthoses Fabrication, Appl Mech Mater 371 (2013) 230-+.
[15] O. Ciobanu, M. Rotariu, Photogrammetric Scanning and Applications in Medicine, Engineering Solutions and Technologies in Manufacturing 657 (2014) 579-583.
[16] A. Hernandez, E. Lemaire, A smartphone photogrammetry method for digitizing prosthetic socket interiors, Prosthet Orthot Int 41(2) (2017) 210-214.
[17] A.D. Jones, Manual of Photogrammetry, eds C.C. Slama, C. Theurer and S.W. Hendrikson, American Society of Photogrammetry, Falls Church, Va., 1980, Fourth Edition, 180 × 260mm, xvi and 1056 pages (with index), 72 tables, 866 figures. ISBN 0 937294 01 2, Cartography 12(4) (1982) 258-258.

[18] E. Parrilla, A. Ballester, C. Solves-Camallonga, B. Nácher, S. Antonio Puigcerver, J. Uriel, A. Piérola, J.C. González, S. Alemany, Low-cost 3D foot scanner using a mobile app, Footwear Science 7(sup1) (2015) S26-S28.
[19] A. Ballester, E. Parrilla, A. Piérola, J. Uriel, C. Perez, P. Piqueras, B. Nácher, J. A. Vivas, S. Alemany, Data-driven three-dimensional reconstruction of human bodies using a mobile phone app, International Journal of the Digital Human 1 (2017) 361.
[20] H.A. Walta, P. Ariese, J.C. Cool, Ergonomic socket design for congenital below elbow amputated children, J Rehabil Sci (2) (1989) 19-24.
[21] C. Lake, The Evolution of Upper Limb Prosthetic Socket Design, Journal of Prosthetics and Orthotics 20(3) (2008) 85-92.
[22] S.-H. Ahn, M. Montero, D. Odell, S. Roundy, P.K. Wright, Anisotropic material properties of fused deposition modeling ABS, Rapid Prototyping Journal 8(4) (2002) 248-257.
[23] C. Schumacher, B. Bickel, J. Rys, S. Marschner, C. Daraio, M. Gross, Microstructures to Control Elasticity in 3D Printing, Acm T Graphic 34(4) (2015).
[24] Ultimaker, Technical data sheet, TPU, 2018. https://ultimaker.com/download/74605/UM180821%20TDS%20TPU%2095A%20RB%20V10.pdf. (Accessed 27/02/2019 2019).
[25] K.M. Robinette, H. Daanen, E. Paquet, The CAESAR project: a 3-D surface anthropometry survey, Second International Conference on 3-D Digital Imaging andModeling, IEEE, Ottawa, Ontario, Canada, 1999, pp. 380-386.
[26] S. International, CAESAR: Civilian American and European Surface Anthropometry Resource Project. http://store.sae.org/caesar/. (Accessed 16-05-2019 2019).
[27] T. Huysmans, J. Sijbers, B. Verdonk, Automatic Construction of Correspondences for Tubular Surfaces, Ieee T Pattern Anal 32(4) (2010) 636-651.
[28] C. Goodall, Procrustes Methods in the Statistical-Analysis of Shape, J Roy Stat Soc B Met 53(2) (1991) 285-339.
[29] H. Li, R.W. Sumner, M. Pauly, Global correspondence optimization for non-rigid registration of depth scans, Comput Graph Forum 27(5) (2008) 1421-1430.
[30] T.F. Cootes, C.J. Taylor, D.H. Cooper, J. Graham, Active Shape Models - Their Training and Application, Comput Vis Image Und 61(1) (1995) 38-59.
[31] D.C. Brown, Close-Range Camera Calibration, Photogramm Eng 37(8) (1971) 855-&.

[32] O. Wasenmüller, J. C Peters, V. Golyanik, D. Stricker, Precise and Automatic Anthropometric Measurement Extraction Using Template Registration, 2015.
[33] Z.Y. Xu, Q.N. Zhang, S.Y. Cheng, Multilevel active registration for kinect human body scans: from low quality to high quality, Multimedia Syst 24(3) (2018) 257-270.
[34] A. Jurca, T. Kolsek, T. Vidic, DOROTHY mass foot measurement campaign, Footwear Science 3 (2011).
[35] Y.J. Sang, X. Li, Y. Luo, Biomechanical design considerations for transradial prosthetic interface: A review, P I Mech Eng H 230(3) (2016) 239-250.

Chapter 8: Fitting the 3D printed hand in low-income countries

Juan Sebastian Cuellar, Madelon Kusters, Hilde Jansen, Dick Plettenburg, Amir A. Zadpoor, Paul Breedveld and Gerwin Smit

Abstract

Providing prosthetic devices in low-income settings is challenging given the precarious situation of healthcare systems. Several research groups and NGOs have reported designs suitable for low-income countries but actually, only a few of them have been fitted in subjects with arm defects who are living under such conditions and almost no measurements of the actual functionality or user satisfaction exists in the scientific literature. Previously, we have developed a new bio-inspired 3D printed hand prosthesis aiming to reduce the manufacturing requirements. The goal of the research described in this paper was, therefore, to measure the functionality and satisfaction of the bio-inspired 3D printed hand prosthesis among subjects living in low-income settings. Five subjects with trans-radial defects were recruited in the city of Ibague, Colombia. Each subject was invited to a local prosthetic workshop where the physical measurements of their stump were taken. The sockets and shafts were then produced using 3D printing. The whole prosthetic arm was later assembled and then fitted to the user. The functionality of the prostheses was assessed through the Box and Blocks Test and satisfaction was assessed with the self-report questionnaire known as the Orthotics Prosthetics User Survey (OPUS). The results showed lower functionality compared to other 3D printed BP hands although the scores are likely to increase with use time. The users reported in general a high level of satisfaction regarding the 3D printed prosthesis, although some aspects of the design require further improvement including the option for users to perform maintenance or repair as well as the comfort of the prosthesis. The results suggest that our production method could increase the accessibility of trans-radial prostheses in the city of Ibague, Colombia among people living in low-income settings.

8.1 Introduction

Providing prosthetic devices in low-income settings is challenging given the precarious situation of healthcare systems. A large group of individuals with arm defects are, therefore, left without proper care [1]. 3D Printing technology could potentially provide a solution for overcoming the production difficulties

encountered when fabricating prosthetic arms. 3D Printing permits the manufacturing of end-use parts with complex and uncommon shapes at relatively low costs. In fact, many 3D printed upper-limb prosthetic devices can already be found in the literature [2]. A number of research groups and NGOs have reported designs suitable for low-income countries, but actually, only a few of them have been fitted in subjects with arm defects who are living under such conditions and almost no measurements of the actual functionality or user satisfaction exists in the scientific literature. Indeed, most of the 3D printed upper limb prostheses are described as proof-of-concepts, providing control schemes for surface muscle electromyography (sEMG) [3, 4], serving as a transitional or a training device [5], demonstrating the possibility to reduce the assembly requirements [6], or as a design study to reduce the production costs [7].

Among the few studies where the 3D printed prosthesis was actually fitted to a patient, Zuniga *et al.* [8] fitted a subject with shoulder disarticulation with a 3D printed body-powered (BP) prosthesis. The device improved the balance of the subject and performance of some activities requiring the function of both hands, such as grabbing a large ball. The researchers also identified some limitations like low grip strength and low durability of the prosthetic device. The same research group also fitted 11 children with a 3D printed prosthesis, reporting increased gross manual dexterity [9] and high satisfaction scores regarding the weight, safety and ease of use after remote-fitting of the same prosthesis on a different group of 8 subjects [10]. Herfat & Moreau [11] also fitted 3D printed cosmetic prostheses to a group of subjects in Amman, Jordan, obtaining high satisfaction scores.

In a previous study, we have developed a new bio-inspired 3D printed hand prosthesis for use in developing countries, aiming to reduce the manufacturing requirements and costs (Chapter 6). In that study, the prosthetic hand was not fitted to subjects with trans-radial defects living in the targeted socio-economic environments. The goal of the research described in the current paper is, therefore, to measure the functionality and satisfaction of the bio-

inspired 3D printed hand prosthesis among subjects living in low-income settings.

8.2 Methodology

Upper limb prosthetic devices need to be custom-made for an individual, which is why they often require local production. A small prosthetic workshop was, therefore, installed on the premises of the Universidad del Tolima in the city of Ibague, Colombia. The workshop consisted of a 3D printer working on the basis of material extrusion technology (Prusa i3 MK3S) and of conventional tools like screwdrivers, tweezers, and scissors.

The prosthetic device consisted of four parts: the prosthetic hand, socket, shaft (the part that couples the socket and the hand) and the driving system, which was based on BP actuation, see Figure 8.1. The prosthetic hands were 3D printed using another material extrusion 3D printer (*i.e.*, Ultimaker 3, The Netherlands) prior to the installation of the prosthetic workshop in Colombia. The Ultimaker 3 machine allows simultaneous deposition of two different materials which is necessary for the manufacturing of this specific prosthetic hand. The prosthetic hand design (Chapter 6) used in this paper has several bio-inspired design features and was successfully manufactured using multi-material 3D printing. The device can execute different grasping patterns thanks to the adaptive grasping delivered by the articulated fingers and the whiffle tree mechanism. The assembly of the hand was minimized to two post-processing steps besides the usual support removal after 3D printing. No extra parts or tools were required. The main body of the hand, the phalanges and the connecting elements are 3D printed simultaneously with PLA and TPU. The prosthetic hand was produced in a standard size set as the average size of human hands, based on a sample of 253 males in the USA, as described in the work of Vicinus [12]. The prosthetic hand is body-powered and has the following features: anthropomorphic shape, light weight, adaptive grasping, articulated fingers, and minimized post-printing assembly. The other parts were produced in Ibague using the Prusa i3 MK3S 3D printer and materials found

locally. The socket and the shaft were designed accordingly to each individual, based on the level and condition of the stump and its size.

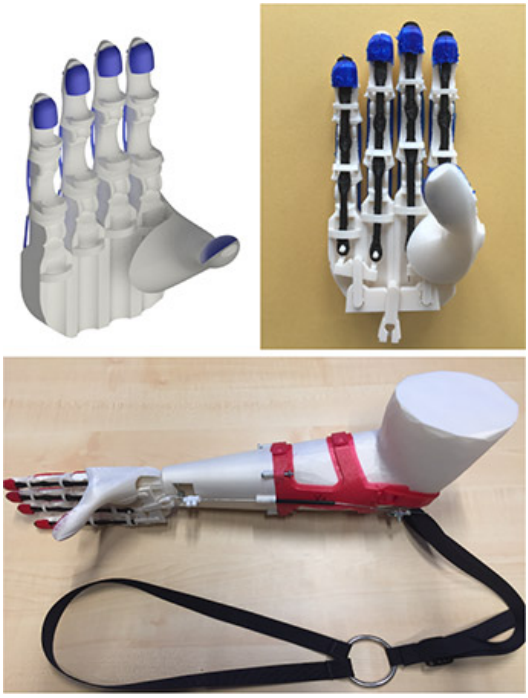

Figure 8.1: The 3D printed prosthetic hand that was used in this study, showing the CAD model of the main body of the prosthetic hand *(top left)*, the 3D printed and fully assembled prosthetic hand *(top right)* and the prosthetic hand with the shaft, socket (red part) and driving system *(bottom)*. The driving system consists of a cable and a harness made with nylon webbing (black part).

The design of the socket was based on the WILMER Open Socket [13, 14], using the same straps size and the same locks as the WILMER Open Socket. The socket was designed for 3D printing enabling custom-made low cost production. The design consisted of two sets of straps (see red parts in Figure 1), one attached above the elbow and the other attached below the elbow, which were connected to each other with a hinge located at the pivot point of

the elbow joint, the so-called epicondyle. As compared with the WILMER Open Socket, this socket maintains the same suspension points and is as breathable, but has been modified for 3D printing by designing flat straps. In contrast, the current WILMER Open Socket design is made of sturdy metal bars. The straps were devised flat for two important reasons. One, because there were no overhangs during 3D printing, hence, support structures were avoided, and two, because large z-direction (direction perpendicular to the building plate) loads during regular use were prevented, see Figure 8.2. The straps were bent and locked in position to conform to the cylindrical-shape that fits around the stump. This custom-made socket was printed in two different ways depending on the length of the stump: for stumps larger than 10 cm starting from the epicondyle, the part below the elbow consisted of two straps. For shorter stumps, only one strap was used. Figure 8.1 shows a socket for a stump larger than 10 cm, the two straps can be seen in red colour.

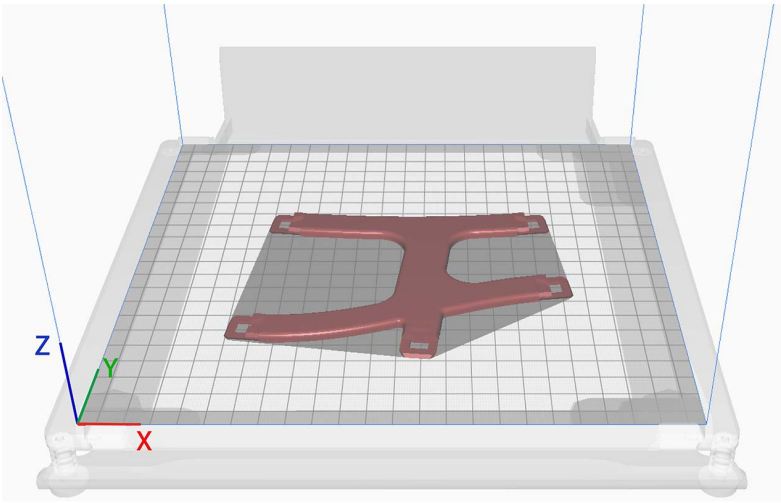

Figure 8.2: A strap of the socket is shown on the building plate of a 3D printer. Note that there are no overhangs; hence, support structures are avoided. Note also that in this 3D printing configuration large forces in the z-direction are avoided; there are no large forces pulling the layers apart when the user is wearing the socket.

A parametric design built upon key anatomical measurements was implemented using the CAD software Inventor® in order to obtain fast custom-made socket and shaft designs. Anatomical measurements were used to resize the socket and shaft accordingly. Figure 8.3 shows the most important anatomical measurements. The midpoint of the straps, both directly below and above the elbow was 45 mm away from the epicondyle. This distance of 45 mm made sure that the straps did not interfere with each other during the flexion/extension of the elbow and also provided good suspension points. The 45 mm distance (Figure 8.3: I) was measured from the epicondyle when the elbow was at a 90 degrees flexion. From there, a measuring tape was used to obtain the circumferences of the stump at these points (Figure 8.3: F,C). For long stumps, a second measurement was performed for the second strap (Figure 8.3: D). This was done by determining the perfect place for the strap considering the dimples, scars, muscles, and painful tissue in the stump. The circumference of that point together with the distance between the straps (Figure 8.3: E) were also determined using a measuring tape. Finally, two measurements of the healthy arm were taken for the design of the shaft (Figure 8.3: J, K). These were used mainly for the length and width of the forearm.

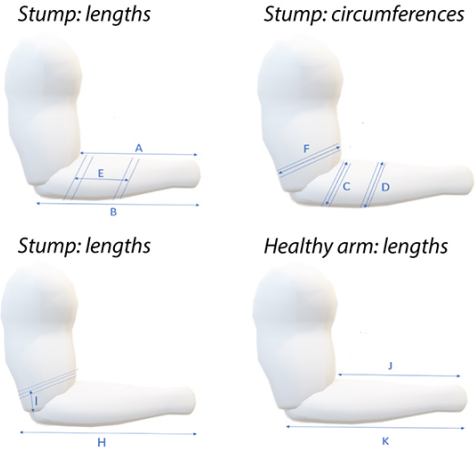

A	*Ventral length stump*
B	*Dorsal length stump*
C	*Proximal circumference lower arm*
D	*Distal circumference lower arm (depends of the stump)*
E	*Length between the two straps (measured in the middle)*
F	*Circumference upper arm*
H	*From the end of the arm till the end of the stump (measured in the middle)*
I	*Dimple elbow beginning of the strap*
J	*Ventral length healthy arm*
K	*Dorsal length healthy arm*

Figure 8.3. The measurements taken on the stump and healthy arm. These measurements were used for the design of the socket and shaft of the prosthesis.

Five subjects with trans-radial defects were recruited in the city of Ibague, Colombia with the help of the Secretary of Healthcare of the city. An invitation message for recruitment was broadcast using the local radio. Table 8.1 shows basic clinical data of the subjects. The number of participants was defined as a convenience sample according to the subjects available, the logistic challenges of the area and the timeframe of the study. Two of the subjects had been previously fitted with a prosthetic device (1 and 5). The study was approved by the Internal Review Board (IRB) of the Universidad del Tolima and all subjects gave written consent to participate. Each subject was invited to the prosthetic workshop where the physical measurements of their stump were taken. The important anatomical points were spotted visually and a measuring tape was used to measure the dimensions required for the design of the socket. The sockets and shafts were then produced using the Prusa i3 MK3S 3D printer and TPU and PLA filaments, respectively. The driving system was manufactured using the cable and housing of a bicycle braking system, nylon webbing, plastic buckles, and fasteners. The whole prosthetic arm was later assembled and then fitted to the user.

Table 8.1. Clinical data of the five subjects recruited for the study.

Subject	Gender	Age	Hand	Etiology
1	Male	42	Right	Trauma
2	Male	68	Left	Trauma
3	Male	35	Left	Trauma
4	Female	23	Right	Congenital
5	Male	21	Right	Trauma

Each subject was then allowed to use the prosthesis freely, adjusting the harness as requested until the user felt comfortable. The functionality of the prostheses was assessed through the Box and Blocks Test (BBT). BBT measures hand functionality by scoring the number of blocks moved from one side to another in a partitioned box [15].

The subjects were instructed to first undertake two warm-up tests in order to familiarize themselves with the experimental setup. The actual experiment then followed and consisted of four repetitions of the BBT. The subjects then took their prosthetic device home and were told to use it as they saw fit, during their regular daily lives. In a months-time, the subjects were contacted again inviting them to complete a questionnaire related to their experience with their prosthetic device. The first eleven items of the module of satisfaction of the Orthotics Prosthetics User Survey (OPUS) instrument were administered as a self-report questionnaire [16] (See the questions in Appendix 1). These first eleven items refer only to the satisfaction with the prosthetic device and not to the clinical service. The questions were all translated to the Spanish language and sent by email to the users. The users scored the different aspects of the prosthesis on a scale from 1 (Strongly Disagree) to 5 (Strongly Agree).

8.3 Results

Five prosthetic arms were produced and fitted onto the users (Figure 8.4). The total time required to produce the whole prosthetic device was one week per subject, including the time for the measurements, the 3D printing of the parts and the assembly. This also included the time to produce the prosthetic hand

(≈28 hours of 3D printing time (See, Chapter 6)), which in this case took place in the Netherlands previous to the installation of the prosthetic workshop in Ibague. The total material costs of the prosthetic device, including 3D printing polymers and other materials, were 50 US dollars. The results of the BBT are presented in Table 8.2. The results of the OPUS questionnaire are shown in Figure 8.5.

Table 8.2. The results of the Box and Blocks Test (BBT).

Subject	1st Trial	2nd Trial	3rd Trial	4th Trial	Mean ± SD	
1	16	14	16	18	16 ± 1.6	10.2 ± 5.4 (Mean ± SD)
2	4	4	4	4	4 ± 0	
3	5	5	4	8	5.5 ± 1.7	
4	9	9	13	12	10.75 ± 2.1	
5	15	11	18	15	14.75 ± 2.9	

Figure 8.4. The subjects fitted with the 3D printed prosthetic device.

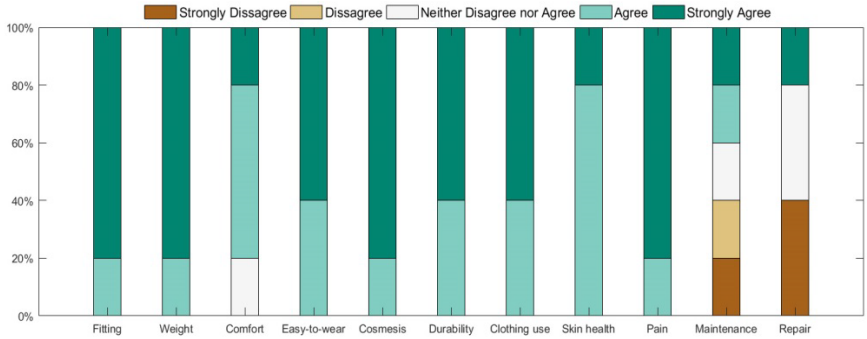

Figure 8.5. The satisfaction scores of the 3D printed prosthetic device.

The users were generally satisfied with all the features of their prosthetic device. The features that did not satisfy all the users are comfort and the ability to perform maintenance and repair. One subject neither disagreed nor agreed regarding the comfort, one subject strongly disagreed regarding the ability to perform maintenance and two subjects strongly disagreed regarding the ability to perform repairs.

8.4 Discussion

Through the manual measuring method and parametric socket and shaft designs, these two components of the prosthetic device were produced easily and locally. The material cost of the prosthesis is relatively low, which makes it an affordable alternative to current BP prostheses. The resulting prosthetic hand is a first working prototype for a low-cost device (less than 30 US dollars of material costs) that provides a solution for transradial amputation in Ibague, Colombia. The prosthetic hand itself was produced with a dual-extrusion 3D printer which is less accessible and more difficult to operate than single-extrusion 3D printers. Equipping a workshop with a dual-extrusion 3D printer would increase the cost of the equipment between 1500 – 2000 US dollars and will increase the training time of the 3D printer operator. These two points must be considered when setting up a workshop that can produce our bio-inspired hand locally.

The scores of the BBT (10.2 ± 5.4 blocks per minute) are the first functionality results ever reported for a 3D printed upper limb prosthesis used by subjects living in low-income settings. Only the research performed by Zuniga *et al*. presents results of the 3D printed prosthetic hand known as the Cyborg Beast, scoring higher (13 ± 12.7 blocks per minute) in a group of children who were also not living in low-income settings [9]. Although the mean value of the BBT results is slightly higher for the Cyborg Beast, the level of variability in those BBT results is much higher than the ones observed in our study. This could be linked to the fact that Zuniga performed an evaluation on children and they are probably less consistent in their behaviour than grown-ups. Moreover, the BBT values for the Cyborg Beast were measured 24 weeks after the fitting of the prostheses. The users, thus, had considerably more training time with the Cyborg Beast [9], which makes a direct comparison of the two prostheses challenging. The results shown in this paper suggest that our 3D printed prosthetic hand (median 10.2) is still not as functional as conventional BP prostheses (median 17 – 30 blocks per minute [17]) or other 3D printed BP hands (median 14 – 21 blocks per minute [18]). It is important to mention that we have previously found that BP prosthesis users improve in their performance of the BBT with practice [17]. It could therefore be hypothesized that the BBT scores would increase in a 24 weeks period following the fitting. In fact, the subjects who had been previously fitted with a BP prosthetic device (Subjects 1 and 5) obtained the best scores (mean 16 and 14.7 blocks respectively). That suggests how important it is for the users to receive proper training on the functionality of the prosthesis. Follow-up tests must be conducted in order to understand the effects of the training and experience with the device as well as the details of a learning curve. Indeed, those two subjects stopped using their previous prosthesis because of the weight of their devices. The BBT is also limited in defining all the functional characteristics of a prosthetic hand. Other functional tests, like the Southampton hand assessment procedure (SHAP) [19], would give more functional outputs, like the ability to perform the different grasping patterns of a human hand. This would help to understand whether further improvements on the grasping action should be

considered and on which particular features (friction properties, force transmission, etc.).

The scores of the questionnaires suggest that the users were in general satisfied with their prosthesis. The cosmetic appearance was scored high even though the colour of the prosthesis didn't match the skin tone of the users. None of them expressed major concerns about the colour, but two asked for the possibility of changing it to one that would better match their personality and/or 'style' rather than their skin tone. The results are hard to compare because of the subjective nature of the answers. Again, it is important to note that two subjects had previous experience with a BP prosthesis and this certainly impacted their satisfaction scores as they compared both devices. Some limitations that were identified included the ability to maintain and repair the prosthesis, which is depending on the economic status of the subject and on a certain level of knowledge about how the prosthesis actually works and the price of the parts. Some basic training could help the subjects to understand the whole assembly and identify easy ways for maintenance and repair. None of the prostheses broke or showed damage during the timeframe of the study and all subjects reported that the prosthesis was used at least four days per week between 1 – 3 hours per day. By prolonging the follow-up, the lifetime of the prosthesis could be also determined. Zuniga *et al.* reported that the subjects fitted with their 3D printed prosthesis also reported high levels of satisfaction although some concerns arose regarding the comfort and the durability of the device [10]. These subjects did not, however, live in low-income settings, and were also children which might have made a difference when it comes to the subjective experience with a new medical device. For instance, it is unlikely that subjects in low-income countries are familiar with the most recent technical advancements, which may lower the expectations on a new device. A follow-up study comparing the satisfaction scores of the two socio-economic groups towards the same 3D printed hand could provide more insights. Another limitation of our study is the limited statistic significance of the data due to the small size of the user groups. The subjects encountered difficulties when travelling from far to the prosthetic workshop either because they did not have

enough financial resources and/or they could not travel by themselves. This limited the number of subjects available. Performing the anthropometric measurements and the experiments via home visits can be considered as a strategy to increase the sample size. Moreover, only adults were recruited in order to facilitate the approval of the Internal Review Board (IRB). There is, therefore, no evidence that children may also accept or be satisfied with our design.

Manual measuring of parameters needed for the socket design is a fast anthropometric method and is easy to implement in terms of hardware. The method proved to be sufficient as the sockets properly fitted the users and were functional after one trial. The main problem lies in the fact that manual measurements are affected by human error. The outcome relies entirely on the skills and expertise of the person performing the anthropometrical measurements. Untrained personnel may provide inaccurate and inconsistent measurements, which can lead to imprecise fittings. The material of the socket lends itself to a certain degree of malleability, which allows for some level of inaccuracy. However, it seems more practical to adjust the socket slightly afterwards to make it perfectly fit the user. An improved design with adjustable straps could be beneficial, so long as the manufacturing requirements are limited to a 3D printer. Generally, the subjects were satisfied with the socket, although two areas for future improvement were identified. The comfort of the prosthesis and the contact with the skin could be improved by exploring other 3D printer settings or by using softer printing materials that lead to smoother surfaces. Amongst other things, the fact that the socket could be easily adapted for long stumps as well as for short stumps was very advantageous and saved design time.

8.5 Conclusion

Five trans-radial 3D printed prosthetic devices were custom-designed, manufactured, and fitted to users in low-resource settings. The functionality was assessed using the BBT, providing the first functionality data of a 3D printed hand manufactured in such settings. These initial results showed lower

functionality compared to other 3D printed BP hands, although the scores are likely to increase with user time. We therefore suggest follow-up experiments to clarify if there is a learning curve. The users reported in general a high level of satisfaction regarding the 3D printed prosthesis, although some aspects of the design require further improvement, including the option for users to perform maintenance or repair as well as the comfort of the prosthesis. Our 3D printed design and manufacturing process proved to be fast and easy to implement and opens a gateway for the production of prosthetic devices in developing countries.

8.6 References

[1] WHO, Standards for P&O Service Provision | ISPO, (2015).
[2] J. ten-Kate, G. Smit, P. Breedveld, 3D-printed upper limb prostheses: a review, Disabil Rehabil Assist Technol 12(3) (2017) 300-314.
[3] C. Joochim, N. Siriwatcharakul, Artificial Human Arm Controlled by Muscle Electromyography (EMG), 2018 Third International Conference on Engineering Science and Innovative Technology (ESIT), 2018, pp. 1-5.
[4] T. Sittiwanchai, I. Nakayama, S. Inoue, J. Kobayashi, Transhumeral prosthesis prototype with 3D printing and sEMG-based elbow joint control method, Proceedings of the 2014 International Conference on Advanced Mechatronic Systems, 2014, pp. 227-231.
[5] S. Mick, M. Lapeyre, P. Rouanet, C. Halgand, J. Benois-Pineau, F. Paclet, D. Cattaert, P.Y. Oudeyer, A. de Rugy, Reachy, a 3D-Printed Human-Like Robotic Arm as a Testbed for Human-Robot Control Strategies, Front Neurorobot 13 (2019) 65.
[6] J.S. Cuellar, G. Smit, A. Zadpoor, P. Breedveld, Ten guidelines for the design of non-assembly mechanisms: The case of 3D-printed prosthetic hands, Proc Inst Mech Eng H (2018) 954411918794734.
[7] J.A. Leal-Naranjo, C.T. Miguel, M. Ceccarelli, H. Rostro-Gonzalez, Mechanical Design and Assessment of a Low-Cost 7-DOF Prosthetic Arm for Shoulder Disarticulation, Appl Bionics Biomech 2018 (2018) 4357602.
[8] J.M. Zuniga, A.M. Carson, J.M. Peck, T. Kalina, R.M. Srivastava, K. Peck, The development of a low-cost three-dimensional printed shoulder, arm, and hand prostheses for children, Prosthet Orthot Int 41(2) (2017) 205-209.

[9] J.M. Zuniga, J.L. Peck, R. Srivastava, J.E. Pierce, D.R. Dudley, N.A. Than, N. Stergiou, Functional changes through the usage of 3D-printed transitional prostheses in children, Disabil Rehabil Assist Technol 14(1) (2019) 68-74.
[10] J.M. Zuniga, K.J. Young, J.L. Peck, R. Srivastava, J.E. Pierce, D.R. Dudley, D.A. Salazar, J. Bergmann, Remote fitting procedures for upper limb 3d printed prostheses, Expert Rev Med Devices 16(3) (2019) 257-266.
[11] S. Herfat, P. Moreau, Evaluating 3D technologies for upper limb prosthesis design (Amman, Jordan), 2018. https://doi.org/10.7490/f1000research.1115497.1. (Accessed 28/04/2020).
[12] J.H. Vicinus, X-ray anthropometry of the hand, Aerospace Medical Research Laboratories, Wright-Patterson AFB, Ohio, 1962.
[13] D.H. Plettenburg, Basic requirements for upper extremity prostheses: the WILMER approach, Proceedings of the 20th Annual International Conference of the IEEE Engineering in Medicine and Biology Society. Vol.20 Biomedical Engineering Towards the Year 2000 and Beyond (Cat. No.98CH36286), Hong Kong, 1998, pp. 2276-2281 vol.5.
[14] H.A. Walta, P. Ariese, J.C. Cool, Ergonomic socket design for congenital below elbow amputated children, J Rehabil Sci (2) (1989) 19-24.
[15] V. Mathiowetz, G. Volland, N. Kashman, K. Weber, Adult norms for the Box and Block Test of manual dexterity, Am J Occup Ther 39(6) (1985) 386-91.
[16] H.Y. Lindner, B.S. Natterlund, L.M. Hermansson, Upper limb prosthetic outcome measures: review and content comparison based on International Classification of Functioning, Disability and Health, Prosthet Orthot Int 34(2) (2010) 109-28.
[17] L. Haverkate, G. Smit, D.H. Plettenburg, Assessment of body-powered upper limb prostheses by able-bodied subjects, using the Box and Blocks Test and the Nine-Hole Peg Test, Prosthet Orthot Int 40(1) (2016) 109-16.
[18] J.S. Cuellar, G. Smit, P. Breedveld, A.A. Zadpoor, D. Plettenburg, Functional evaluation of a non-assembly 3D-printed hand prosthesis, Proc Inst Mech Eng H 233(11) (2019) 1122-1131.
[19] C.M. Light, P.H. Chappell, P.J. Kyberd, Establishing a standardized clinical assessment tool of pathologic and prosthetic hand function: normative data, reliability, and validity, Arch Phys Med Rehabil 83(6) (2002) 776-83.

Chapter 9: Discussion

9.1 3D Printed prosthetic hands

This PhD project started by envisioning a new paradigm for the fabrication of prosthetic mechanisms such that fully functional mechanisms could be fabricated in a single step without any requirements for post-manufacturing assembly. By replacing the traditional manufacturing process with 3D printing, robust assemblies could be produced on-demand and *in situ*, thereby eliminating several logistic challenges. Indeed, such customized devices could be produced for any kind of engineering applications. For example, prosthetics and orthotics could be produced in low-income settings without the need for a well-equipped workshop or laboratory.

This thesis began exploring possibilities of non-assembly fabrication by 3D printing techniques. Chapter 2 contains a literature review describing a number of mechanisms fabricated in a non-assembly manner by 3D printing. That exercise enabled us to explore the advantages of this manufacturing technique and discover strategies that could improve the design of mechanisms created by non-assembly manufacturing. Chapter 3 reviews the results of fatigue testing in 3D printed polymers in order to determine the 3D printing material and 3D printing settings that ensure best fatigue performance. Due to the synergy between all of the 3D printing parameters, it was unfeasible to characterize the best settings for maximizing the fatigue life with the data available in literature. Looking at the materials of 3D printing techniques based on material extrusion, it proved to be inconclusive as to whether ABS or PLA had the best fatigue resistance. ABS specimens typically had the longest fatigue life, but there were also instances where PLA had the best fatigue life.

Chapter 4 continues with a number of design considerations that were formulated for the fabrication of non-assembly mechanisms with 3D printing. We followed these guidelines to design a functional multi-articulated hand prosthesis that was then manufactured by material extrusion 3D printing

(Figure 1). This design procedure concluded in a hand prosthesis concept that reduces manufacturing requirements to a single 3D printer and its building material. Additional material or laborious post-manufacturing steps were eliminated. In addition to fulfilling the functional requirements proposed, the material costs of this prosthetic hand are low (20 US dollars) as compared to commercial prosthetic devices and similar 3D printed prosthetic hands [1]. Chapter 5 contains a functional evaluation of the 3D printed prosthetic hand including mechanical and user testing. The mechanical evaluation showed that the thin sheet of PLA material fabricated to serve as a leaf spring component in the finger joints of the hand, functions well under the static loading conditions proposed in our prosthetic design. On the other hand, the fatigue life experiments showed that the leaf spring is unable to withstand cyclic loading for a prolonged period. Our prosthetic hand needs a considerably lower amount of energy to close as compared to other Body Powered (BP) prosthetic hands, however, the pinch force achieved by the index and middle fingers given a force input of 100 N is low as compared to other BP prostheses [2]. The results of the Box and Blocks Test (BBT) and the Southampton Hand Assessment Procedure SHAP indicated a lower functionality of the device as compared to other BP alternatives [3-6]. This could be explained partly by the low pinch forces and the lack of friction between the fingertips (made of PLA material) and the objects involved in the test. Chapter 5 also shows that an increase of the friction coefficient of the finger pads leads to better performances of the box and blocks test, reaching scores comparable to those of other BP hands. This highlights the importance of the friction at the fingertips for improving the performance of 3D printed prosthetic hands.

Figure 9.1: The non-assembly prosthetic hand described in Chapter 4 of this thesis.

To further explore the capabilities of non-assembly 3D printing, in Chapter 6 we initiated a new design process aimed at producing articulated fingers (two degrees of freedom per finger) under this manufacturing framework. For this process, we adopted a bio-inspired design approach by studying the anatomical structures of the human hand that can be translated into components of prosthetic hands and have the potential of offering improved functionality. This bio-inspired designed prosthetic hand (Figure 2) achieved superior pinch force as compared to our previous non-assembly BP prosthetic hand [7], but still below the pinch force of conventional BP hand prostheses [2, 8]. Commercial BP hands that are produced in a factory or a specialized workshop with conventional production processes generally deliver higher pinch forces but are also much more expensive and weigh more and/or have no articulated fingers [8]. Due to the lack of data on the mechanical performance of other 3D printed BP hands in the literature, it is impossible to establish direct comparisons [1]. The increase in the pinch force as compared to the current 3D printed prosthetic hands, including our previous prosthetic hand design described in Chapter 4, is noteworthy. The input force and energy required needed to initiate a pinch grasp are, however, higher than in the

previous design[7], but still lower than in most of the conventional BP prosthetic hands [2, 8]. The data acquired indicate that our bio-inspired prosthetic hand is capable of applying a suitable pinch force for the activities of daily living at the expense of larger driving forces on the shoulder. Because of this, our prosthesis may be challenging to use for a part of the user population [2, 9]. More testing is required to evaluate user fatigue, given that the proposed design consumes more energy than other 3D printed hands, but still less energy than conventional prostheses. The implications of this are user-dependent: contractions up to 15-20% of a muscle's peak force can be largely fatigue-free [10], meaning that the user's physical strength plays a major role in the incidence of fatigue.

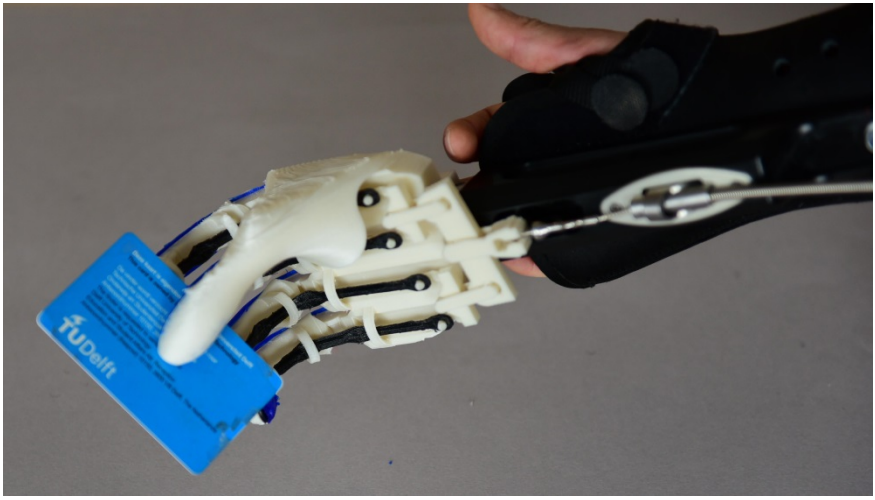

Figure 9.2: The bio-inspired prosthetic hand described in Chapter 6 of this thesis.

9.2 Use in developing countries

Another aspect addressed in this thesis was the 3D modeling of the residual limb of transradial amputees. Chapter 7 describes the method employed to obtain and process the 3D models of a stump. The method is based on photos

from a smartphone and a Statistical Shape Model (SSM). The algorithm translates the photos into a 3D digital shape and then introduces the digital outcome into the process of automatic anthropometry. The outcome was later used for determining the parameters of a parametric design of a transradial socket that can be 3D printed and fitted onto the user's residual limb. The automatic anthropometry process has proven to be fast and easy to use, only requiring an easy-to-build photo shoot set, which consisted of an A0-sized green background and a smartphone. On the other hand, the error resulting from the automatic measurement was still too large (>20 mm) for an acceptable socket design.

The thesis ends in Chapter 8 with a pilot study of our new bio-inspired 3D printed hand design in Colombia (Figure 3). We employed a manual measuring method using visual cues of the stump and a measuring tape to obtain the dimensions required for the design of the socket. Through the manual measuring method and parametric socket and shaft designs, the components of the prosthetic device were produced easily and locally on a material extrusion 3D printer. The material costs are relatively low, making our prosthesis an affordable alternative to commercial BP prostheses. Our bio-inspired 3D printed prosthetic hand is a first working prototype of a low-cost prosthetic device (less than 30 US dollars of material costs) that provides a solution for transradial amputation in Ibague, Colombia. We evaluated our prosthetic hand with a BBT to measure functionality as well as with a questionnaire to measure satisfaction. The scores of the BBT (10.2 ± 5.4 blocks per minute) are the first functionality results ever reported for a 3D printed upper limb prosthesis used by subjects living in low-income settings. It is important to mention that subjects improve their performance in the BBT as the hand is used more often [3]. It could be hypothesized that BBT scores would increase in a 24 weeks period following the fitting. In fact, two subjects who had been previously fitted with a BP prosthetic obtained the best scores, which shows how important it is for the users to receive proper training on the functionality of the prosthesis. Follow-up tests must be conducted in order to

understand the effects of the training and experience with the device as well as the details of a learning curve.

The resulting sockets are lightweight (~57-70 g) and easy to put on and put off, which are important characteristics that increase the general acceptance of prosthetic devices by users [11]. Generally, the subjects were satisfied with the socket, although two areas for future improvement were identified. The comfort of the prosthesis and the contact with the skin could be improved by exploring other printing settings or by using other soft printing materials that lead to smoother surfaces. Among other things, the fact that the socket could be easily adapted for long stumps as well as for short stumps was very advantageous and saved design time.

Figure 9.3: Users with our 3D printed bio-inspired prostheses in Colombia.

The scores of the questionnaires suggest that the users were in general satisfied with their prosthesis. The results are challenging to compare with previous research because of the subjective nature of the answers. Some limitations that were identified included the ability to maintain and repair the prosthesis, which is expected to be dependent on the economic status of each subject and certain level of knowledge about the price of the parts. By prolonging the follow-up, the lifetime of the prosthesis could be also determined. The socioeconomic status of the subjects participating in a satisfaction study of prosthetic devices may play an important role when it comes to the subjective experience with a new medical device. A study comparing the satisfaction scores of the two socioeconomic groups towards the same 3D printed hand could provide more insights. Another drawback of our study is the limited statistical significance due

to the small size of the user groups. The subjects encountered difficulties when travelling to the prosthetic workshop either because they did not have enough financial resources and/or they could not travel by themselves. This limited the number of subjects available.

9.3 Design for 3D printing

This thesis began exploring possibilities of non-assembly fabrication by 3D printing techniques. That exercise enabled us to explore the advantages of this manufacturing technique and discover strategies that could improve the design of non-assembly 3D printed mechanisms. Throughout the literature search, material jetting was found to be the most widely used AM technique for the fabrication of non-assembly mechanisms. Both compliant and traditional mechanisms were successfully conceived achieving reasonable levels of (geometrical) complexity. The remarkable capability of some 3D printers (*e.g.*, Objet, Stratasys) for parallel deposition of parts and soluble support material has been found to offer significant advantages over other 3D printing fabrication principles. Material jetting technology is, however, less commonly used because the required equipment and printing material are more expensive than those for other 3D printing processes. As far as other printing techniques are concerned, material extrusion and in particular fused deposition modelling (FDM) stand out as the most accessible 3D printing technology. Although material extrusion-based processes are generally perceived to be less precise as compared to other commercially available AM techniques, recent developments in FDM technology have enabled it to reach reasonable levels of geometric fidelity while enabling dual deposition of parts and soluble support materials. As shown by Wei *et al.* [12], industrial-grade FDM printers could equate other AM technologies in terms of minimum achievable clearance when building non-assembly joints. In addition of being the most affordable among AM techniques, the high versatility and easy accessibility makes the FDM technology a viable choice for manufacturing non-assembly constructs especially in settings where high-end technology is out of reach.

The design considerations conceived here for non-assembly fabrication could serve as guidelines enabling the circumvention of the many limitations that are commonly faced when using AM to build mechanisms. These guidelines were followed to build a prosthetic hand with FDM. Reference values (*i.e.* joint clearances, gaps and printer settings) used to fulfil the design considerations proposed are, therefore, based on the characteristics of FDM. Considering the used AM machine (*i.e.*, Ultimaker 3) and its relatively low building accuracy, the dimensions used in the design cases presented in Chapters 4 and 6 are an appropriate starting point for building non-assembly mechanisms with all AM techniques currently available. More strict tolerances and the use of water soluble support structures could address the mechanical problems that tend to arise from a large clearance between joints, provided that the required AM technology and equipment are available.

Although a large joint clearance is often seen as a significant concern in traditional mechanical design, it is usually necessary in FDM-based mechanical design and can be addressed using the unique features of AM. Without proper joint clearances the parts could fuse together during material deposition. The form-freedom offered by AM allows for the design of mechanical linkages that conveniently limit the joint clearance when actuated or reconfigured. The forces that activate the mechanisms can reposition the moving components into their desired locations when needed. Extra components that could remove joint clearance by manually reconfiguring their position inside the device are other options to deal with large clearances. Once 3D printed, these extra components can be clicked using, for instance, snap fit joints to couple the elements and complete the assembly. Compliant components might be also considered when joint clearance is undesired and the range of motion is compatible with the deformation limits of the widely available 3D printing materials. Compliant configurations can be also included when a spring behaviour is required as shown by the fabrication of the semi-circle leaf springs in Chapter 4 Here, compliancy was achieved by shaping the geometry of the constructs. The design of thin sheets of PLA as curved shapes allowed for

relatively small deformations and sufficient spring behaviour even when a material such as PLA, which is usually considered brittle, was used.

Additional possibilities of 3D printing for non-assembly fabrication can be found in Chapter 5. The bio-inspired design approach described there identified elements, based on the anatomical parts of the human finger, such as the joints, the stabilizing tendon elements and the pulling driving tendons, that were successfully incorporated in a prosthetic hand design and were then entirely manufactured by 3D printing. The process resulted in a bio-inspired prosthetic hand that possesses articulated fingers and minimizes post-printing assembly. The assembly of the hand was minimized to two post-processing steps, besides the usual support removal after 3D printing. The prosthetic has low production costs and is, therefore, potentially suitable for places where state-of-the-art prosthetic workshops are absent. In this design, the manufacturing advantages of the used 3D printing technology were conveniently used to fabricate an assembled mechanical hand with a complex shape and advanced functionality. During its fabrication, we used multi-material 3D printing, which has proven to be particularly advantageous when realizing different mechanical properties at specific areas. It is worth noting that different material combinations can be 3D printed, even if the materials are not bonding properly onto one another during their deposition. In our design, two materials (PLA and TPU) can be 3D printed simultaneously by embedding one of the materials into the other, thereby creating mechanical shape interlocking.

9.4 Automatic vs manual anthropometry

The dimensional error resulting from the automatic measurement in Chapter 7 was outside the acceptable boundaries for the design of the socket. The dimensional errors in the digital models obtained with our SSM based method may have originated from multiple possible sources. First, the process of generating the training database for the SSM can introduce small errors at different stages. The surface registration process ideally repositions the points to match the same location across surfaces. However, when the source and target shapes are significantly different, the repositioning process is not entirely

accurate and the new locations may not truly represent a match between both surfaces. This can lead to an SSM that does not describe the shape variations accurately. The outcome could be improved by manually aligning the points. This is, however, a long and time-consuming process. Second, the pictures were assumed to be taken from a specific location and with a specific orientation, which in reality is challenging, as precise positioning of the limbs for photo shooting is difficult to achieve. This can considerably influence the outcome, because the projections of the SSM using the pinhole camera model are based on three cameras positioned orthogonal to each other. An attempt was made to reduce this source of error by placing the smartphone in a fixed position with respect to the position of the limb and moving the limb to perform the photo shooting for all the view planes. This modification reduced the effects of moving the smartphone between the photo shoots, which can cause imprecise camera positioning. For that reason, we also used an optimization algorithm to find the position of the SSM that minimizes the error of the comparisons between the projections and the silhouettes. Third, the landmarks used for the automatic 3D anthropometry method were annotated manually using visual cues, which makes the process somewhat subjective. Finally, an artificial database based on healthy subjects was constructed. An early assumption was that the shape of a residual limb could be directly derived from healthy limb shapes with no significant modifications. This may not be entirely true for some special cases of transradial defects where the shape is significantly different due to specific arm conditions. An extended SSM trained with a larger database including actual surfaces of limbs with transradial defects would be, therefore, desirable. In addition, we have used a relatively small number of shapes to train the SSM (40 stump 3D models were used to train each SSM). The 3D modelling of the test setup could be better performed, if the training dataset of the residual limb models was larger.

During this research, we acquired the photos using an average quality camera (iPhone 6 camera) but under controlled conditions. While it is expected that the required photographic conditions can be easily met due to the low level of hardware requirements (*i.e*. smartphone camera, tripod and colored

background), the photo shooting process could pose some challenges, because three orthogonal photographs are required. This may be difficult to arrange for all users particularly those living in remote, isolated areas. While the proposed methodology in Chapter 7 makes the whole 3D modelling process faster, it leads to less accurate measurements in comparison to other scanning methods, such as laser scanning. While the proposed way of processing images is promising, its accuracy needs to be improved considerably and its practicality is yet to be proven both for the prosthetist and the user.

Manual measuring is a fast anthropometric method and is easy to implement in terms of hardware. The method proved to be sufficient as the sockets properly fitted the users and were functional at the first attempt. The main problem lies in the fact that the measurements are affected by human error. The outcome relies entirely on the skill and expertise of the person performing the anthropometrical measurements. Untrained personnel may provide inaccurate and inconsistent measurements, which can lead to imprecise fittings. The material of the socket lends itself to a certain degree of malleability, which allows for some level of inaccuracy. In the end, it seems more practical to manually adjust the socket slightly afterwards to make it perfectly fit the user and be optimal to use.

9.5 Future directions

We performed a 1-month follow-up after the fitting of our bio-inspired prosthesis in Colombia, in which the user satisfaction of the prosthetic device was measured. Other circumstances, such as the failure of parts, are more likely to happen at a later point in time. A follow-up over a longer period is, therefore, required in order to observe any changes to the prosthesis. These changes can have an important effect on the functionality and the user satisfaction of the prosthesis. Furthermore, while BBT is a fast and reliable method to assess gross manual dexterity, it does not prove that the user is able to execute other tasks in daily life apart from moving wooden blocks. The 1-month follow-up can be extended by measuring functionality through other functional tests such as SHAP or the Nine-Hole Peg Test and also through questionnaires. The BBT can

be applied again after a specific amount of time to measure how much their grasping function has improved as the users continued using the prosthesis.

To expand the scope of the project in Colombia, the equipment can be set and calibrated for multi-material 3D printing in order to build more prosthetic hands locally. More subjects can be included in the study once the printer is capable of producing more hands. Other 3D printed prosthetic designs can be also produced locally and a comparative study between different designs can be initiated. This research could be also expanded by testing different designs of sockets for other levels of amputation, since we only provided fitting to transradial cases.

Additionally, we could also continue exploring the 3D scanning method using a smartphone. However, at this stage, the automatic anthropometry method needs significant further development. Considering the rate at which technology is advancing, it may be possible to find low-cost 3D scanners in the near future or even integrated 3D scanners inside smartphones. But even with an accurate 3D scanner, the practicality of the entire fitting process using 3D models of stumps remains unknown and needs further investigation. In fact, we constructed acceptable fittings using just a measuring tape. Maybe this measuring method using a tape combined with an adjustable socket is good enough for producing well-working sockets. In any case, using both fitting methods, the one using a measuring tape and the one using a 3D scanner, and comparing or combining them could be an interesting direction for future research.

In a more general view, we would like to discuss two points regarding the development of 3D printed prosthetic hands. First, the design process has to be customized to the anatomy of the user, but it should be also customized for his/her needs. Prosthetic users prioritize different characteristics of their prosthetic device depending on their taste, culture, job, etc. For instance, a user may prefer cosmetics over the number of achievable grasping patterns. This difference in priority can be easily integrated in the design process if a certain database of prosthetic hand designs for 3D printing is available. Following the previous example, in this database the user can select designs that are more

cosmetic as opposed to designs that have more functions. This means that the design process must take the personal preference of the end user into account from step one. The information provided by the user holds crucial value and should also be used for further developments on prosthetic hands because one, the users can instantly refer to the problems they have, or would like to solve, with a new prosthetic hand, and two, because the users can relate to problems specifically to the location and socio-economic status of the targeted group. For example, problems with the prosthetic device could be related to the temperature of the environment, or the user's ability to perform the assembly of the prosthesis, maintenance or repair.

Second, comfort is more important than dexterity in active prosthetic hands. In accordance to previous research [13-15], the subjects involved in the evaluation of the bio-inspired hand in Chapter 8 also reported that the total weight and the interaction of the socket with the skin have to be a top priority over the rest of the functional features of the prosthesis. In fact, two subjects that previously used a prosthesis were relieved and satisfied with our new prosthesis mostly because it is lightweight. Further research on 3D printed prosthetic designs should pursue more comfort in 3D printed sockets. Lastly, more testing data of functional characteristics of 3D printed hand prostheses is clearly needed. By the end of this project, only a few research groups reported functionality results in scientific literature, which makes it difficult for having direct comparisons and also to define whether improvements have been made. We encourage developers of 3D printed hand prostheses to append their new designs with functional evaluations, preferably user evaluations, in order to have a good baseline for comparison.

The knowledge acquired in this project serves as a starting point towards the implementation of low-cost prosthetic workshops throughout the Colombian territory and hopefully in other regions in the developing world as well. The prosthetic designs conceived during this project will be open source so that 3D printing communities around the globe can produce them, build upon them and develop new improved designs based on them. In the near future, we hope that with the technology developed in this project , proper treatment can

be provided to people with arm defects or amputation regardless of their country and living conditions. We also expect that the ideas discussed in this thesis foster local entrepreneurship and innovation, hopefully beyond the prostheses world. We believe that the successful outcomes of this project demonstrates how technology can be developed and introduced in settings where technical practices are outdated and do not measure up to the local challenges. Nowadays , given that 3D printing technology is becoming more and more accessible and knowledge can be transferred faster than ever, the opportunities are plentiful.

9.6 Conclusion

A 3D modelling procedure for the anthropometry of upper limbs with trans-radial defects based on 2D pictures was proposed, implemented, and tested. The resulting anatomical measurements were less accurate than manual measurements and need to be further improved before the application of this technique in actual practice can be realized. Manual measurements were used instead to design a socket that properly fits the residual limb of the users. The resulting socket was lightweight, easy to put on and put off and affordable. Two hand prosthesis were designed and 3D printed with an inexpensive FDM™ machine. Both prosthetic designs meet basic user requirements and reduced the number of post assembly operations to zero (Chapter 4) and two (Chapter 6). The prosthesis in Chapter 6 also incorporates new bio-inspired features that allowed articulated fingers. Field testing in Colombia concluded that our design and manufacturing processes based on 3D printing are fast and easy to implement and opens a gateway for the production of prosthetic devices in developing countries.

9.7 References

[1] J. ten-Kate, G. Smit, P. Breedveld, 3D-printed upper limb prostheses: a review, Disabil Rehabil Assist Technol 12(3) (2017) 300-314.
[2] G. Smit, D.H. Plettenburg, Efficiency of Voluntary Closing Hand and Hook Prostheses, Prosthetics and Orthotics International 34(4) (2010) 411-427.

[3] L. Haverkate, G. Smit, D.H. Plettenburg, Assessment of body-powered upper limb prostheses by able-bodied subjects, using the Box and Blocks Test and the Nine-Hole Peg Test, Prosthet Orthot Int 40(1) (2016) 109-16.
[4] T.R. Farrell, R.F. Weir, The optimal controller delay for myoelectric prostheses, IEEE Trans Neural Syst Rehabil Eng 15(1) (2007) 111-8.
[5] I.A. Ramirez, C.P. Lusk, R. Dubey, M.J. Highsmith, M.E. Maitland, Crossed four-bar mechanism for improved prosthetic grasp, J Rehabil Res Dev 46(8) (2009) 1011-20.
[6] J.T. Belter, M.T. Leddy, K.D. Gemmell, A.M. Dollar, Comparative Clinical Evaluation of the Yale Multigrasp Hand, P Ieee Ras-Embs Int (2016) 528-535.
[7] J.S. Cuellar, G. Smit, A. Zadpoor, P. Breedveld, Ten guidelines for the design of non-assembly mechanisms: The case of 3D-printed prosthetic hands, Proc Inst Mech Eng H (2018) 954411918794734.
[8] G. Smit, D.H. Plettenburg, F.C.T. van der Helm, The Lightweight Delft Cylinder Hand: First Multi-Articulating Hand That Meets the Basic User Requirements, Ieee T Neur Sys Reh 23(3) (2015) 431-440.
[9] M. Hichert, A.N. Vardy, D. Plettenburg, Fatigue-free operation of most body-powered prostheses not feasible for majority of users with trans-radial deficiency, Prosthet Orthot Int 42(1) (2018) 84-92.
[10] H. Monod, Contractility of Muscle during Prolonged Static and Repetitive Dynamic Activity, Ergonomics 28(1) (1985) 81-89.
[11] Y.J. Sang, X. Li, Y. Luo, Biomechanical design considerations for transradial prosthetic interface: A review, P I Mech Eng H 230(3) (2016) 239-250.
[12] X. Wei, Y. Tian, A. Joneja, A study on revolute joints in 3D-printed non-assembly mechanisms, Rapid Prototyping Journal 22(6) (2016) 901-933.
[13] E. Biddiss, D. Beaton, T. Chau, Consumer design priorities for upper limb prosthetics, Disabil Rehabil Assist Technol 2(6) (2007) 346-57.
[14] C. Pylatiuk, S. Schulz, L. Doderlein, Results of an Internet survey of myoelectric prosthetic hand users, Prosthet Orthot Int 31(4) (2007) 362-70.
[15] J.T. Belter, J.L. Segil, A.M. Dollar, R.F. Weir, Mechanical design and performance specifications of anthropomorphic prosthetic hands: a review, J Rehabil Res Dev 50(5) (2013) 599-618.